DATA REPORT:
SEDIMENT INCUBATIONS AND SUPPORTING STUDIES FOR ONONDAGA LAKE SEDIMENT MANAGEMENT UNIT (SMU) 8

Prepared For:

Honeywell

301 Plainfield Road
Suite 300
Syracuse, New York 13212

Prepared By:

Exponent®
420 Lexington Avenue, Suite 1740
New York, NY 10170

Michigan Technological University
Upstate Freshwater Institute

and

Syracuse University
Environmental Systems Engineering
Syracuse University
51 Link Hall
Syracuse, New York 13244

JULY 2011

TABLE OF CONTENTS

TABLE OF CONTENTS (CONTINUED)

Page

TABLE OF CONTENTS
(CONTINUED)

Page

TABLE OF CONTENTS (CONTINUED)

LIST OF TABLES

Page

TABLE OF CONTENTS (CONTINUED)

LIST OF FIGURES

Page

TABLE OF CONTENTS (CONTINUED)

LIST OF FIGURES (CONT.)

Page

TABLE OF CONTENTS (CONTINUED)

LIST OF FIGURES (CONT.)

Page

TABLE OF CONTENTS
(CONTINUED)

LIST OF APPENDICES

LIST OF ACRONYMS

DIW	distilled water
DNR	dissimilatory NO_3 reduction to ammonium
DO	dissolved oxygen
EA	electron acceptors
ERS	ecological redox series
LCS	laboratory control sample
MS	matrix spike
MSD	matrix spike duplicate
NYSDEC	New York State Department of Environmental Conservation
QA/QC	quality assurance/quality control
qPCR	quantitative time polymerase chain reaction
ROD	Record of Decision
SMU	sediment management unit
USEPA	United States Environmental Protection Agency

EXECUTIVE SUMMARY

This report documents the results of sediment incubations and other studies undertaken for Honeywell by various universities and research groups to assist in the evaluation of nitrate addition and oxygenation as required in the Record of Decision (ROD) for the Onondaga Lake Bottom Subsite (NYSDEC and USEPA 2005) and the Statement of Work appended to the Consent Decree between Honeywell and the New York State Department of Environmental Conservation (NYSDEC) for remediating the lake bottom. This work is applicable to the deep water portion of Sediment Management Unit 8 (SMU 8) where water depths exceed 9 meters (30 feet). The objectives of the work were to establish the efficacy of oxygen and nitrate addition in blocking methylmercury production, the quantities of nitrate and oxygen required to meet sediment demand, and the interplay between conditions in the water column and sediment dynamics.

Michigan Technological University designed and implemented the sediment incubation studies with the assistance of Upstate Freshwater Institute and Syracuse University. These studies examined the accumulation of methylmercury in water overlying sediment cores in the laboratory as a result of varying oxygen and nitrate concentrations in overlying water.

Syracuse University designed and implemented the mercury and nitrogen fate experiments. Detailed analysis of sediment porewater under different oxygen and nitrate conditions in overlying water showed that the zones of microbial nitrate and sulfate reduction respond to changes in oxygen and nitrate concentrations in overlying water. When nitrate is depleted in overlying water, the sulfate reduction zone and thus the zone of methylmercury production moves up to the sediment-water interface resulting in increases in methylmercury concentration in overlying water. Regarding the fate of nitrate in Onondaga Lake, most nitrate reduction was in the form of complete denitrification to dinitrogen gas, with no trend towards increased nitrous oxide or ammonium production even at ten times ambient nitrate concentrations

The microbiological analyses in SMU 8 sediment supported the observations made during the sediment incubations and the mercury and nitrogen fate studies. During stratification when the hypolimnion was anaerobic and nitrate was still present in water overlying the sediment, denitrifying bacteria predominated in surface sediments. When nitrate was depleted, iron/sulfate reducing bacteria increased in abundance in surface sediment. Methanogenic bacteria were most abundant when redox potential was low, following oxygen and nitrate depletion.

Results from the sediment incubation, mercury and nitrogen fate, and microbiological studies are summarized in this report. The results will need to be interpreted in conjunction with water column observations from the ongoing baseline monitoring program as well as results from the nitrate application field trial being conducted in 2009. Taken together, these efforts will help inform the decision to implement oxygenation and/or nitrate addition and the design of such processes.

SECTION 1

INTRODUCTION

The remedy for Onondaga Lake, as described in the ROD for the Onondaga Lake Bottom Subsite prepared by the NYSDEC and the United States Environmental Protection Agency (USEPA) (NYSDEC and USEPA 2005) includes performance of a pilot study in the deep water portion of Onondaga Lake (called the profundal zone or SMU 8) to evaluate the potential effectiveness of oxygenation at reducing the formation of methylmercury in the water column, while preserving the normal cycle of stratification within the lake. In addition, the Statement of Work appended to the Consent Decree requires Honeywell to conduct a study to determine if nitrate addition would effectively reduce methylmercury formation in the water column while preserving the normal cycle of stratification. This study of nitrate addition is ongoing and may later include performance of a nitrification pilot test (or demonstration). Both oxygen and nitrate are electron acceptors potentially capable of blocking the biogeochemical pathway leading to methylmercury production.

This report documents the results of sediment incubations and other studies undertaken to assist in the evaluation of nitrate addition and oxygenation as described in the *Work Plan for Onondaga Lake Sediment Management Unit 8 (SMU 8) Sediment Incubations and Supporting Studies* (Parsons et al. 2008). The decision to implement oxygenation and/or nitrate addition will be informed by the outcome of these studies.

1.1 PROJECT OBJECTIVES AND COMPONENTS

The work plan (Parsons, Exponent, Syracuse University and Upstate Freshwater Institute, 2007) approved by NYSDEC for the results presented in this report describes a series of laboratory measurements, supported by field monitoring and mathematical modeling activities, to provide the information required to design pilot demonstrations for oxygenation and nitrate addition and to enable a comparison of the relative advantages of both of these electron acceptors, establishing:

- Efficacy of oxygen and nitrate addition in blocking methylmercury production
- Quantities of nitrate and oxygen required to meet the sediment demand
- Interplay between conditions in the water column and sediment dynamics

Results presented in this report are based upon sediment samples collected from Onondaga Lake in 2007 and 2008, sub-sampled for chemical and microbiological analysis and applied in laboratory microcosm experiments. Individual, self-standing chapters specifically address three main components of the work: methylmercury flux from Onondaga Lake sediments, the fate of mercury and nitrogen in Onondaga Lake water and sediments, and microbiological analyses of SMU 8 sediments. The fourth component proposed in the work plan was redox modeling (described in Appendix B of work plan). Three models (i.e., a diagnostic model, a sediment diagenesis (chemical, physical, or biological changes occurring in sediment following initial deposition) model, and a coupled sediment-water column model) were developed to support the

design of the incubation chambers, describe sediment diagenesis, and predict electron acceptor demand and hypolimnetic methylmercury concentrations as functions of carbon fluxes, respectively. A report on this modeling effort will be submitted separately.

1.2 REPORT ORGANIZATION

Section 2 of this report describes the theoretical basis for the electron acceptor augmentation technology by applying results from microprobe measurements and porewater analysis; uses multiple approaches to establish the contemporary baseline (no augmentation) methylmercury flux for Onondaga Lake sediments; evaluates the efficacy (relative to baseline conditions) of oxygen and nitrate augmentation in mediating that flux; and provides guidelines relating to the concentrations of nitrate or oxygen required in augmentation, supporting those recommendations through analysis of laboratory incubations and sediment porewater profiles.

Section 3 of this report describes the results of a batch experiment to assess the fate of mercury under different oxidation-reduction regimes; patterns of mercury speciation and distribution in the sediment porewater and the water immediately overlying the sediment; and vertical profiles of ancillary parameters (nitrate, sulfate, and phosphate). In addition, this section attempts to delineate redox regions in the surficial sediment under different regimes and assesses the fate of nitrogen by quantifying nitrate removal to dinitrogen gas, nitrous oxide, and ammonium.

Section 4 of this report describes the results of a survey undertaken for the purpose of characterizing the microbial populations in the sediments of Onondaga Lake both temporally and spatially. Nitrate reduction and sulfate reduction, key processes for carbon and mercury cycling in Onondaga Lake, are both mediated by bacteria. Therefore, bacterial presence and abundance was investigated to shed light on the relative location and magnitude of these processes in SMU 8 sediment.

The report concludes with several appendices. Appendix A was prepared by Dr. Edwin A. (Todd) Cowen of Cornell University and describes the results of hydrodynamic studies. These studies provided the basis for generating turbulence in the incubation chambers that is representative of turbulence experienced in SMU 8 bottom waters.

Appendices B and C were prepared by Dr. Martin Auer of Michigan Technological University. Appendix B discusses electron acceptor addition and regulation of ammonia and phosphorus flux from lake sediments. Appendix C covers induced oxygen demand and electron acceptor amendment developed in conjunction with Dr. Stephen Chapra of Tufts University.

1.3 REFERENCES FOR SECTION 1

New York State Department of Environmental Conservation and United States Environmental Protection Agency Region 2. 2005. Record of Decision. *Onondaga Lake Bottom Subsite of the Onondaga Lake Superfund Site*. July 2005.

Parsons, Exponent, Syracuse University, and Upstate Freshwater Institute, 2007. *Work Plan for Onondaga Lake SMU 8 Sediment Incubations and Supporting Studies.* Prepared for Honeywell. Revised December 2008.

SECTION 2

METHYLMERCURY FLUX FROM THE SEDIMENTS OF ONONDAGA LAKE, NEW YORK, AS DETERMINED USING FLOW-THROUGH SEDIMENT MICROCOSMS

Martin T. Auer[1], David A. Matthews[2], Charles T. Driscoll[3], Steven W. Effler[2], G. Albert Galicinao[1], Brandon J. Ellefson[1] and Svetoslava Todorova[3]

2.1 INTRODUCTION: THE BIOGEOCHEMICAL BASIS FOR ELECTRON ACCEPTOR AMENDMENT

2.1.1 Carbon Diagenesis and the Ecological Redox Series

Particulate organic carbon delivered to the lake bottom undergoes diagenesis with the labile (biodegradable) fraction being converted to carbon dioxide, water and various extrametabolites through microbially-mediated reactions and the refractory (non-biodegradable) fraction passing deeper into the sediment for ultimate burial. Organic carbon diagenesis is a redox reaction involving an electron donor (organic carbon; nominally $C(H_2O)$) and one of several electron acceptors (EAs). The utilization of a particular electron acceptor is dictated by the thermodynamic favorability, as reflected in a sequence termed the ecological redox series (ERS; Table 2.1). In lake sediments, the ERS may be manifested vertically, with EAs and their attendant reactions and end products arrayed in bands in the downcore direction (Figure 2.1). The thickness (and in fact the simple presence) of each band is determined by the availability of EAs in the overlying water and the amount of labile organic carbon present. In oligotrophic (i.e., low primary productivity (algal production) as a result of low nutrient content) waters, where labile organic carbon is limited to the surface sediments, much of the diagenesis may be supported by aerobic metabolism (oxygen is the EA) and some components of the ERS (e.g. methanogenesis may be absent). In eutrophic (i.e., high primary productivity (algal production) as a result of high nutrient content) waters, where organic carbon is likely present at depth, all ERS processes may be present and active and the zone dedicated to the terminal process (methanogenesis) may be extensive.

2.1.2 Redox Chemistry and Methylmercury Dynamics

Redox chemistry and the activity and distribution of several members of the ERS impact methylmercury dynamics in the sediment. It is generally accepted that sulfate-reducing bacteria are the primary agents of mercury methylation (Compeau and Bartha 1985; Gilmour et al. 1992) and thus the production of methylmercury may be expected to be localized in the region of active

[1] Michigan Technological University
[2] Upstate Freshwater Institute
[3] Syracuse University

sulfate reduction (Figure 2.1). Three things are required to sustain sulfate-reduction and attendant mercury methylation:

1. A source of inorganic mercury, a reactant in the methylation process
2. A source of sulfate, the electron acceptor in the sulfate reduction process
3. A source of labile organic carbon, the electron donor in the sulfate reduction process

Changes in the availability of any of these components would be expected to be similarly manifested in the rate of methylmercury production.

Methylmercury is produced then diffuses toward the surface where it may enter the water column and become available to the lake's biota (Mason and Morel 1995). Prior to release, however, the methylmercury must pass through ERS zones favoring aerobic decomposition and denitrification, regions thought to support microbial demethylation and/or physicochemical sorption (Oremland et al. 1991; Gagnon et al. 1996). Thus, with oxygen and/or nitrate available, the uppermost layers of sediment act in the capacity of a filter, reducing or eliminating the flux of methylmercury from the sediment.

2.1.3 Electron Acceptor Resources and Demand

The EAs supporting organic carbon diagenesis in lake sediments are drawn from the overlying water through diffusive mass transport. In lakes exhibiting thermal stratification, the EAs available to the sediments over the stratified interval are largely those present in the hypolimnion at the time of stratification. In (eutrophic) systems where the demand on EAs is great, hypolimnetic EA resources may be depleted over the course of the stratified interval. The classic depletion of oxygen and nitrate in the hypolimnia of stratified lakes is well known to limnologists. As EAs become depleted from the hypolimnion and thus the sediments, the attendant microbial reactions become inactive. The effect of this is that processes further along in the ERS 'move up' and dominate both sediment metabolism and exchange of extrametabolites across the sediment water interface (Figure 2.1). The depletion of oxygen and nitrate and the attendant elimination of aerobic metabolism and denitrification have two effects. First, the capacity of the sediment to 'filter' the up-core diffusion of sulfide and methylmercury is lost. Second, sulfate reducers no longer have to compete with microbes higher on the ERS for labile organic carbon resources. The result includes both an increase in gross sulfate reduction and methylmercury production and an increase in net sulfide and methylmercury flux. This process is manifested in the almost sudden co-appearance and subsequent accumulation of sulfide and methylmercury in hypolimnetic waters.

It should be noted, however, that the loss of the oxygen and nitrate components of the ERS from sediments is not an instantaneous occurrence. The depth of penetration of oxygen and nitrate into the sediment, and thus the thickness of the 'filtering layer,' reflects the interplay of labile organic carbon concentrations and the rate of diffusion of these EAs across the sediment-water interface. The rate of diffusion is, in turn, governed by the EA concentration at the sediment-water interface. This concentration decreases systematically as sediment EA demand proceeds and the rate of downcore diffusion decreases accordingly. The result is a 'thinning' of the sediment layers in which aerobic metabolism and denitrification occur and, potentially, a concomitant reduction in the efficiency of the 'filter effect' (i.e. sorption and demethylation capacity). It is expected that such a condition would be reflected in a transition phase during

which rates of sulfide and methylmercury flux would gradually increase, eventually arriving at the maximum rates associated with complete oxygen and nitrate depletion.

2.1.4 Electron Acceptor Amendment as a Mercury Remediation Technology

The addition of oxygen or nitrate to the hypolimnion of mercury-impacted lakes, here termed EA amendment, is based on the biogeochemical processes driving methylmercury production and its transport across the sediment-water interface. The long-term response of a contaminated system will be governed by the three driving forces outlined above: the availability of ionic mercury as a precursor to methylmercury formation and the availability of labile organic carbon and sulfate as the raw materials driving the sulfate reduction engine thought to foster methylation. Because inorganic mercury is strongly sorbed, dissolved-phase mercury remains in proximity to the solid phase matrix with which it was associated at deposition, tracking that material as it is moved downcore through burial. Because mercury is closely held to particulate matter and because soluble phase mercury must be resident within the zone of sulfate reduction in order to undergo methylation, a reduction in mercury inputs to the sediments holds promise for providing long-term relief from contamination for the waters overlying the sediment.

The addition of EAs to the system offers to limit methylmercury impacts over the period in which the sediments come into equilibrium with new levels of mercury input (i.e. cleaner sediment) in two ways. First, by providing an alternative pathway for organic carbon diagenesis, energy resources are diverted from the sulfate reduction pathway known to support methylation. Second, by establishing sediment layers rich in oxygen and/or nitrate sorption and/or demethylation are promoted, creating a 'filter effect' that limits transport of methylmercury across the sediment-water interface. Thus, nitrate and/or oxygen addition offers to reduce both the production and flux of methylmercury over the interval necessary for sediments to reach equilibrium with their remediated condition. The research results presented here evaluate the efficacy of EA amendment in reducing methylmercury flux from intact sediment cores and present evidence for the reduction in methylmercury production associated with EA diversion of energy resources from the sulfate reduction pathway.

2.2 TASK SPECIFIC OBJECTIVES AND APPROACH

The engineering objective driving this research relates to the use of electron acceptor augmentation as a means of blocking methylmercury flux while the lake sediment come to steady state with the post-cleanup depositional environment. The research objective is to evaluate this approach using bench-scale sediment microcosms as a prelude to a field scale technology demonstration program of electron acceptor (oxygen and/or nitrate) addition. Specifically, we seek to:

1. Quantify the distribution of electron acceptors, reduced species end products and methylmercury in the sediment porewater as relates to the theoretical foundations of the electron acceptor augmentation technology.
2. Examine the efficacy of augmentation with oxygen and nitrate in blocking methylmercury flux, identifying requirements for the maintenance of specific electron acceptor concentrations.

3. Apply the findings of porewater and flux measurements in considering contemporary changes in electron acceptor depletion in the hypolimnion and methylmercury flux from the sediments as they influence future needs for augmentation.

The approach will involve utilization of microprobe and manual porewater measurements in support of the first objective and flow-through sediment microcosms in support of the second.

2.3 METHODS AND MATERIALS

2.3.1 Clean Protocols

Research focusing on trace metals requires that clean protocols be observed. Clean techniques for these experiments were developed and maintained under the auspices of the laboratory of Dr. Charles T. Driscoll of Syracuse University, an experienced researcher in the field of mercury biogeochemistry.

The focus of clean techniques operations was the setup, operation and sampling of the sediment microcosms used to evaluate the impact of electron acceptor amendment on methylmercury flux. Deionized water (0.22 μm Millipak 40, Millipore Corporation), testing negative (limit of detection, 0.2 ng mercury $\cdot L^{-1}$) for the presence of total mercury, was used in preparing all chemical solutions and in washing laboratory materials. The containers and tubing used to construct the microcosms were made of Teflon and glass, cleaned by washing with a 10 percent HCl solution [trace metal grade] followed by three rinses in deionized water. A short section of C-Flex tubing (thermoplastic elastomer) was used within the contact portion of the peristaltic pumps. The feed stock for the microcosms, prepared from deionized water and analytical trace-metal grade chemicals, tested negative for the presence of total mercury. Gas feeds were drawn from ultra-pure/zero grade quality sources and passed through carbon and gold traps to ensure that no mercury was introduced.

A clean protocols test was performed on the microcosms prior to initiation of experiments. A feed stock of deionized water was run through an otherwise empty microcosm for six hours with the effluent collected and sampled for total mercury. The observed absence of mercury confirmed that the experiment could be initiated in a mercury-free state. The pumping system was then attached to a microcosm containing mercury-contaminated sediments from the study site and operated for an additional six hours. The entire system was then emptied, cleaned and set up again for operation with only a deionized water feed. The system was operated in this condition for six hours with the effluent collected and sampled for total mercury. The observed absence of mercury confirmed that clean-up techniques prevented carryover of mercury between experiments.

2.3.2 Sediment Collection and Processing

Sediments were collected from the South Deep depositional basin of Onondaga Lake between November 2007 and August 2008 using a stainless steel box corer (Model 1260, Ocean Instruments, Inc., San Diego, CA). The South Deep basin (maximum depth, 19 m) is considered to be representative of conditions in the remainder of the lake's profundal zone (Effler 1996). Teflon containers (10 cm in diameter by 30 cm tall; Savillex Corporation) were used to subsample the box core, yielding approximately 7 cm of hypolimnetic water over 12 cm of sediment. Additional collections, termed short cores, were collected using 5 cm in diameter by

10 cm tall sections of cellulose acetate butyrate core liner material (Wildlife Supply Company). Short cores contained approximately one-half hypolimnetic water and one-half sediment. Upon collection, sediment samples were placed in an ice chest and transported to the laboratory for storage at 4°C until used. Particular care was taken to minimize disturbing the sediment-water interface during box coring and transportation to the laboratory.

Processing and disposition of sediment samples varied with the application. Short cores and selected Teflon-contained cores were used for sediment microprofiling (as described below) and were simply held at 4°C until used. Other Teflon-contained cores were extruded in a nitrogen environment and sliced at 0.5 – 1.0 cm intervals. The slices were placed in plastic bags and frozen. Later, the slices were thawed and centrifuged in a nitrogen environment with the supernatant retained for total mercury and methylmercury analysis (as described below). The majority of the Teflon-contained cores were utilized in sediment microcosm experiments. Cores were outfitted with a friction-fit bottom, side-wall inlet and outlet ports and a threaded top containing ports for various applications. Cores to be used in microcosm experiments were maintained at 4°C until used.

2.3.3 Sediment Microprofiling

Microelectrode technologies provide a means for developing high resolution (50-100 μm) downcore profiles of selected chemical analytes (e.g., oxygen, nitrate, pH and sulfide). Instrumentation developed by Unisense A/S (Aarhus, Denmark) was utilized here and consisted of analyte-specific electrodes mounted on a computer-controlled, motor-driven micromanipulator. Electrodes were standardized for each use and offered a limit of detection entirely suitable for chemical rich sediment porewater [0.01 $mg \cdot L^{-1}$ for oxygen, nitrate and sulfide and 0.1 unit for pH. In addition to its role in motor control, the computer served in a data acquisition role and provided near real time feedback of conditions within the core. Ms. Heidi Brixen of the University of Aarhus (Denmark) provided assistance with the particularly challenging nitrate microelectrode measurements.

2.3.4 Sediment Microcosms

A microcosm approach to laboratory determination of flux across the sediment-water interface using a completely-mixed flow reactor is applied here. While batch core incubations have successfully been employed to measure flux (e.g. ammonia, oxygen and nitrate), the need to maintain electron acceptor concentrations at specified levels over the course of the incubation precludes their use here.

2.3.4.1 Microcosm Construction and Operation

A sediment microcosm consists of a cylindrical Teflon container, 10 cm diameter by 30 cm tall, outfitted with opposing inlet-outlet ports located approximately 2 cm below the top rim (Figure 2.2). The microcosm container is filled with 7 cm of hypolimnetic water over 12 cm of sediment, leaving approximately 11 cm of headspace. A friction fit Teflon bottom provides a seal against leakage following sample collection. A threaded Teflon top is outfitted with six peripheral ports to provide mixing and a single, central port where gas may be introduced.

Artificial lake water (Table 2.2), with an ionic composition similar to that of Onondaga Lake, serves as feed stock to the reactor with the rate of input regulated by metered gravity flow or a peristaltic pump. Gas (air, N_2 or an air-N_2 mix) is bubbled into the microcosm as a means of

regulating redox conditions. A digital gas mixer (Mix 1000 model, Applied Analytics, Inc.) was used to achieve the desired concentrations. Mixing in the microcosm is provided by three re-circulating channels (Teflon tubes; six ports) attached to a computer-controlled peristaltic pump. The pump is set at a re-circulating rate that provides random mixing at a turbulence level comparable to that observed at the sediment-water interface of Onondaga Lake (Ellefson, In Preparation). The objective of regulating turbulence levels is to eliminate artificial barriers to mass transport that might be associated with development of a stagnant boundary layer. All experiments were conducted in a temperature-controlled room or incubator maintained at 8°C, a representative hypolimnetic temperature for Onondaga Lake. Where experimental conditions required the absence of oxygen, experiments were conducted in an anaerobic chamber (mixed gas, N_2 with 5% H_2 and 1600 ppm CO_2, Coy Laboratory Products). Oxygen concentrations were monitored daily in the anaerobic chamber.

The experimental design is outlined in Table 2.3. Three experimental treatments, roughly corresponding to the sequential depletion of electron acceptors of Onondaga Lake, were examined: high oxygen – high nitrate, low oxygen plus nitrate and no oxygen – no nitrate. Additionally, treatments with oxygen alone and nitrate alone were evaluated to consider the separate effects of the electron acceptors. The desired oxygen concentrations for the gas feed were obtained through simple penetration of the Teflon tubing by ambient air (low levels, 0.3-0.8 $mgO_2 \cdot L^{-1}$) or through use of a gas blender (high levels, 2.0-11.8 $mgO_2 \cdot L^{-1}$). For experiments requiring anaerobic conditions, the mixed gas supply for the anaerobic chamber was passed through the microcosm. Nitrate levels were maintained by setting the nitrate concentration of the feed stock and then adjusting the feed stock flow rate until the desired nitrate concentration was achieved.

2.3.4.2 Microcosm Monitoring and Analysis

The theory of microcosm operation establishes that chemical flux may be calculated once the system has reached steady state, i.e., chemical conditions in the effluent stream are unchanged with respect to time. Analytical logistics prohibit real-time monitoring of methylmercury as a means of verifying establishment of that steady state. Instead, the feed stock flow (Figure 2.3; measured by direct collection) and gas feed are adjusted until the desired electron acceptor level is achieved in the microcosm. Effluent concentrations of oxygen (Figure 2.3; Hach Model LBOD 10101 luminescent dissolved oxygen probe) and nitrate (Figure 2.3; Thermo Fisher Scientific Inc., Model 9707BNWP Ionplus® Nitrate Combination Electrode) are measured (or calculated from feed stock concentration and sediment demand). Once effluent monitoring of electron acceptor levels indicates a steady state condition (typically achieved in one week, but occasionally as long as three weeks), samples for mercury analysis were collected for a period of several days; flow and electron acceptor levels continue to be monitored over this interval (Figure 2.3). Additional samples were collected on an occasional basis for phosphorus, ammonia and sulfide analysis. Samples for mercury analysis were filtered (0.45 μm disc filter, Vipor Inc.), placed in 500 mL Teflon bottles with 2 mL of hydrochloric acid (34-37% HCl) and stored in double-sealed polyethylene bags in a temperature-controlled room at 8°C. Details of the analytical techniques employed are summarized in Table 2.4.

2.3.4.3 Flux Calculations

Methylmercury flux is calculated by assuming that the sediment microcosm is a completely-mixed flow reactor. The mass balance on that reactor may be given as,

$$V \cdot \frac{dC}{dt} = Q \cdot C_{in} - Q \cdot C + J_{MeHg} \cdot A \quad (1)$$

where: V = microcosm volume, m^3

Q = feed stock flow rate, $m^3 \cdot d^{-1}$

C = microcosm mercury or methylmercury concentration, $ng \cdot m^{-3}$

C_{in} = influent mercury or methylmercury concentration, $ng \cdot m^{-3}$

$J_{Methyl\ mercury}$ = mercury or methylmercury flux, $ng \cdot m^{-2} \cdot d^{-1}$

A = area of the sediment surface, m^2

Given that the influent mercury and methylmercury concentrations are zero and that, at steady-state dC/dt = 0, Equation 1 becomes,

$$J_{MeHg} = QC / A \quad (2)$$

Thus for any set of electron acceptor conditions, the total and methylmercury flux may be calculated as a function of the flow, the effluent mercury concentration and the sediment surface area of the reactor.

2.4 RESULTS AND DISCUSSION

2.4.1 Electron Acceptor Distribution and its Relation to the Amendment Process

The conceptual basis for the electron acceptor amendment technology lies in the maintenance of an environment near the sediment surface where methylmercury produced at depth (zone of sulfate reduction) may be sorbed or demethylated as it diffuses toward the sediment-water interface. It is proposed that this environment is characterized by a zone in which aerobic respiration occurs (oxygen is present) overlays a zone in which denitrification is active (nitrate is present). Implementation of electron acceptor amendment seeks to sustain this environment by preventing depletion of oxygen and/or nitrate in the overlying waters. While this conceptual model is consistent with observed behaviors of electron acceptors, reduced species end products and methylmercury in the water column, the downcore distributions of these analytes have not been quantified for Onondaga Lake and thus the model remains conceptual. The utility of the conceptual model and opportunities to conduct prognostive explorations of the impact of changes in electron acceptor and donor availability require that these distributions be quantified.

To this end, a series of porewater profiles were developed for methylmercury, two electron acceptors (oxygen and nitrate) and one reduced species end product (sulfide). Methylmercury was determined by wet chemistry on sliced and processed sediment while the other analytes were

measured on intact cores using microprobe instrumentation. Porewater profiles of redox species are highly dynamic and thus there are only two alternative methods of measurement: *in situ* by deployment of submersible instrumentation and in the laboratory by manipulating conditions in the water overlying the sediment to mimic the desired environment. The latter approach was adopted here for its adaptability to studies of the effect of changes in water column concentrations of electron acceptors on porewater profiles. The nature of microprofiling is such that some analytes (e.g. pH and sulfide) can be measured on intact cores and be representative of ambient conditions, while others (oxygen and nitrate) could not be measured for ambient conditions, except through *in situ* deployment of microprofilers. The profiles presented here were developed at different times and are thus a compilation of 'ambient' profiles for pH and sulfide and profiles for oxygen and nitrate where conditions at the sediment-water interface were controlled to match the ambient environment. The composite profiles portray conditions during the sequential depletion of oxygen and nitrate from the water column and the sediment.

2.4.1.1 Oxygen Profile

As the first electron acceptor option in the ecological redox series, oxygen is the first to be depleted with depth in the sediment. In Onondaga Lake sediment, oxygen penetrates to a depth of ~1.5 mm with an interfacial oxygen concentration of 8.2 $mgO_2 \cdot L^{-1}$ (Figure 2.4, upper panel). Variation in the depth of oxygen penetration as a function of the oxygen concentration in the overlying water is also illustrated in Figure 2.4 (lower panel), with conditions ranging from near stratification to near depletion. The limited penetration of oxygen into the sediments of Onondaga Lake reflects the abundance of labile organic carbon there. By comparison, oxygen penetrates to depths of 4 mm in the eutrophic waters of Green Bay (Lake Michigan) and as deep as 200 mm in the oligotrophic waters of Lake Superior (Klump et al. 1989).

2.4.1.2 Nitrate Profile

Nitrate is the second electron acceptor in the ecological redox series. A paired nitrate profile (Figure 2.4, upper panel) is presented here to complement the oxygen profile introduced previously. In this profile, nitrate penetrates the sediment to a depth of ~3 mm for a nitrate concentration in the overlying water of 1.9 $mgN \cdot L^{-1}$. Additional nitrate profiles are presented in Figure 2.4 (lower panel), illustrating the variation in nitrate penetration with changes in the nitrate concentration of the overlying water. These results are consistent with observations made by Jensen et al. (1994) for eutrophic Lake Vilhelmsborg, Denmark both with respect to the relationship to the oxygen profile and the maximum depth of penetration of nitrate. It is noteworthy that the maximum total thickness of the combined oxygen and nitrate layers, hypothesized to control methylmercury release from Onondaga Lake sediments is on the order of 3-4 mm, essentially coincident in location with the thickness of fresh sediment deposited annually.

2.4.1.3 Total Sulfide Profile

Profiles of total sulfide reflect the activity of sulfate reduction, the process known to co-occur with mercury methylation. Sulfide produced through sulfate reduction is oxidized as it migrates toward the sediment-water interface when oxygen and/or nitrate are present in the surface sediments. Thus, like oxygen and nitrate, the shape and position of sulfide profiles would be expected to vary seasonally with the electron acceptor resources of the hypolimnion. In

Onondaga Lake sediments, with oxic conditions present at the sediment-water interface, sulfide is absent from the profile above a depth of ~ 0.6 cm (Figure 2.5a). The peak in sulfide (assumed peak in sulfate reduction) occurs at a depth of ~2.5 cm, the approximate point where sulfate is depleted (Figure 2.5a). Above and below this peak, sulfide levels are attenuated through diffusion and/or reaction. With anoxic conditions at the sediment-water interface, no sulfide is lost to oxidation (by oxygen and nitrate) and the profile 'stands up' permitting diffusion of the reduced species end product into the water column (Figure 2.5b). The transition between these two conditions corresponds to the depletion of oxygen and nitrate from the hypolimnion and the attendant accumulation of sulfide in the water column. An overlay of the oxic and anoxic profiles (Figure 2.5c) further illustrates this transition.

2.4.1.4 Methylmercury Profile

Based on the demonstrated association of methylmercury with sulfate reduction, one would expect the peak in the methylmercury profile to co-occur with the peak in the sulfide profile. This is, in fact, the case (Figure 2.6). The methylmercury profile (based on an average of triplicate samples) tracks the total sulfide profile except that it is not attenuated as rapidly as it moves toward the surface. This may be due to the absence of kinetic sinks operative on sulfide that do not impact methylmercury. It would be anticipated that, with anoxic conditions at the sediment-water interface, the methylmercury profile would 'stand up' in a manner similar to that for sulfide leading to a flux of methylmercury from the sediments.

2.4.1.5 Porewater Profile Summary

The development of porewater profiles for oxygen, nitrate, sulfide and methylmercury support the theoretical construct of a sequential downcore distribution of electron acceptors and reduced species end-products consistent with operation of the ecological redox series. Downcore depletion of electron acceptors follows the pattern oxygen → nitrate → sulfate. It would be anticipated that Fe and Mn reduction would occur between the denitrification and sulfate reduction bands. These electron acceptors are often disregarded in the Onondaga Lake system due to their low concentrations. Below the zone of sulfate reduction, methanogenesis would be the operative process for organic carbon diagenesis.

The profiles for methylmercury and total sulfide support the hypothesis of co-occurring production within the layer of sulfate reduction. The distributions of oxygen and nitrate are consistent with our operating hypothesis that as sulfide and methylmercury approach the sediment-water interface, they are acted upon by sink terms, oxidation in the case of sulfide and demethylation and adsorption in the case of methylmercury. Differences in the magnitude of the various sink terms result in the lack of a relationship between sulfide and methylmercury with the approach to the sediment-water interface. These observations provide an observational basis and support a theoretical foundation not only for the methylmercury flux inhibition studies that follow, but also for considering short- and long-term changes in methylmercury dynamics.

2.4.2 Electron Acceptor Amendment and Methylmercury Flux

As outlined in Table 2.3 above, three electron acceptor treatments were applied, roughly corresponding to the intervals observed in the sequential depletion of oxygen and nitrate from the hypolimnion and the sediment (Figure 2.7): high oxygen - high nitrate, low oxygen plus nitrate and no oxygen – no nitrate. Fundamental to this series of experiments is the determination of a

baseline flux representing conditions following the depletion of oxygen and nitrate from the hypolimnion. Two additional treatments, addition of oxygen alone and addition of nitrate alone, were applied to compare the efficacy of oxygen addition with nitrate addition (see Auer et al., 2010).

2.4.2.1 Baseline Flux

The baseline flux, i.e. that corresponding to the period when oxygen and nitrate have been depleted from the sediment, forms the basis for evaluating the efficacy of electron acceptor amendment. Because of the significance of this estimate to the study, a 'multiple lines of evidence' approach was followed, incorporating: (1) fluxes based on measured methylmercury hypolimnetic accumulation rates, (2) fluxes based on methylmercury porewater profiles and (3) fluxes based on sediment microcosm measurements.

The application of hypolimnetic accumulation rates in estimating chemical flux across the sediment-water interface has been successfully demonstrated for a host of analytes in Onondaga Lake (oxygen, nitrate, sulfate, methane; Matthews et al. 2008). Here, we calculated a baseline methylmercury flux as being equivalent to the areal rate of methylmercury accumulation in the hypolimnion in 2007 and 2008. The calculations are based on volume-weighted methylmercury concentrations measured at 1 m increments over the depth range 10-19 m from the first incidence of accumulation until turnover (Upstate Freshwater Institute, unpublished). The methylmercury fluxes, so determined, were 180 and 128 $ng \cdot m^{-2} \cdot d^{-1}$ for 2007 and 2008, respectively.

Calculations based on porewater concentration gradients may be used to estimate fluxes across the sediment-water interface (Lavery et al. 2001). The approach is based on Fick's First Law,

$$J = -D \cdot \frac{\partial C}{\partial z} \qquad [3]$$

where, for methylmercury :

J = methylmercury flux, ng methylmercury $\cdot m^{-2} \cdot d^{-1}$

D = diffusion coefficient, $m^2 \cdot d^{-1}$

C = methylmercury concentration, $ng \cdot m^{-3}$

z = depth in sediment, m

The value for the diffusion coefficient (1.5×10^{-5} $cm^2 \cdot s^{-1}$) was determined for Onondaga Lake sediments using chemically-conservative tracers. The concentration gradient in Equation 3 was calculated from methylmercury porewater concentrations made on cores collected in November 2008 (oxic conditions), assuming a concentration of zero at the sediment-water interface (Upstate Freshwater Institute, unpublished). Values for the diffusion coefficient, the concentration gradient and the resultant methylmercury flux are detailed in Table 2.5. The average methylmercury flux, based on porewater methylmercury gradients, was 112 ± 24 $ng \cdot m^{2} \cdot d^{-1}$.

A baseline methylmercury flux was also determined using the sediment microcosm approach described above. Triplicate microcosms, receiving a no oxygen – no nitrate feed, were

operated for 36 days in an anaerobic chamber with samples collected and fluxes calculated at 5-day intervals. Unlike the plus oxygen and plus nitrate incubations described subsequently, no definitive steady state was achieved. Instead, pulses in methylmercury concentration were observed at intervals over the course of the incubation (Figure 2.8). We believe that this non-steady state or pulse response reflects an inability to consistently maintain anoxia. We have therefore calculated the baseline flux (135 $ng \cdot m^{-2} \cdot d^{-1}$) as the mean of those fluxes associated with pulses in methylmercury concentration. An ability to consistently maintain anoxia in microcosm measurements has been subsequently demonstrated using an anoxic chamber.

A summary of the multiple line of evidence analysis of baseline methylmercury flux is presented in Figure 2.9. The three flux estimates, hypolimnetic accumulation, porewater gradient calculation and microcosm measurement do not differ significantly from one another ($p < 0.05$). Given the comparable nature of the results, the baseline flux determined through microcosm measurement (135 $ng \cdot m^{-2} \cdot d^{-1}$) is carried forward as it is based on the same experimental protocols as the electron acceptor amendment determinations.

2.4.2.2 Fluxes Associated with Sequential Electron Acceptor Depletion

The three periods of sequential electron acceptor depletion, corresponding to conditions regularly experienced in the hypolimnion, are: high oxygen – high nitrate, low oxygen plus nitrate and no oxygen – no nitrate (the baseline condition developed above). A single experiment was conducted for the high oxygen – high nitrate treatment, with steady state oxygen and nitrate concentrations of 11.8 $mgO_2 \cdot L^{-1}$ and 8.5 $mgN \cdot L^{-1}$. The objective here was to determine the minimum achievable flux, i.e. that corresponding to an excess of electron acceptor resources. The resulting flux, 3.8 $ng \cdot m^{-2} \cdot d^{-1}$, was the lowest amongst the 32 microcosm experiments conducted and essentially equivalent to that obtained through observations of methylmercury hypolimnetic accumulation for the interval when oxygen and nitrate resources are abundant.

Conditions for the low oxygen plus nitrate treatment seek to represent the interval over which oxygen resources become depleted and nitrate resources are then depleted over time. For these eight experiments, the oxygen concentration averaged 0.57±0.04 $mgO_2 \cdot L^{-1}$ and the nitrate concentration ranged from 0.4 – 10.5 $mgN \cdot L^{-1}$. Fluxes varied somewhat over the range of nitrate concentrations tested here (mean, 30.2±6.4 $ng \cdot m^{-2} \cdot d^{-1}$) and, although there was a tendency toward lower fluxes with increasing nitrate levels, the relationship was not strong ($r^2 < 0.2$). Variability would be expected for a treatment such as this where conditions bracket the border between oxygen/nitrate control and simple nitrate control of methylmercury flux. Average fluxes for the high oxygen – high nitrate and low oxygen plus nitrate treatments are compared with the baseline (no oxygen – no nitrate) treatment in Figure 2.10. The resulting reductions in methylmercury flux were 97 and 79 percent for the high oxygen – high nitrate and low oxygen plus nitrate treatments, respectively. Differences between fluxes were significant ($p < 0.05$) for all treatments.

2.4.2.3 Oxygen and Nitrate Amendment

Oxygen and nitrate are utilized concurrently in the sediments of Onondaga Lake and are depleted concurrently within the water column. As a result of the rates and stoichiometry of the reactions and their respective initial conditions, oxygen is exhausted from the hypolimnion several weeks before nitrate.

Amendment with oxygen would likely be initiated when oxygen levels reached some pre-determined level (e.g. 2 $mgO_2 \cdot L^{-1}$), maintaining oxygen concentrations at that level until turnover (while nitrate continues to be depleted and is eventually exhausted). This is the situation corresponding to the oxygen amendment described here. Ten experiments were conducted with zero nitrate and oxygen concentrations ranging from 0.2 – 12.2 $mgO_2 \cdot L^{-1}$. The average flux with oxygen amendment was 11.9±1.5 $ng \cdot m^{-2} \cdot d^{-1}$, a 92% reduction from the baseline (no oxygen – no nitrate) condition. There was no trend in flux with increasing oxygen levels, suggesting that the simple maintenance of an aerobic environment is sufficient to control methylmercury flux.

Amendment with nitrate would be similarly initiated when nitrate levels reached some pre-determined level (e.g. 0.5 or 1 $mgN \cdot L^{-1}$), maintaining nitrate concentrations at that level until the fall when deeper waters turn over and mix with upper waters. This is the situation corresponding to the nitrate amendment described here. Two experiments were conducted with zero oxygen and nitrate concentrations of 0.3 and 1.0 $mgN \cdot L^{-1}$. The average flux with nitrate amendment was 49.6±3.0 $ng \cdot m^{-2} \cdot d^{-1}$, a 65% reduction from the baseline (no oxygen – no nitrate) condition. As with the case for oxygen amendment, there is no apparent benefit from the maintenance of increasing nitrate concentrations. Average fluxes for the oxygen amendment and nitrate amendment are compared with the baseline (no oxygen – no nitrate) in Figure 2.11. Differences between fluxes were significant ($p < 0.05$) for all amendments.

There have been several changes since 2005 associated with organic carbon and the availability of alternate electron acceptors. First, less particulate organic carbon is reaching the sediments of Onondaga Lake today than in recent years. The average organic carbon content of the top 2.5 cm of sediment (~ corresponding to the past 5 years of deposition) is approximately 25 percent less than that of the next two lower 2.5 cm increments (Figure 2.12). This is a conservative portrayal of deposition conditions because the sediment at depth will have lost comparatively more organic carbon to diagenesis since deposition. Thus, it appears that the amount of carbon available to drive sulfate reduction has been significantly reduced in the past 5 years.

Second, the relative contributions of the various electron acceptors to carbon metabolism have changed over this period. Increases in nitrate resources in the hypolimnion of Onondaga Lake resulting from the implementation of enhanced nitrification at the Syracuse Metropolitan Wastewater Treatment Plant have markedly increased the role of denitrification in organic carbon diagenesis in the sediment (Figure 2.13). Because more nitrate is available to the sediments and because freshly deposited sediment lies resident almost entirely within the region where aerobic respiration and denitrification dominate, it is likely that less labile organic carbon is delivered to the site of sulfate reduction. Consequently, with the sulfate reduction engine scaled back, rates of mercury methylation, porewater methylmercury concentrations, and methylmercury fluxes are all lower (as observed in the lake since 2005).

The interplay of changes in organic carbon deposition and electron acceptor availability, together with potential reductions in mercury inputs, bode well for Onondaga Lake sediments. Changes in redox dynamics in the sediment additionally favor the maintenance of oxygen and nitrate in the hypolimnion, offering the potential to place less demand on external sources of electron acceptors.

2.5 REFERENCES FOR SECTION 2

Auer M.T.; Galicinoo, G.A.; Matthews, D.A.; Driscoll, C.T.; Chapra, S.C.; Effler, S.W.; and S.G. Todorova. 2010. Response of Sediment Methylmercury Flux to Nitrate and Oxygen amendment as determined through Microcosm Incubations. Draft manuscript for submission to Water Research.

Berg P, Rysgaard S, Thamdrup B. 2003. Dynamic Modeling of Early Diagenesis and Nutrient Cycling. A case study in an arctic marine sediment. Am J Sci 303:905–955.

Boudreau, B. P. 1996. Diffusive Tortuosity of Fine-Grained Unlithified Sediments. Geochim. Cosmochim. Acta 60: 3139–3142.

Compeau, G.C. and R. Bartha. 1985. Sulfate-Reducing Bacteria: Principal Methylators of Mercury in Anoxic Estuarine Sediment. Appl Environ Microbiol. 50(2): 498-502.

Effler S.W. 1996. Limnological and Engineering Analysis of a Polluted Urban Lake. Prelude to Environmental Management of Onondaga Lake, New York. Springer-Verlag.

Gagnon C., Pelletier, E., Mucci, A. and W. F. Fitzgerald. 1996. Diagenetic Behavior of Methylmercury in Organic-Rich Coastal Sediments. Limnology and Oceanography, 41: 428-434.

Gilmour C.C., Henry E.A., Mitchell R. 1992. Sulfate stimulation of mercury methylation in freshwater sediments. Environ Sci Technol. 26:2281-2287.

Jensen K, Sloth NP, Risgaard Petersen N, Rysgaard S, Revsbech NP (1994) Estimation of Nitrification and Denitrification from Microprofiles of Oxygen and Nitrate in Model Sediment Systems. Appl Environ Microbiol 60:2094–2100.

Klump, J.V., Paddock, R., Remsen, C.C., Fitzgerald, S., Boraas, M. and P. Anderson. 1989. Variations in Sediment Accumulation Rates and the Flux of Labile Organic Matter in Eastern Lake Superior Basins. Journal of Great Lakes Research, 15: 104-122.

Lavery, P.S., Oldham, C.E. and M. Ghisalberti. 2001. The Use of Fick's First Law for Predicting Porewater Nutrient Fluxes Under Diffusive Conditions. Hydrological Processes, 15: 2435-2451.

Mason, R.P., J.R. Reinfelder, and F.M.M.Morel. 1995. Bioaccumulation of Mercury and Methylmercury. *Water Air & Soil Pollution*, 80: 915-921.

Matthews, D.A., Effler, S.W., Driscoll, C.T., O'Donnell, S.M. and C.M. Matthews. 2008. Electron Budgets for the Hypolimnion of a Recovering Urban Lake, 1989–2004: Response to Changes in Organic Carbon Deposition and Availability of Electron Acceptors. Limnology and Oceanography, 53: 743-759.

Oremland, R.S., Culbertson, C.W. and M.R. Winfrey. 1991. Methylmercury Decomposition in Sediments and Bacterial Cultures: Involvement of Methanogens and Sulfate Reducers in Oxidative Demethylation. Applied and Environmental Microbiology, 57: 130-137.

Table 2.1. The Ecological Redox Series (stoichiometry after Berg et al. 2003 and Boudreau 1996).

Oxygen Reduction

$$CH_2O + O_2 \rightarrow CO_2 + H_2O$$

Nitrate Reduction

$$5CH_2O + 4NO_3^- + 4H^+ \rightarrow 5CO_2 + 2N_2 + 7H_2O$$

Manganese Oxide Reduction

$$CH_2O + 2MnO_2 + 4H^+ \rightarrow CO_2 + 2Mn^{2+} + 3H_2O$$

Iron Oxy-Hydroxide Reduction

$$CH_2O + 4FeOOH + 8H^+ \rightarrow CO_2 + 4Fe^{2+} + 7H_2O$$

Sulfate Reduction

$$2CH_2O + SO_4^{2-} + 2H^+ \rightarrow 2CO_2 + H_2S + 2H_2O$$

Methanogenesis

$$2CH_2O \rightarrow CH_4 + CO_2$$

Table 2.2. Composition of artificial lake water, mimicking the ionic composition of Onondaga Lake for sediment microcosm applications.

Salt	Final Concentration (mM)	Final Concentration ($mg \cdot L^{-1}$)
$CaCl_2 \cdot 2H_2O$	5.84	858.83
$NaHCO_3$	4.24	356.2
Na_2SO_4	1.67	237.21
$MgCl_2 \cdot 6H_2O$	0.99	200.87
KCl	0.44	32.43
NaCl	3.21	187.45
NaF	0.02	1.01

Anions	($meq \cdot L^{-1}$)	(mM)	($mg \cdot L^{-1}$)
Cl^-	17.303	17.303	611.54
HCO_3^-	4.241	4.241	258.64
F^-	3.340	1.670	160.42
$SO_4^=$	0.024	0.024	0.46
Total	24.908		

Cations	($meq \cdot L^{-1}$)	(mM)	($mg \cdot L^{-1}$)
Ca^{++}	11.684	5.842	234.14
K^+	0.435	0.435	17.01
Mg^{++}	1.977	0.988	24.03
Na^+	10.812	10.812	248.57
Total	24.908		

Table 2.3. Microcosm evaluation of electron acceptor augmentation as a means of inhibiting methylmercury flux from the sediments.

a) Experimental Design

Incubation Type *Tracking hypolimnetic conditions*	**Representing Conditions**
1. High oxygen – High nitrate	early in the stratified period when oxygen and nitrate resources are replete
2. Low oxygen – Plus nitrate	when oxygen is becoming depleted from the hypolimnion but nitrate remains
3. No oxygen – No nitrate	when oxygen and nitrate have become depleted from the hypolimnion
Incubation Type *Evaluating electron acceptor response*	**Representing Conditions**
4. Oxygen Added	where oxygen is maintained in the hypolimnion, but nitrate becomes depleted
5. Nitrate Added	where nitrate is maintained in the hypolimnion, but oxygen becomes depleted

b) Box Core Collection and Application

Date of Core Collection	# of Cores Collected	Incubation Number(s)*	Incubation Type(s)**,***	Antecedent Conditions	
				Oxygen ($mgO_2 \cdot L^{-1}$)	Nitrate ($mgN \cdot L^{-1}$)
Nov 2007	8	1, 2, 3	1(1),2(4), 4(3)	0.3 – 8.7	0.1 – 1.8
May 2008	7	4, 5	2(2), 4(5)	5.3 – 8.9	1.8 – 1.9
Jun 2008	7	6, 7	2(4), 3(1), 4(2)	0.2 – 4.8	1.1 - 1.8
Jul 2008	2	8	3(2)	0.1 - 0.3	0.4 – 1.2
Aug 2008	8	9, 10	3(5), 4(1), 5(2)	0.1 - 0.3	0.1 – 0.8

* as detailed in the data file submitted to NYS DEC; ** number of replicates in parens; *** as defined in Table 2.3a above

Table 2.4. Analytical methods supporting porewater analysis and sediment flux measurements.

Analyte	Analytical Method Description	Reference
Nitrate[1,3]	A filtered sample enters through a column containing copper-cadmium to convert nitrate to nitrite. The nitrite is determined by diazotizing with sulfanilamide and coupling with N-(1-naphyl)-ethylenediamine dihydrochloride to form a highly colored azo dye which is measured colorimetrically.	U.S. EPA Method 353.2
Sulfide[1]	Excess iodine is added to a sample that has zinc acetate added to it to form zinc sulfide. The iodine oxidizes the sulfide to sulfate under acidic conditions. The excess iodine is then back titrated with sodium thiosulfate.	Hydrogen Sulfide > 1.0 mg/L SM 20th ed 4500 S 2- F
Phosphorus[1]	Ammonium molybdate and potassium antimonyl tartrate react in an acid medium with orthophosphate to produce a heteropoly acid (phosphomolybdic acid) that is reduced to an intensely colored molybdenum blue by ascorbic acid. Analysis for soluble reactive phosphorus is done with the aid of Genesys 2 Spectrophotometer	Soluble Reactive Phosphorus Standard Methods 20th Edition (Method 4500-PE)
Ammonia[1]	Alkaline phenol and hypochlorite react with ammonia sample to form indophenol blue that is proportional to the ammonia concentration present in the sample. Ammonia (TNH_3) analysis is done using an expanded range (ER) photometric detector	U.S. EPA method 350.1
Methyl mercury[2]	Methyl Mercury in Water by Distillation, Aqueous Ethylation, Purge and Trap, and CVAFS Draft	EPA Method 1630
Total mercury[2]	Mercury in Water by Oxidation, Purge and Trap, and Cold Vapor Atomic Fluorescence Spectrometry	Method 1631 Revision E
Oxygen[3]	Dissolved Oxygen Measurement	Hach Electrode

[1] Upstate Freshwater Institute

[2] Department of Civil & Environmental Engineering, Syracuse University

[3] Michigan Technological University

Table 2.5. Determination of methylmercury flux using porewater concentrations.

Core	MeHg @ (0.25 cm) ($ng \cdot L^{-1}$)	$\partial c/\partial z$ ($10^3 ng \cdot m^{-3} \cdot m^{-1}$)	J (D^1) ($ng \cdot m^{-2} \cdot d^{-1}$)
A	3.1	1240	107
B	1.8	720	62
C	1.6	640	55
		Mean ± S.E.	75±16

Figure 2.1. The Ecological Redox Series as manifested in lake sediments, illustrating changes in the distribution of contributing processes as electron acceptors are depleted from the hypolimnion. Mercury methylation is localized within the zone of sulfate reduction. This illustration is tailored to conditions in Onondaga Lake where the roles of manganese and iron are thought to be minor and where a natural abundance of sulfate sustains sulfate reduction through the thermally stratified interval.

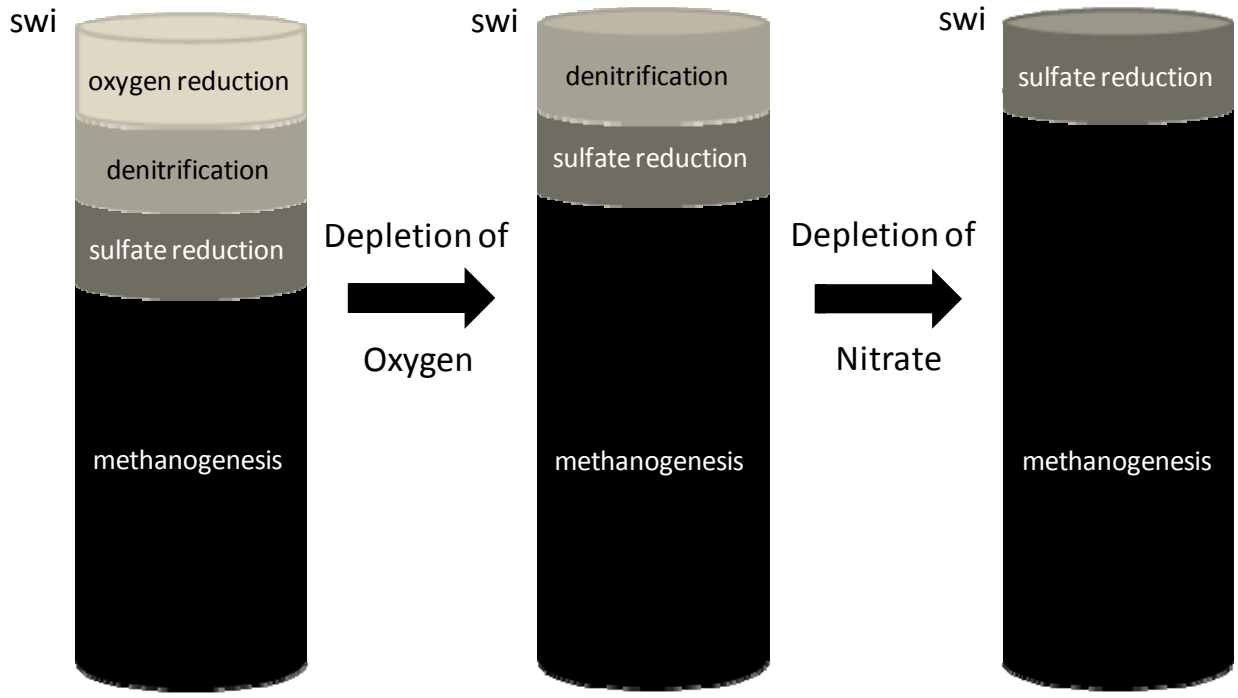

Figure 2.2. Schematic drawing (left) and photograph (right) of the sediment microcosm used to measure methylmercury flux under controlled conditions of mixing and electron acceptor concentration. Only two of six mixing jets are included in the schematic drawing.

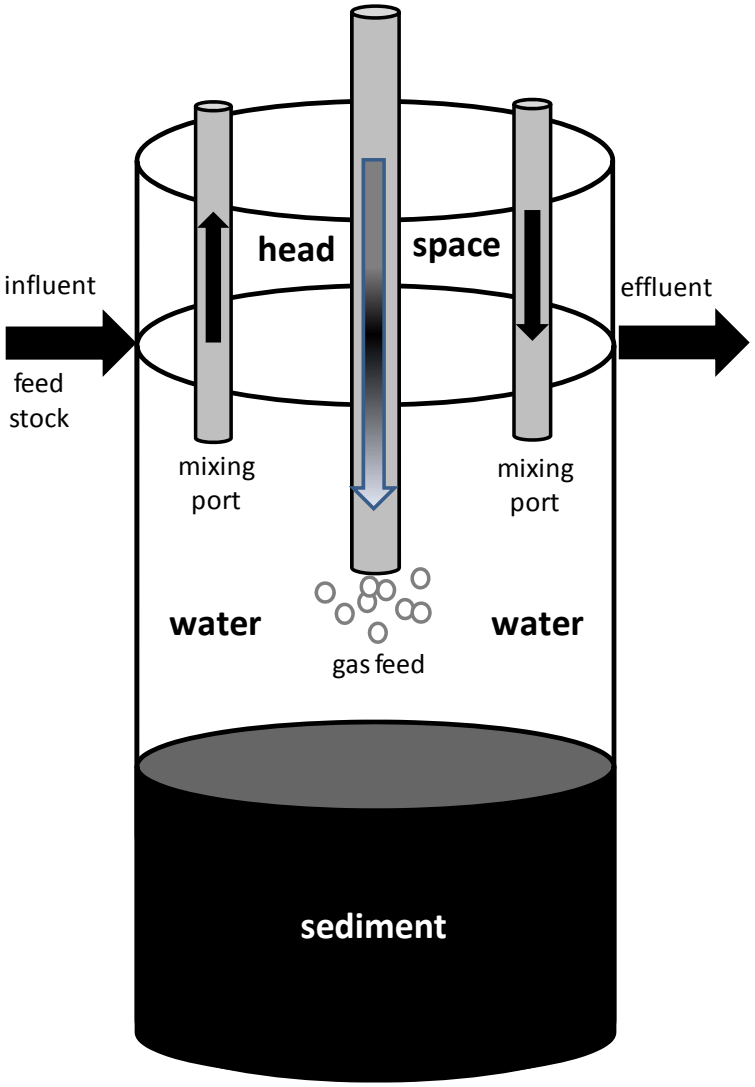

Figure 2.3. Establishment of steady state conditions in the sediment microcosm. The system was operated at a constant flow. Effluent electron acceptor concentration reached a steady state. Results below for flow and methylmercury are paired data from a single experiment. Performance at several different concentration levels is illustrated for effluent electron acceptor concentrations with labels referring to nominal concentration.

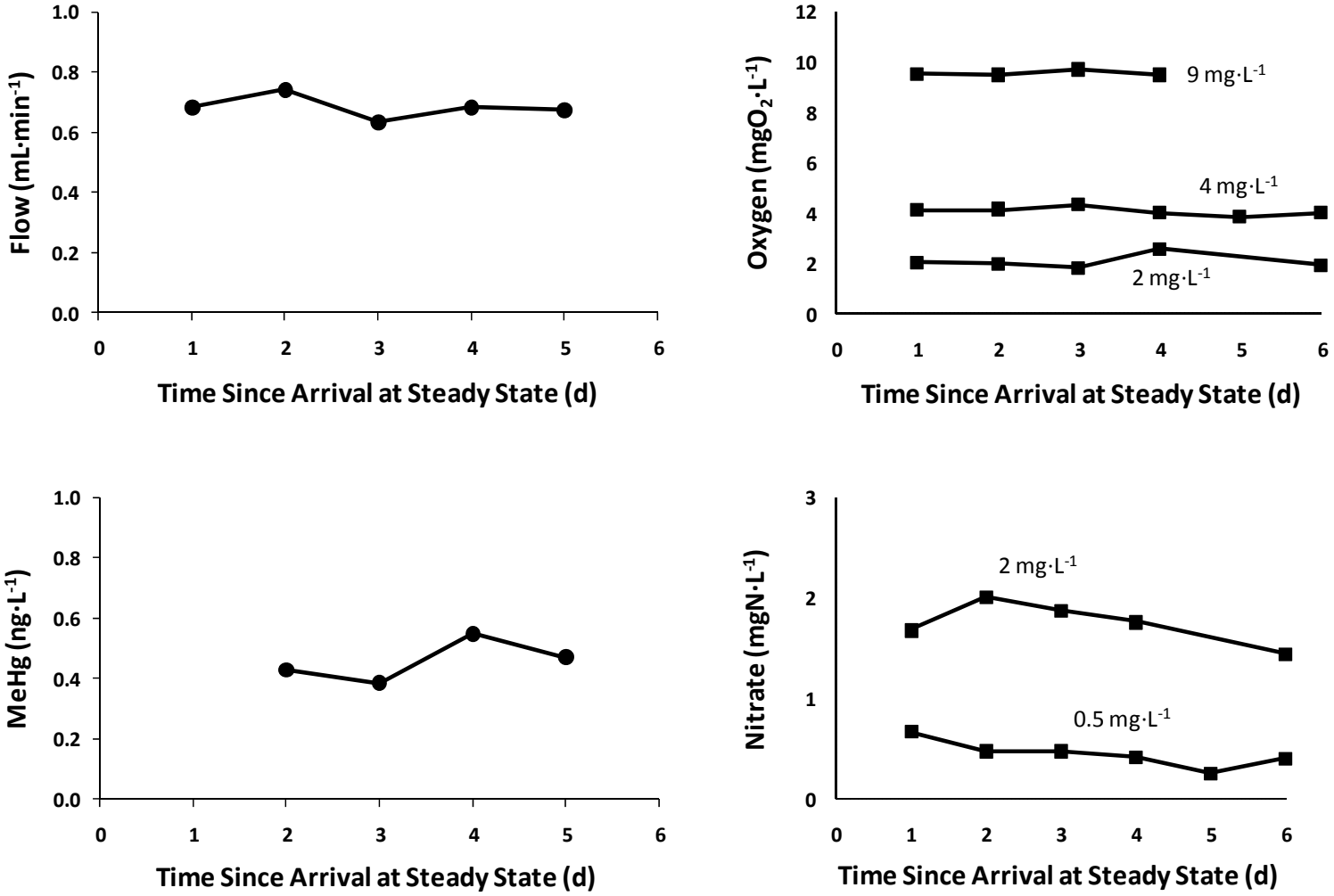

Figures 2.4. Paired (upper panels) and nested (lower panels) porewater profiles for oxygen and nitrate.

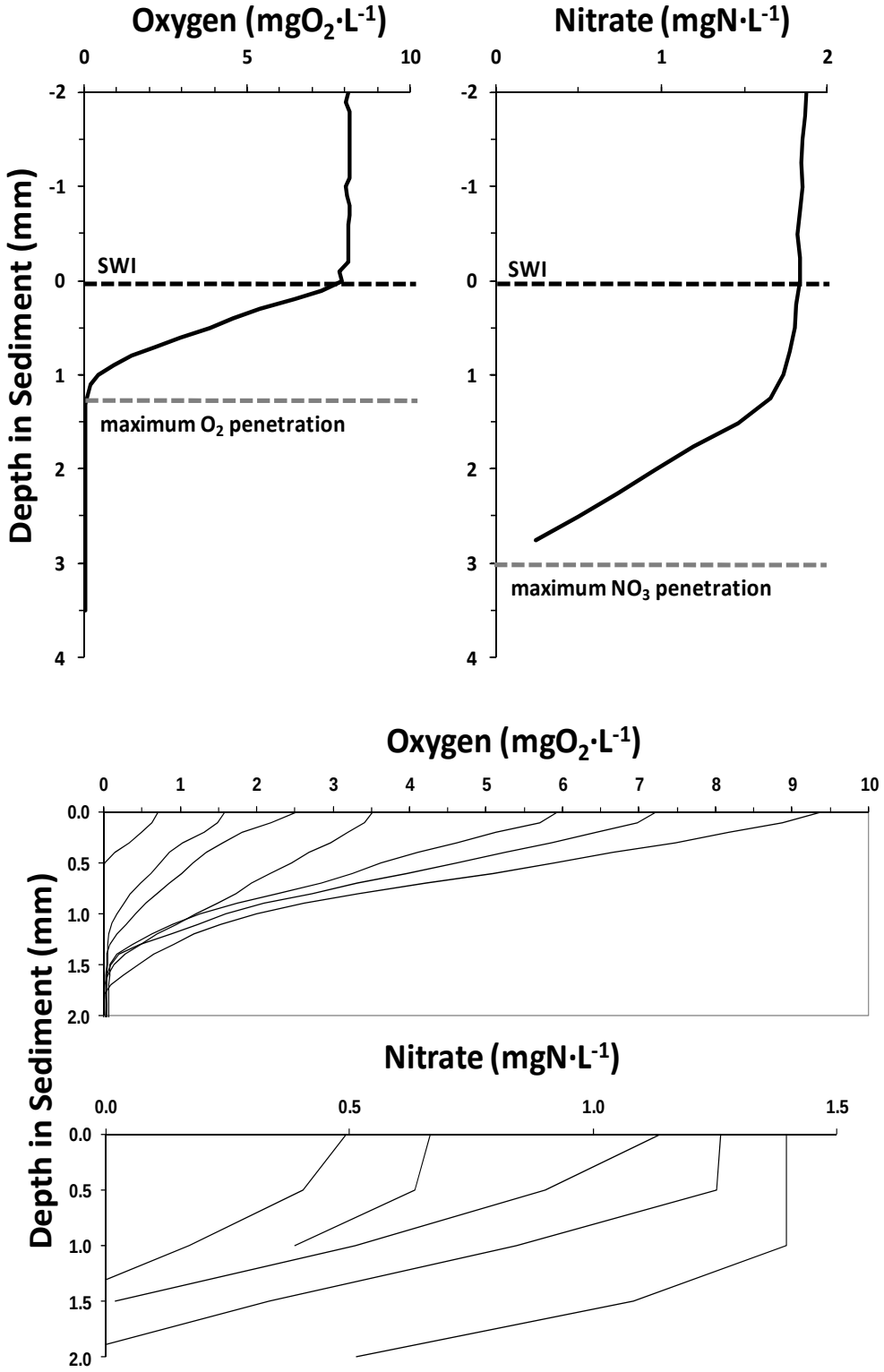

Figure 2.5. Downcore sediment porewater profiles: (a) sulfate, gray line with symbols, and sulfide, black line, with an oxic sediment-water interface, (b) sulfide with an anoxic sediment-water interface, (c) overlay of sulfide with oxic and anoxic interfaces.

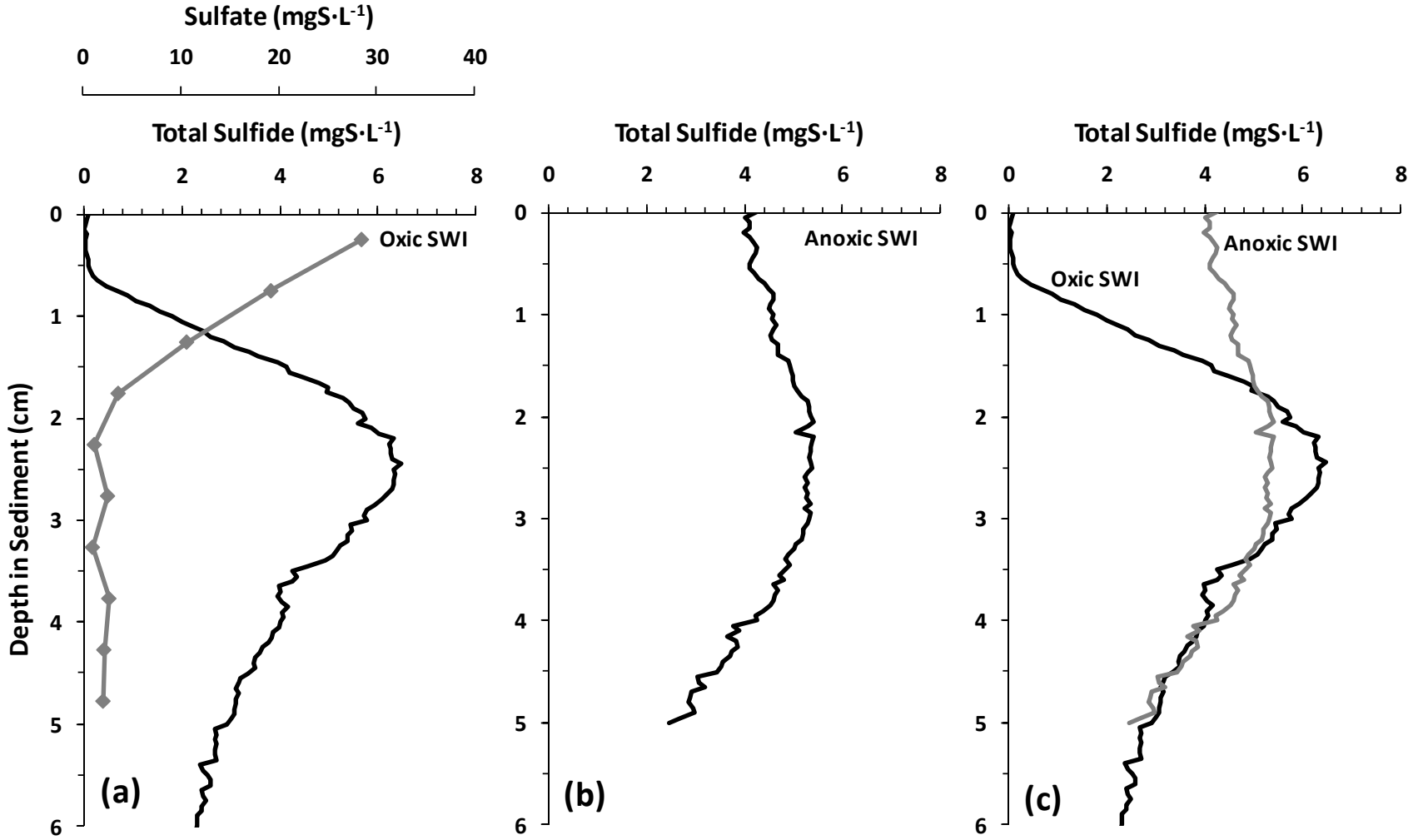

Figure 2.6. Composite illustration of porewater profiles for oxygen, nitrate, total sulfide and methylmercury with an oxic sediment-water interface.

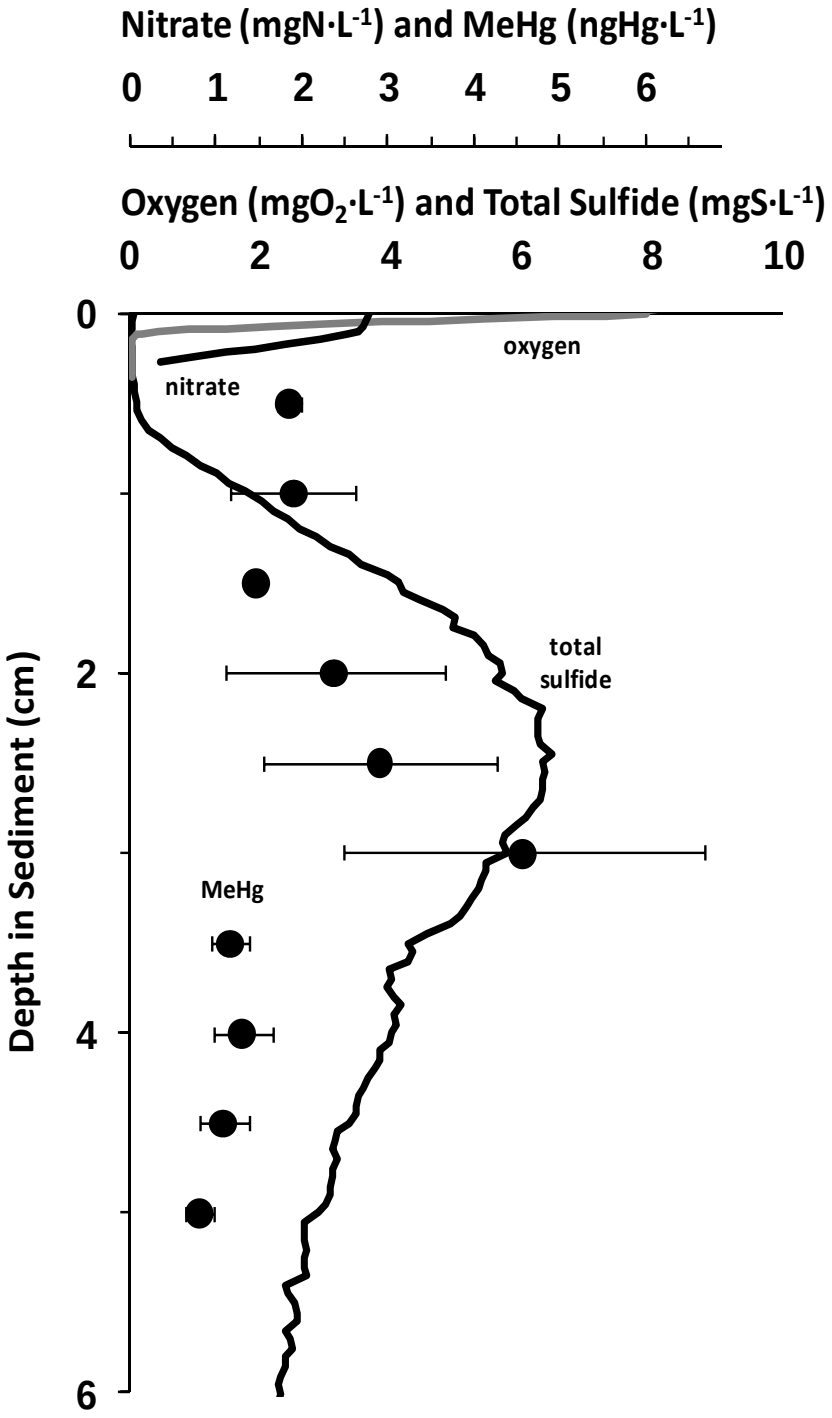

Figure 2.7. Time course of depletion of oxygen and nitrate (both 16-18 m average) and the release of methylmercury (12-19 m average) in the hypolimnion of Onondaga Lake as measured at the South Deep Station.

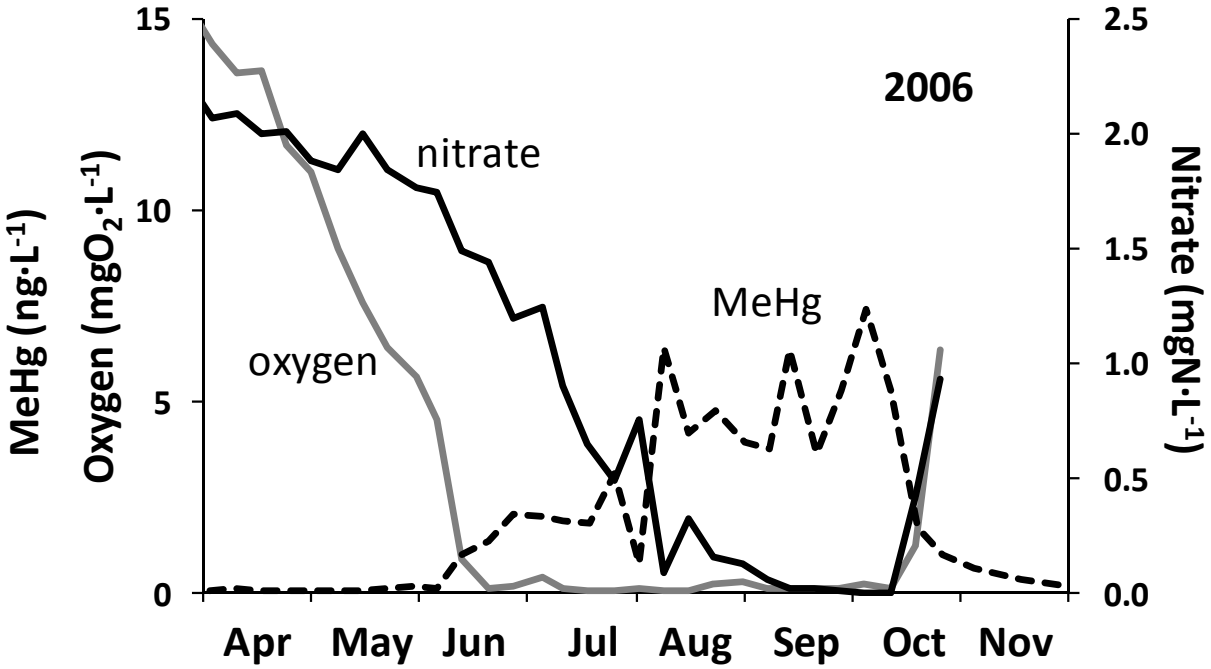

Figure 2.8. Comparison of methylmercury concentrations in the effluent of (a) a 'plus oxygen' incubation and (b) triplicate 'no oxygen – no nitrate' incubations. It is estimated that steady state was achieved in the time necessary to flush the reactor three times, i.e. ~ 1d.

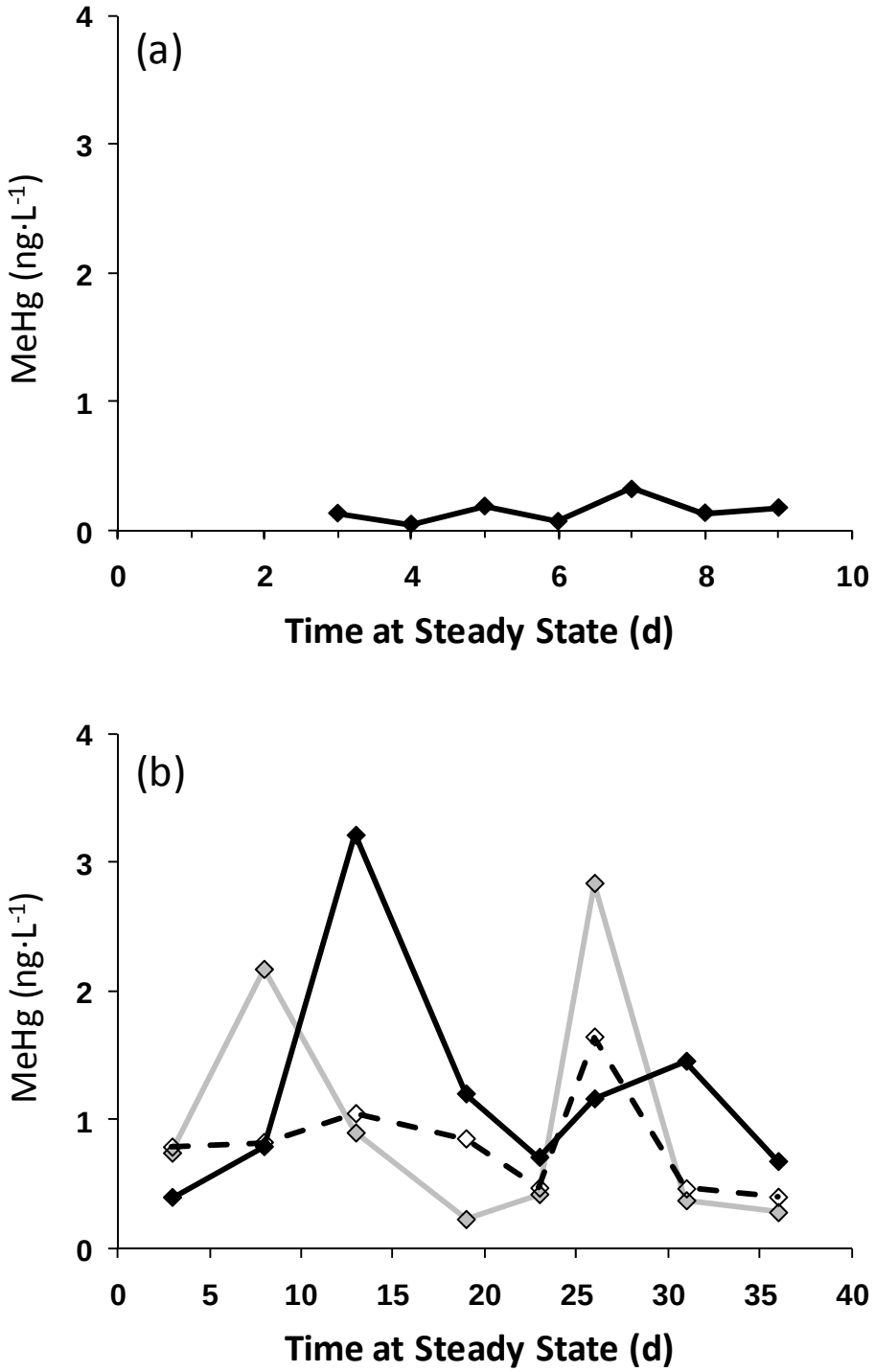

Figure 2.9. The multiple lines of evidence result for determining the baseline methylmercury flux, based on hypolimnetic accumulation rate (data from 2008), porewater profiles and sediment microcosm measurements.

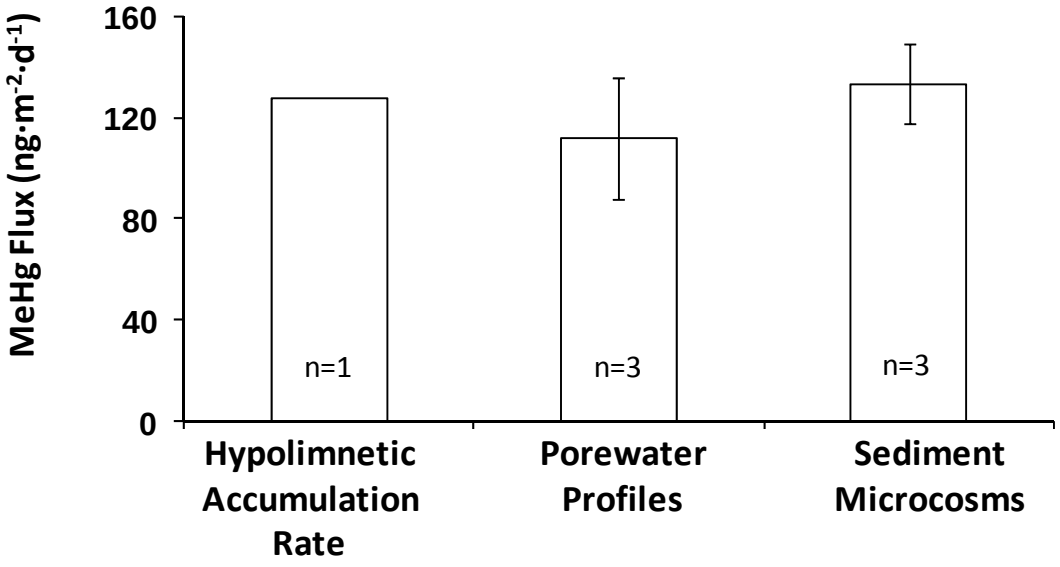

Figure 2.10. Summary of sediment microcosm results for the 'high oxygen – high nitrate' and 'low oxygen plus nitrate' compared with the baseline (no oxygen – no nitrate) case.

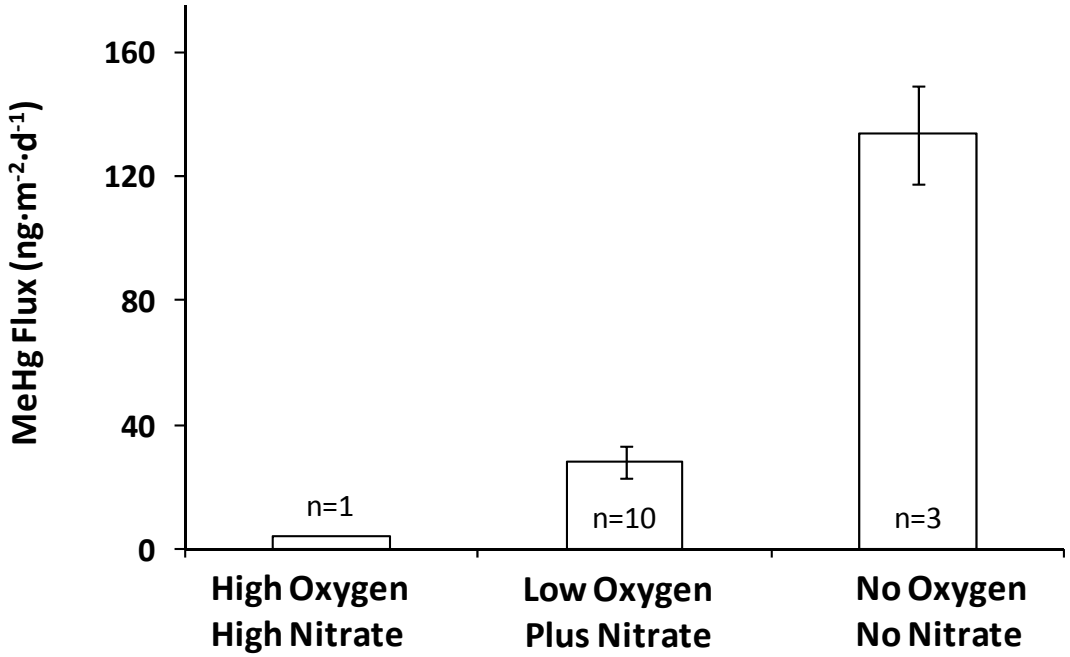

Figure 2.11. Summary of sediment microcosm results for the 'plus oxygen' and 'plus nitrate' compared with the baseline (no oxygen – no nitrate) case.

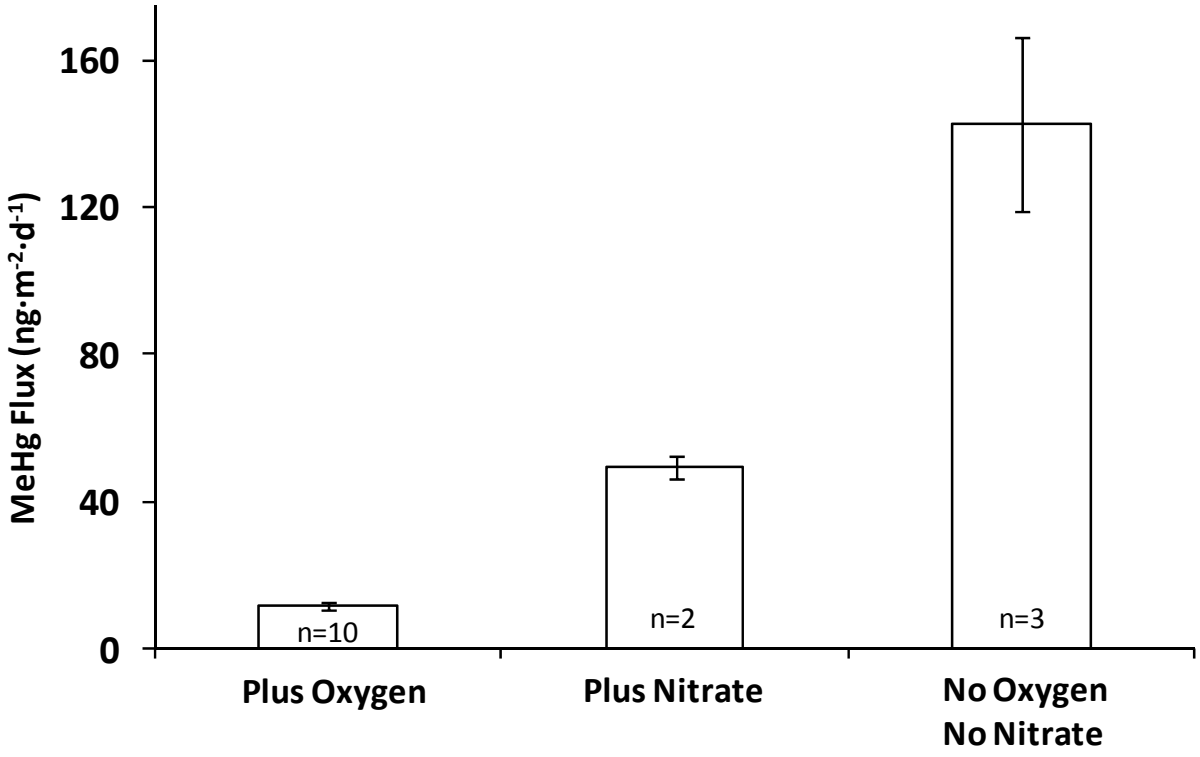

Figure 2.12. Sediment profile of total organic carbon illustrating reductions in deposition.

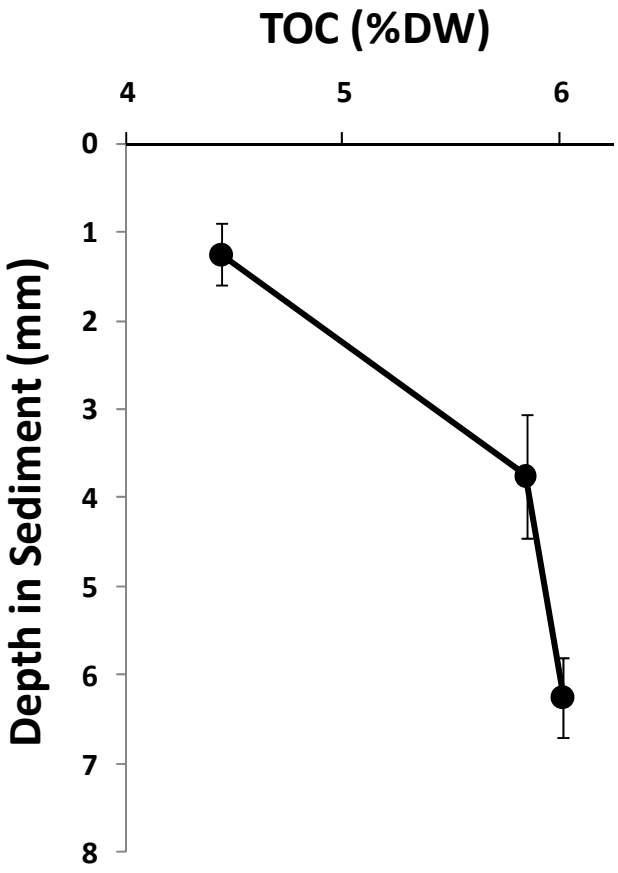

Figure 2.13. Contributions to carbon metabolism as evidenced by the accumulation and depletion of chemical species in and from the hypolimnion.

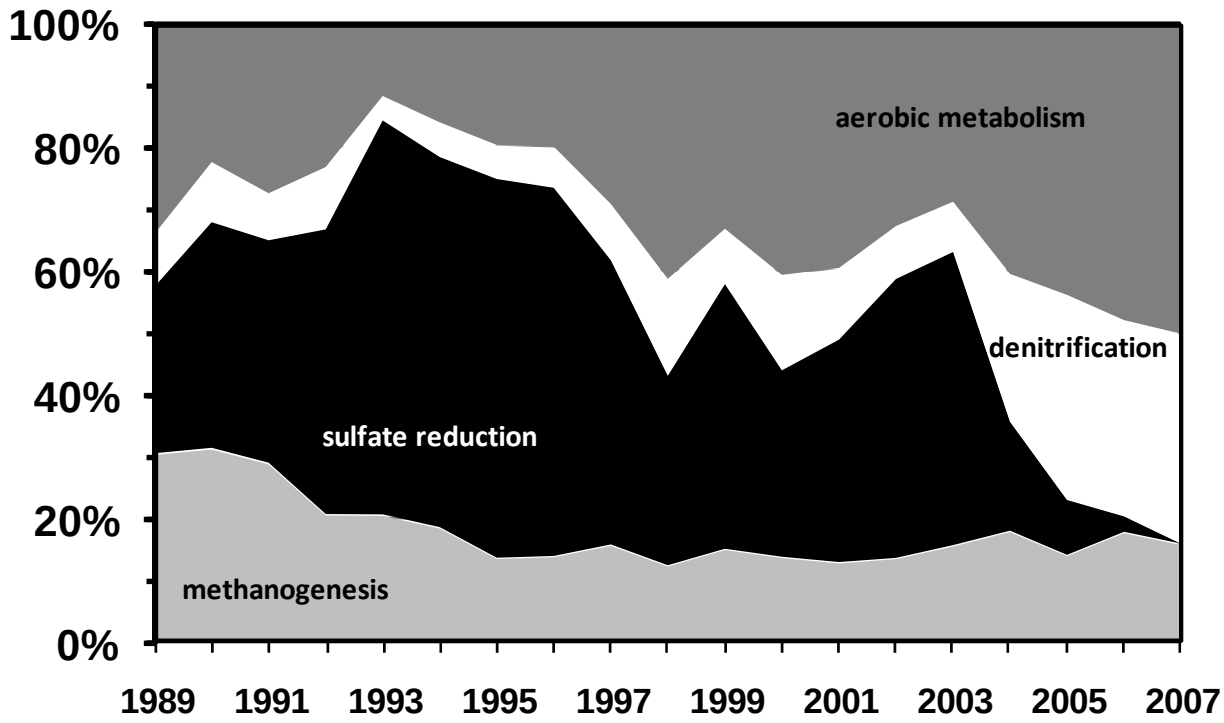

SECTION 3

THE FATE OF MERCURY AND NITROGEN IN THE WATER AND SEDIMENTS OF ONONDAGA LAKE

Prepared by

Svetoslava Todorova
Charles Driscoll

SYRACUSE UNIVERSITY

151 Link Hall
Syracuse, NY 13244
(315) 443-3434

3.1 INTRODUCTION

Freshwater ecosystems are the final recipients of mercury contamination from atmospheric deposition and terrestrial drainage. These ecosystems play an essential role in the cycling of mercury and biological transformation between the inorganic (Hg^{2+}) and organic mercury forms. The mercury contaminant of concern is monomethylmercury (CH_3Hg^+), which is retained in fish tissue to levels that exceed the recommended consumer public health limits (USEPA 2001).

The accumulation of CH_3Hg^+ is the net result of inputs and production (methylation) exceeding loss processes (demethylation and export). Methylation and demethylation are redox sensitive and their interplay is an important determinant of the fate and effects of mercury. Numerous geochemical factors influence production of CH_3Hg^+ (Ullrich 2001), one of them being the availability of sulfate (SO_4^{2-}) (Branfireum et al. 1999). SO_4^{2-} addition promotes methylation of ionic mercury by shifting the decomposition of organic matter to anaerobic SO_4^{2-} metabolism. Biological demethylation of CH_3Hg^+ is less well understood but it is believed to occur via two major pathways: reductive demethylation, which is expressed under aerobic conditions and oxidative demethylation, which predominates under anaerobic conditions (Barkay et al. 2003). SO_4^{2-}-rich anaerobic environments stimulate production of CH_3Hg^+ (Gilmour et al. 1992). Lake sediments and hypolimnetic waters have been found to be active zones of CH_3Hg^+ production, with summer anaerobic periods largely contributing to the accumulation of CH_3Hg^+ (Sellers et al. 2001, Eckley and Hintelman 2006).

Thermodynamic principles govern the sequential use of electron acceptors in the decomposition of organic matter. The electron acceptors with higher energy yields are utilized first, following the decreasing order oxygen (O_2) > nitrate (NO_3^-) > manganese (Mn^{4+}) > iron (Fe^{3+}) > SO_4^{2-} > carbon dioxide (Stumm and Morgan 1996). It is reasonable to expect that the abundance of electron acceptors preceding SO_4^{2-} would restrain SO_4^{2-}-reducing activity and production of CH_3Hg^+ in anaerobic environments. Kinetically and thermodynamically, NO_3^- has the capacity to suppress SO_4^{2-} reducing activities (Stumm and Morgan 1996). The distinct difference in electrochemical potentials between NO_3^--reduction and SO_4^{2-}-reduction suggests the existence of discrete zones for these reactions in time and space.

Under oxygen-limiting conditions, NO_3^- can be reduced to nitrous oxide (N_2O), or dinitrogen gas (N_2) by denitrification, or to ammonium (NH_4^+) by dissimilatory NO_3^- reduction to ammonium (DNRA) (Burgin and Hamilton 2007). From these three processes, only denitrification removes nitrogen (N) from the ecosystem. DNRA produces NH_4^+, which is highly bioavailable to algae and toxic to fish (USEPA 1985).

The objective of the current study was to examine the fate of mercury and nitrogen in the surficial sediments of Onondaga Lake under different oxidation-reduction regimes. This study is a supplement to the sediment incubation study reported in Section 2.

3.2 MATERIAL AND METHODS

3.2.1 Sediment Incubation Experiment

PFA Chambers. High purity 2L Teflon® PFA chambers with threaded closure were special-ordered from Savillex, Inc. The chambers have a removable bottom and a push-through plate (Figure 3.1). The chambers were cleaned with acid and thoroughly rinsed with reagent-grade distilled water (DIW) before sampling.

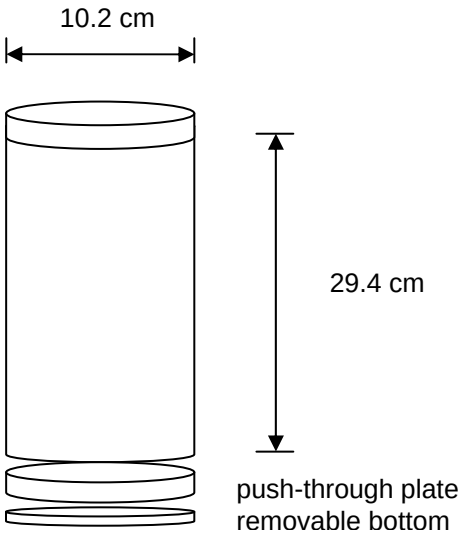

Figure 3.1. Schematic diagram of the incubation chambers. Chambers are made of perfluoroalkoxy (PFA) copolymer resin and were custom-built by Savillex, Inc.

Sediment Core Sampling. Sediments were collected with a box corer from the South Deep station of Onondaga Lake in November and December of 2008 (Figure 3.2). Water depth at the time of sampling was between 19.5 and 20.0 m. The air temperature was between 1 and 3 °C. The temperature of the lake water was 6.7 °C and 5.1 °C in November and December, respectively. Two intact cores of surface sediment sample and overlain water were collected from a single box corer using the Teflon® PFA chambers. A total of 10 cores were collected during each sampling event. Between 12 and 20 cm sediment was collected in each chamber in November and between 10 and 15 cm in December, with overlain water comprising the rest of the chambers. Sediments were transported on ice to the Syracuse University laboratory. Eight of the cores were immediately placed in an anaerobic chamber (Plas Labs Inc., Figure 3.3). The remaining two cores were kept at atmospheric conditions.

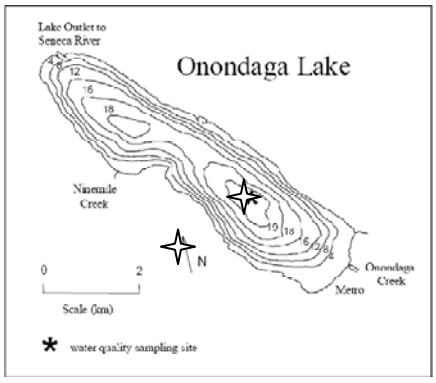

Figure 3.2. Onondaga Lake and sampling sites for denitrification and DNRA analysis. Samples collected at one location in the pelagic sediments (South Deep station, ~20 m depth, asterisk), and two location s in the littoral sediments along a latitudinal transect (8 m depth, 4-point star).

Sediment Incubations. After cores have settled overnight under the appropriate conditions, the overlying water was pipetted out and replaced with artificial lake water. The concentrations of NO_3^- introduced with the artificial lake to each chamber are given in Table 3.1. Each chamber received 1L of artificial lake water (concentrations of the major ion constituents in the lake) or less, depending on the sediment depth. Sediment incubations proceeded under three different regimes: oxic (O_2 present in the overlying water), anoxic (O_2 absent in the overlying water but NO_3^- present), and anaerobic (O_2 and NO_3^- absent in the overlying water). For each experimental batch, two chambers were incubated under oxic condition and eight chambers were incubated under reducing conditions (4 for anoxic and 4 for anaerobic condition). The chambers reached anoxia after 24-48 hours of incubation in a glove box with a continuous Ar flow (Figure 3.3).

Table 3.1. Concentrations of NO_3^- in artificial lake water.

Sample Batch/ Regime	Oxic	Anoxic	Anaerobic
November	-	0.602 mM	-
December	0.223 mM	0.520 mM	0.223 mM

Note: The amount of NO_3^- exceeds the levels observed in Onondaga Lake. An initial experiment conducted with NO_3^- levels within the range observed in the lake resulted in rapid depletion in NO_3^- and failure to maintain anoxic conditions.

The absence of O_2 in the overlying water was continuously verified during the experiment using a portable O_2 probe. We encountered problems with the anaerobic treatment in December. The chambers designated as anaerobic were depleted in O_2 but maintained elevated concentrations of NO_3^- and never reached complete anaerobiosis. The data from these chambers were combined and analyzed with the data from the other anoxic chambers.

Once the chambers reached the desired condition, 0.18 ng (November experiment) and 0.36 ng (December experiment) of $^{199}HgCl_2$ was introduced in the upper 1 cm of the sediment. The spike was injected with a long-length pipette in 13 and 18 locations during November and December experiment, respectively to avoid single localized concentration of the added ionic mercury. Sediment cores were incubated with the added amount of $^{199}Hg^+$ for 0, 5, 10, and 24 hours. The duration of the incubations under each regime are summarized in Table 3.2.

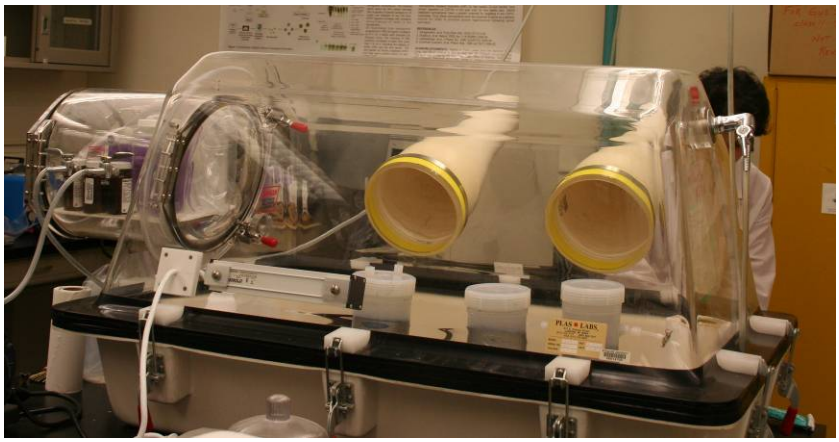

Figure 3.3. Plas Labs acrylic glove box with continuous Ar flow, model818-GB was used for anoxic and anaerobic incubations.

Table 3.2. Regimes and length of incubation

Regime/Incubation Time	0 hour	5 hours	10 hours	24 hours
Oxic	*		*	
Anoxic	*	*	*	*
Anaerobic	*	*	*	*

Note: The anaerobic sediment at 0 hour was lost during incubations in December. The bottom of the sediments at 10 hours were lost during sectioning in November (below 1 cm) and December (below 3 cm).

Water and Sediment Sample Collection. Overlying water from the chambers was removed by pipetting out into acid-washed Teflon® bottles. The water was filtered through 0.45 µm Supor® membranes, acidified with 0.2% HCl, and stored at 4 °C until analysis. Sediment cores for chemical analyses were removed carefully from the glove box and immediately sectioned in a custom-built anaerobic chamber with continuous Ar flow (Michigan Technological University). Cores were sectioned into 0–1, 1–2, 2–3, 3–4, 4-5, and 5-6 cm depth increments using a vertical extruder placed in the anaerobic chamber. The porewater was extracted by centrifugation at 4500 rpm and the supernatant was filtered through 0.45 µm Supor® membranes. The recovered porewater volume ranged between 30 and 60 mL, with lesser amounts collected at deeper sediment. Filtered porewater, containing both dissolved and colloidal size fractions, was placed in centrifuge tubes and stored frozen at −20 °C until analysis. Following centrifugation, a portion of each sediment section was frozen at −20 °C for isotopic mercury analysis. The remaining sediment was freeze-dried for regular total and methylmercury analysis.

The porewater samples were preferentially used for analysis of Hg species and then for ancillary chemistry. The analysis for the ancillary parameters (nitrate, sulfate, and phosphate) were carried out to assess the redox state of the sediments and to locate the boundary between the aerobic and anoxic/anaerobic sediments. Nitrate and sulfate are the electron acceptors utilized in the oxidation of organic matter under nitrate-reducing and sulfate-reducing conditions, respectively. The depletion of these chemical constituents would be an indirect indication of the occurrence of the respected redox reactions. Phosphate was exploited as another indicator for anoxic conditions. Based on the classical concept of Mortimer (1941), phosphate is absorbed to iron oxyhydroxides under oxic conditions and is dissolved from the iron minerals under anoxic conditions. Therefore, an increase in phosphate concentrations in the porewater would be an indirect indication that anoxic conditions (iron-reducing conditions) were established.

3.2.2 Denitrification and DNRA Essay

Sample collection and storage. Sediment samples were collected in late June 2008 from the South basin of Onondaga Lake. The sites were chosen to lie on a latitudinal transect that passes through the South Deep station of the lake (Figure 3.2), representing pelagic sediments (~ 20 m water depth) and littoral sediments (~ 8 m water depth). Sediment samples from the upper 4 cm were collected using a dredge box. The bulk sediment was sub-sampled with a 5-cm in diameter polycarbonate tubing and sediment was sectioned into 0-2 and 2-4 cm. A composite of 4 samples was used to obtain the desired amount of sediment for the experiment. The sediment was transported on ice to the laboratory and stored at 4°C until analysis.

Denitrification and DNRA assays. Denitrification rates were determined by incubating sediment samples in 140 mL serum bottles at room temperature for 6 hours. Each 5-replicate group of vials received 10 g of sediment and 40 mL DIW, lake water (0.21 mM), or NO_3^--amended water (2.35mM). Vials were crimped with rubber septa and aluminum rings to form an airtight seal and flushed with helium for a minimum of 1h to eliminate ambient N_2 and O_2. Samples were analyzed for N_2O, CO_2, and N_2 on a gas chromatograph immediately after flushing (t=0h), after 3 hours of incubation (t=3h), and after 6 hours incubation (t=6h). Between samplings, the transparent vials were covered with aluminum foil to prevent photosynthesis and incubated upside-down underwater in plastic extraction cups on a shaker table. Vials containing DIW were used a control for N_2 leakage.

DNRA were determined by measurement of NO_3^- and NH_4^+ in the sediment-water slurry at the beginning and end of incubation. For the initial measurement, 5 g sediment was mixed with 20 g water in a plastic extraction cup (because vials were already sealed and flushed, filtration and subsequent analysis were not performed). After 30 min incubation on a shaker table, sediment was allowed to settle and overlying water was filtered through a 1µm glass filter. For the final measurement, vials were decrimped, allowed to settle, and filtered through 1µm filter paper. Subsamples from each site were dried at 65°C for 48 h to determine moisture content.

3.3 ANALYTICAL PROCEDURES

3.3.1 Total and Methyl Mercury Analysis

Total Mercury Analysis. Total mercury analyses were performed following USEPA Method 1631, revision E using pre-oxidation with BrCl, followed by reduction of Hg^{2+} to Hg^0 with $SnCl_2$, and purge and trap of Hg^0 (USEPA 2002). Quality assurance and quality control (QA/QC) protocol was carried out by using a laboratory control duplicate, matrix spike (MS) and matrix spike duplicate (MSD). In addition, instrument precision was verified by method blank, continuous calibration verification, continuous calibration blanks, and on-going precision and recovery samples. The spike recovery was between 95.1±6.7 % for both MS and MSD. Instrumentation QA/QC samples were within the method limits. Detection limit of the method calculated from spiked blanks is 0.2 ng L^{-1}.

Methylmercury Analysis. CH_3Hg^+ analysis were performed following USEPA Method 1630 (USEPA 2001). Samples were distilled in 100 ml aliquots, adjusted for to pH = 4.9 with acetate buffer, ethylated with $NaBEt_4$, and purged and trapped. Custom-built automated gas chromatography-cold vapor atomic fluorescence system was used to desorb and detect Hg^0. The precision of the analyses and instrumentation was carried using a laboratory control sample (LCS) and laboratory control duplicates. The small amount of sample did not allow for MS/MSD validation. Instrument precision was verified by method blank, continuous calibration verification, continuous calibration blanks, and on-going precision and recovery samples. The mean recovery of the LCS was 93.2±7.6 %. Detection limit of the method calculated from spiked blanks is 0.02 ng L^{-1}.

3.3.2 Denitrification and DNRA Essay

Analysis. Rates of N_2O, CO_2, and N_2 production were calculated as µmol g^{-1} h^{-1} (dry weight) using a best-fit slope of amount vs. time for each vial's t=0, t=3h, and t=6h timepoints. Rates of NO_3^- removal and NH_4^+ production were derived from t=0 and t=6h timepoints. ANOVA analyzed overall and site-specific effects of treatment on changes in NO_3^-, N_2, N_2O, and NH_4^+.

3.4 RESULTS AND DISCUSSION

3.4.1 Porewater Geochemistry

Several ancillary parameters were measured to help assess patterns of mercury speciation and distribution in the porewater and overlying water. For the oxic treatments, the initial dissolved O_2 (DO) concentrations at the sediment–water interface ranged between 1.9 and 3.3 mg O_2/L in November and between 3.1 and 3.3 mg O_2/L in December. All chambers maintained DO levels above 1 mg O_2/L during the course of the incubations, except for the November chamber at t=10 hours, in which DO decreased to 0.5 mg O_2/L. DO was not detected in the overlying water of the anoxic and anaerobic treatments during the course of the experiment.

Vertical profiles of NO_3^-, SO_4^{2-}, and phosphate (PO_4^{3-}) in the porewater were obtained for the upper 6 cm of sediment for each core. There were no direct measurements of O_2

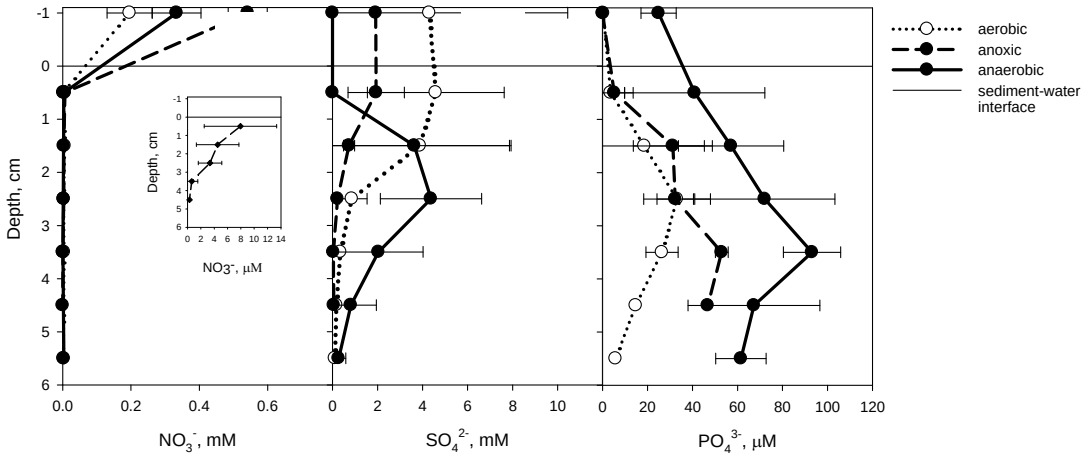

Figure 3.4. Comparison of porewater profiles for (A) NO_3^-, (B) SO_4^{2-}, and (C) PO_4^{3-} under oxic (open circles, dotted line), anoxic (closed circles, dashed line), and anaerobic (closed circles, solid line) conditions. NO_3^- and SO_4^{2-} are given in mM, PO_4^3 is given in µM. Concentrations represent an average of all the cores incubated under the respected condition for both November and December batches. Error bars indicate one standard deviation. Negative depth values represent the overlying water, while positive depths represent porewaters below the sediment-water interface. A line through zero indicates the relative position of the sediment-water interface.

The inserted graph is a magnification of the NO_3^- concentration profile of the anaerobic treatment.

concentrations in the porewater. All treatments maintained NO_3^- concentrations in the overlying water above 0.2 mM (Figure 3.4A). Although oxic and anaerobic treatments in November did not receive NO_3^- additions with the artificial lake water, NO_3^- was detected in the overlying water. NO_3^- concentrations rapidly decreased below the sediment-water interface, which indicated its utilization as terminal electron acceptor in denitrification (Tiedje 1988). SO_4^{2-} concentrations in the overlying water of the oxic and anoxic treatments were 4.31±6.14 mM and 1.92±0.03 mM (average±one standard deviation), respectively and gradually decreased with depth (Figure 3.4B). Overlying water and the upper 1 cm of sediment of the anaerobic treatment were depleted in SO_4^{2-}. An additional supply of SO_4^{2-} was observed at mid-depth of the anaerobic core possibly because of release of S mineral (Shippers and Jorgensen 2002).

PO_4^{3-} concentrations were not detected in the overlying water in the oxic and anoxic treatments. PO_4^{3-} concentrations were elevated to 25 µM in the anaerobic chambers (Figure 3.4C) likely as a result of the dissolution of iron-oxyhydroxo-phosphates from the reduced sediments (Mortimer 1941). Vertical profiles of PO_4^{3-} indicate gradual increase in PO_4^{3-} concentrations with depth, with maximum at 2-3 cm in the sediments overlain by oxygenated water, and at 3-4 cm for sediments overlain by O_2 depleted water. Concentrations of PO_4^{3-} did not show significant change between the sediments overlain by oxygenated water and anoxic sediments but increased two to three times in the porewater of the sediments that reached anaerobic conditions (Figure 3.4C).

The vertical distributions of the ancillary geochemical parameters in sediment porewater (Figure 3.4) were used to delineate zones of NO_3^- reduction and SO_4^{2-} reduction. The rapid depletion of NO_3^- near the sediment-water interface precluded proper delineation of the NO_3^- -reduction zone. The lower boundary of the NO_3^- -reducing conditions was inferred to extend no further than 0.5 cm under the sediment-water interface for oxic conditions (Fig. 3.5A) and close to the sediment-water interface for anoxic conditions (Figure 3.5B). The upper limit of the zone of SO_4^{2-} reduction occurred 1.5 cm and 1 cm below the sediment water interface for the aerobic and anoxic treatments, respectively. Anaerobic conditions in the overlying water, in turn, promoted the extension of the SO_4^{2-} reduction zone to the sediment-water interface (Figure 3.5C). The lower boundary of the SO_4^{2-} reduction is undefined.

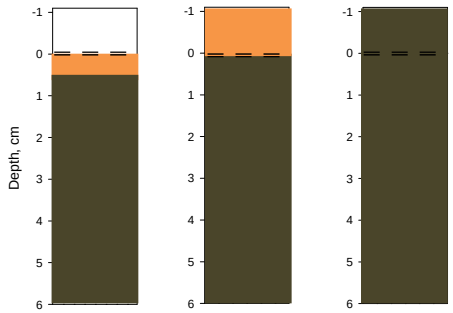

Figure 3.5. Delineation of the redox phases under different treatments (A) aerobic, (B) anoxic, and (C) anaerobic. White area indicates aerobic metabolism, orange area indicates the intermediate anoxic metabolisms including NO_3^- reduction, and brown area indicates anaerobic metabolism.

3.4.2 Distribution of Mercury Species

Average concentrations of mercury species by redox regime. One goal of this work was to investigate the speciation and distribution of mercury in the upper sediments under three different regimes – oxic, anoxic, and anaerobic. Depth profiles of total mercury and CH_3Hg^+ depict the variation of mercury species under these three treatments (Figure 3.6). Under oxic and anoxic conditions the average concentrations of CH_3Hg^+ in the overlying water were in the range of 0.62±0.77 ng L^{-1} and 0.50±0.69 ng L^{-1}, respectively and increased to 4.06±0.28 ng L^{-1} for the anaerobic sediments (Figure 3.6A). Subsurface maxima in the average CH_3Hg^+ concentrations were observed in all cores and treatments, localized within the upper 3 cm. Total mercury concentrations varied between core and treatments but had a general pattern of increasing below 2-3 cm depth (Figure 3.6B).

Changes in percent mercury as CH_3Hg^+ can be used to approximate the zone of CH_3Hg^+ production. The percent of total as CH_3Hg^+ in the overlying water increased from 9.3±3.9% and 5.9±3.8% in the oxic and anoxic treatments, respectively to 48.2±18.3% in the anaerobic treatments (Figure 3.6C). The maxima of percent mercury as CH_3Hg^+ in the porewater was relatively stable among treatments with 27.9±14.9% and 19.8±20.1% in the oxic and anoxic treatments, respectively, and 29.7±14.3% in the anaerobic treatments.

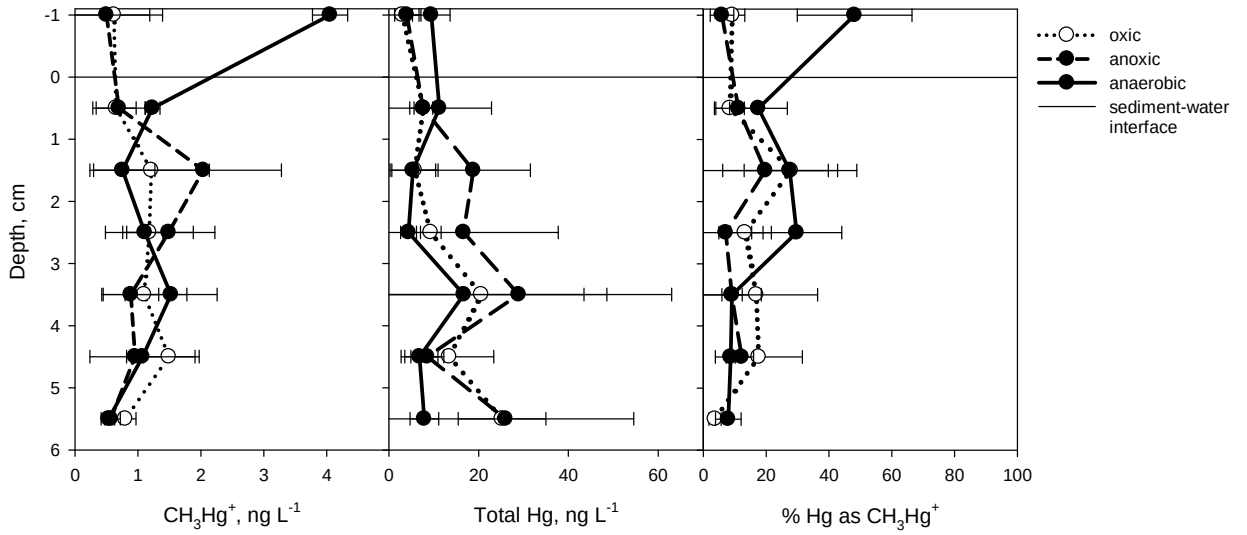

Figure 3.6. Depth profiles of CH_3Hg^+ (A), total mercury (B) and percent mercury as CH_3Hg^+ (C) under oxic (open circles, dotted line), anoxic (closed circles, dashed line), and anaerobic (closed circles, solid line) conditions. NO_3^- and SO_4^{2-} are given in mM, PO_4^3 is given in µM. Concentrations represent an average of all the cores incubated under the respected condition for both November and December batches. Error bars indicate one standard deviation. Negative depth values represent the overlain water, while positive depths represent porewaters below the sediment-water interface. A line through zero indicates the relative position of the sediment-water interface.

Cycling of mercury species under oxic conditions. The oxic treatments in November gave us the opportunity to observe the progression from oxic (t=0 hour) to anoxic (t=10 hours) conditions in the overlying water and the respected changes in the speciation of mercury (Figure 3.7). Using the sequential changes in redox constituents, zones of NO_3^- reduction and SO_4^{2-} reduction were delineated (Figure 3.7A). At time zero (t=0 hour), NO_3^- reduction was contained within the first 2 cm, followed by the zone of SO_4^{2-} reduction. Ten hours later (t=10 hours), DO concentrations were 0.5 mg O_2/L, SO_4^{2-} concentrations in the overlying water decreased to below the analytical detection limit, and PO_4^{3-} concentrations were elevated in the upper 2 centimeters, an indication that the SO_4^{2-} reduction zone migrated closer to the sediment-water interface (Figure 3.7B). PO_4^{3-} concentrations were not detected in the overlying water neither at t=0 hour or at t=10 hours.

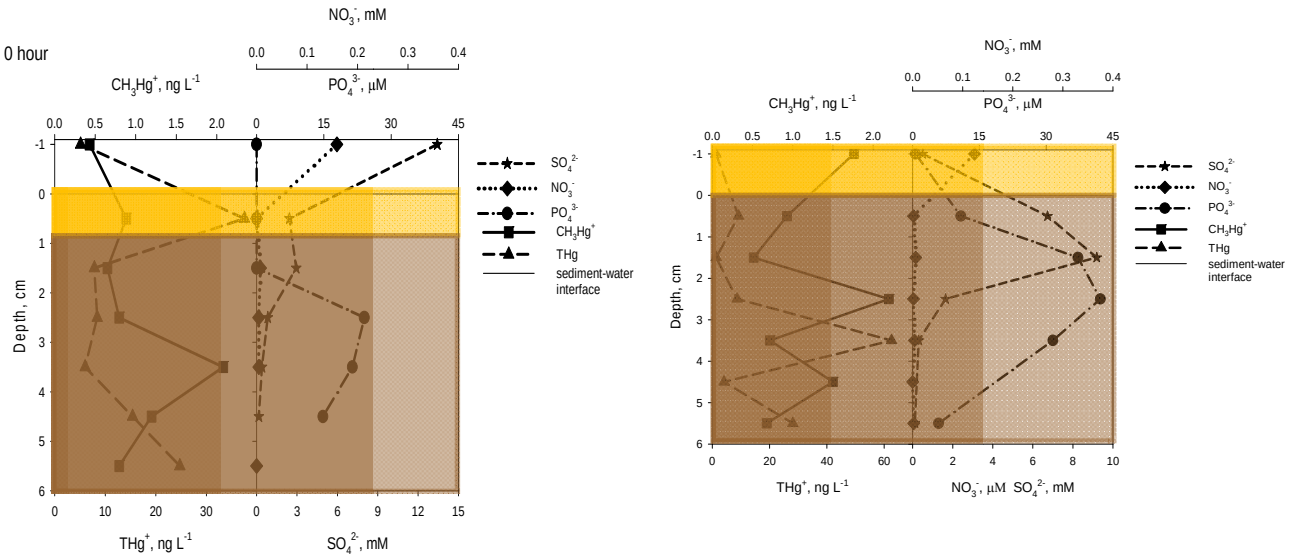

Figure 3.7. Depth profiles of mercury species and major anions during the transition from oxic (A) t=0 hour to anoxic (B) t=10 hours conditions in overlying water. Negative depth values represent the overlying water, while positive depths represent porewaters below the sediment-water interface. A line through zero indicates the relative position of the sediment-water interface.

The transport of the redox elements within the sediments coincided with the movement of the peak CH_3Hg^+ concentrations closer to the sediment-water interface (Figure 3.7B) and a four-fold increase in the CH_3Hg^+ concentration in the overlying water (from 0.43 ng L^{-1} at t=0 hour to 1.76 ng L^{-1} at t=10 hours). The conditions in the overlying water at t=10 hours transitioned from oxic to anoxic. The concentration of NO_3^- in the overlying water at t=10 hour was 0.11 mM, a concentration corresponding to lake conditions at 19 m depth when O_2 has just depleted. NO_3^- concentrations in the sediments decreased below 0.06 mM.

Cycling of mercury species under anoxic conditions. In the anoxic treatment, the concentrations of NO_3^- in the overlying water were maintained at 0.54±0.06 mM and rapidly decreased to 0.07±0.05 mM below the sediment-water interface (Figure 3.8). Concentrations of SO_4^{2-} remained constant in the overlying water throughout the experiment at 1.92±0.03 mM, gradually decreasing with depth. Average concentrations of CH_3Hg^+ in the overlying water (average of all incubation times) were 0.50±0.67 ng L^{-1}. The maximum CH_3Hg^+ concentrations were reached between 1 and 2 cm depth, in the zone of SO_4^{2-} reduction. The maximum in the % mercury as CH_3Hg^+ of 19.8±20.1% was reached at the same depth interval.

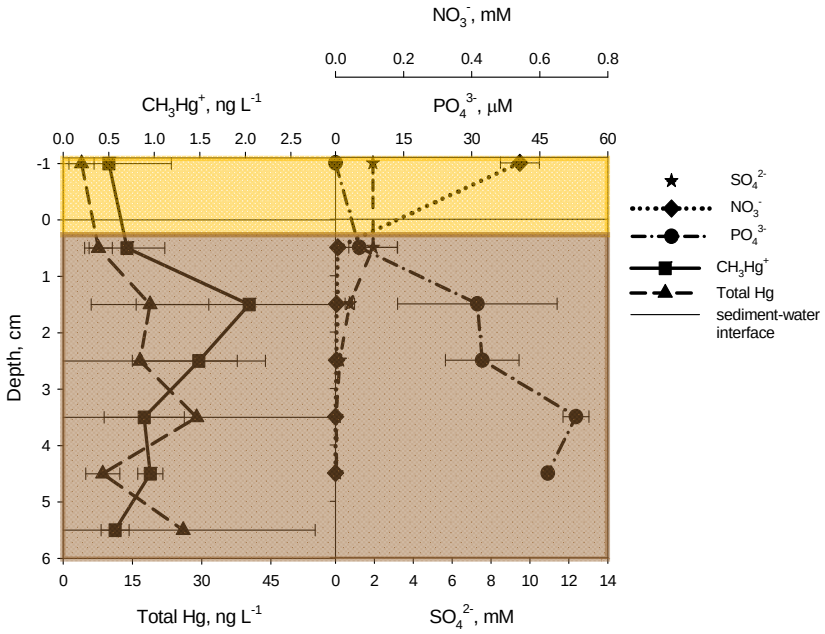

Figure 3.8. Depth profiles of mercury species (A), and major anions (B) at time t=10 hours under sustained anoxic conditions in the overlying water. Negative depth values represent the overlying water, while positive depths represent porewaters below the sediment-water interface. A line through zero indicates the relative position of the sediment-water interface.

Cycling of mercury species under anaerobic conditions. SO_4^{2-} was below the analytical detection limit in the overlying water and upper 1 cm in the anaerobic treatment, which corresponded to increase in concentrations of soluble P and its release in the overlying water, an indication that anaerobic conditions were established (Figure 3.9B). The average CH_3Hg^+ concentrations in the porewater were not statistically different from the average concentrations observed in the oxic and anoxic treatments (F_{oxic}= 0.788, p=0.28; F_{anoxic}=0.777, p=0.30). However, CH_3Hg^+ in the overlying water reached 4.06±0.28 ng L^{-1} (Figure 3.9A), which corresponded to an average 48 percent of the total mercury.

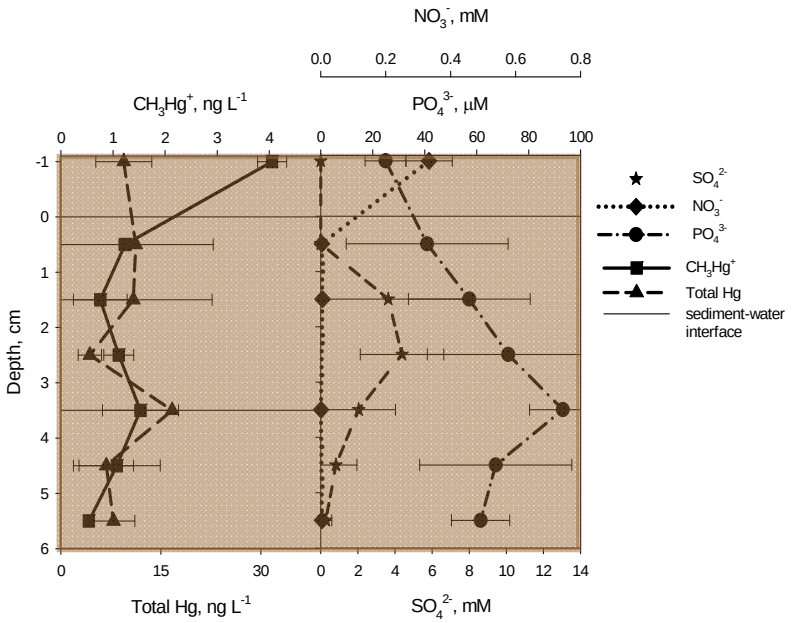

Figure 3.9. Concentration profiles of mercury species (A), and major anions (B) under sustained anaerobic conditions in the overlying water. Negative depth values represent the overlying water, while positive depths represent porewaters below the sediment-water interface. A line through zero indicates the relative position of the sediment-water interface.

An interesting observation was evident in the incubations performed in December. As mentioned in the methods, these treatments received NO_3^- through the artificial lake water and anaerobic conditions were not developed in all the chambers. However, these treatments allowed us to follow the progression from anoxic (t=5 hours) to anaerobic (t=10 hours) conditions and the corresponding changes in the speciation of mercury (Figure 3.10).

The overlying water was depleted in DO in both chambers. Concentrations of SO_4^{2-} in the overlying water were 1.79 mM and 1.69 mM at time t=5 hours and t=10 hours, respectively (Figure 10A and B). PO_4^{3-} concentrations were not detected at t=5 hours and increased to 3.79 µM at t=10 hours. These soluble P concentrations are lower that the concentrations observed in the anaerobic treatments in November (Figure 3.9B). Given the distribution of the redox constituents, we believe that at the time of 10 hours the core was at the interface between anoxic and anaerobic conditions.

The progression between anoxic and anaerobic conditions marked substantial changes in the depth distribution of mercury species. At t=5 hours a definitive maximum in CH_3Hg^+ concentrations was observed between 2 and 3 cm depth in the porewater (Figure 3.10A), which was not seen at t=10 hours (Figure 3.10B). A peak of % mercury as CH_3Hg^+ was observed at 2-3 cm depth (25.6%) at t=5 hours, which migrated to the upper 2 cm (18-20%) at t=10 hours. Following this transition, the concentrations of CH_3Hg^+ in the overlying water at t=10 hours were four times higher (4.32 ng L^{-1}) than the concentration at t=5 hours (1.02 ng L^{-1}). These values are close to the average CH_3Hg^+ concentration observed in the anaerobic treatments (Figure 3.9A).

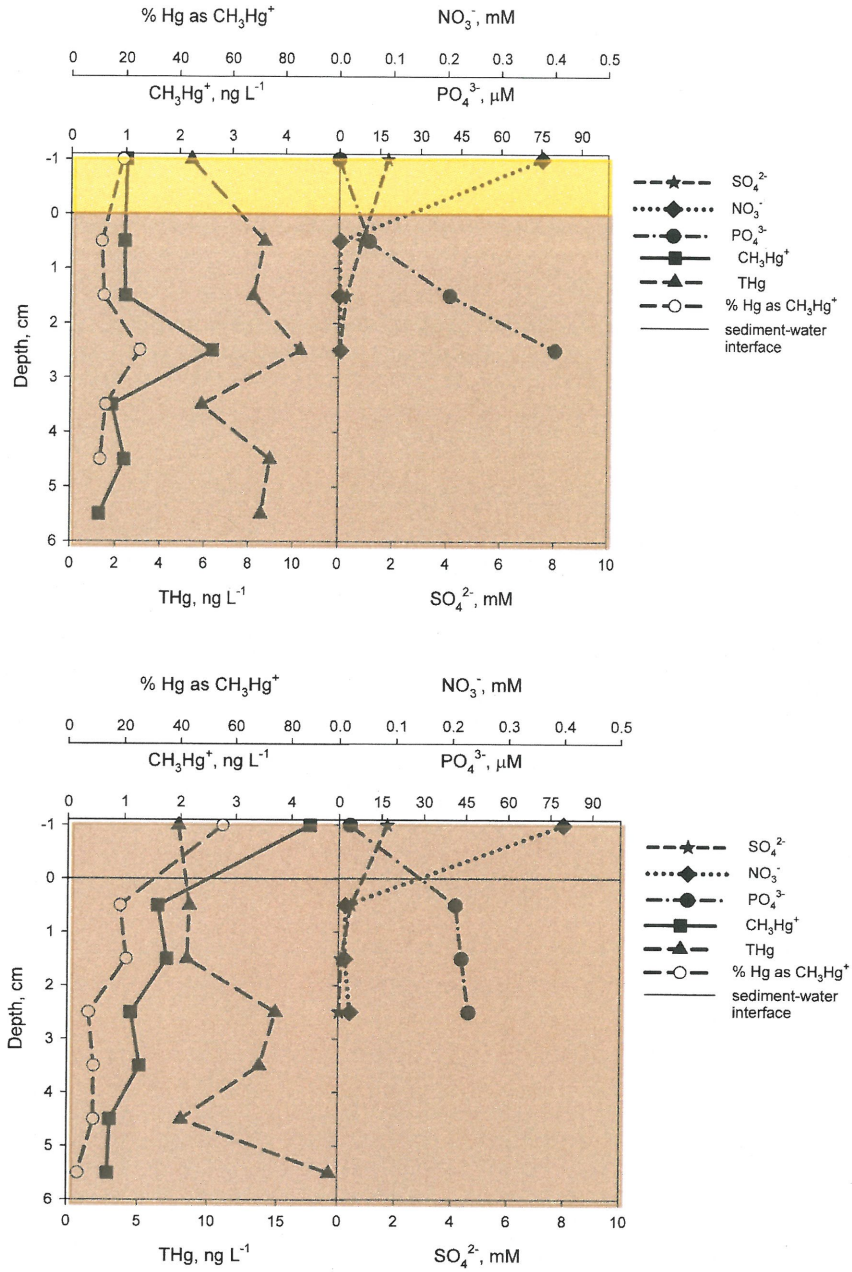

Figure 3.10. Depth profiles of mercury species and major anions during the transition from anoxic (A) t=0 hour to anaerobic (B) t=10 hours conditions in overlying water. Negative depth values represent the overlying water, while positive depths represent porewaters below the sediment-water interface. A line through zero indicates the relative position of the sediment-water interface.

3.4.3 Products of Nitrate Reduction

Littoral and pelagic sediments were incubated with DIW, lake water, and NO_3^- amended lake water. NO_3^- reduction rates at ambient conditions were higher in the littoral sediments than in pelagic sediments (Figure 3.11). Both overall (F=11.042, p=0.000) and within each site (East littoral sediment: F=43.294, p=0.000; West littoral sediment: F=147.134, p=0.000; pelagic sediment: F=940.536, p=0.000), sediments increased rates of NO_3^- removal in response to NO_3^- addition.

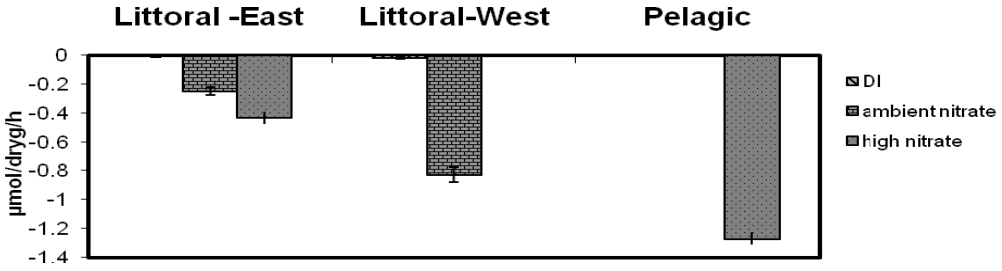

Figure 3.11. Rates of NO_3^- reduction in the littoral and pelagic sediments of Onondaga Lake. Error bars represent one standard error from the mean.

In all treatments, a majority of the NO_3^- reduction occurred through complete denitrification to N_2 (Figure 3.12), with the highest rates detected in the west littoral sediments. Both across the 3 sites (F=11.06, p=0.000) and within each site, there was significant increase in N_2 production with NO_3^- addition (East littoral sediment: F=8.095, p=0.010; West littoral sediment: F=12.423, p=0.005; pelagic sediment: F=157.585, p=0.000). Little NO_3^- was reduced to N_2O (Figure 3.13), or NH_4^+ (Figure 3.14), even in the high NO_3^- treatment. There were no statistical trends toward increased N_2O or NH_4^+ production with additional NO_3^-.

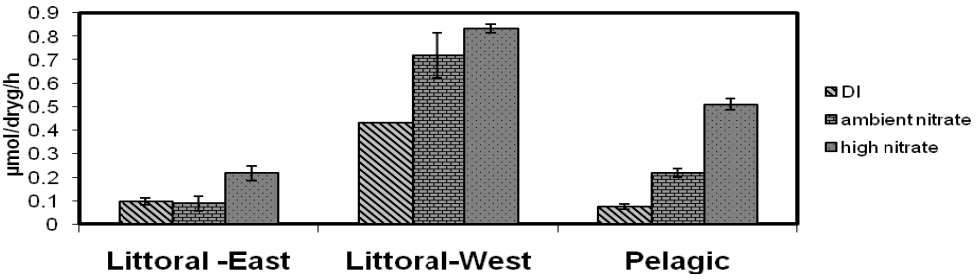

Figure 3.12. Rates of N_2 production in the littoral and pelagic sediments of Onondaga Lake. Error bars represent one standard error from the mean.

NO_3^- reduction in Onondaga Lake appears dominated by denitrification over DNRA. Sediments are below NO_3^--reducing capacity at 0.21 mM; rates of NO_3^- reduction increase with NO_3^- addition. Most NO_3^- reduction is in the form of complete denitrification to N_2, with no trend towards increased N_2O or NH_4^+ production even at ten times ambient NO_3^- concentrations. Although our observations showed a minimal role for DNRA, we caution that our assay was

relatively insensitive to NH_4^+ production. NH_4^+ was measured in water filtered from sediment-water slurries through 1µm glass filters. This filtering did not collect NH_4^+ sorbed to the negatively charged clay particles in the sediment.

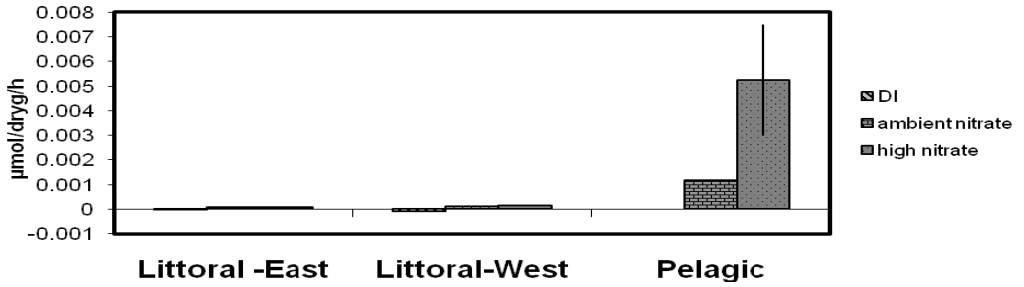

Figure 3.13. Rates of N_2O production in the littoral and pelagic sediments of Onondaga Lake. Error bars represent one standard error from the mean.

This study did not account for either the effects of cold storage or seasonal variables that might influence denitrification patterns. Sediments were sampled at a time when O_2 was still present in the water column. Development of anoxic and anaerobic conditions in the water column and upper sediments could hinder denitrification (Brunet and Garcia-Gil 1996), perhaps favoring NO_2^-, N_2O or NH_4^+ production.

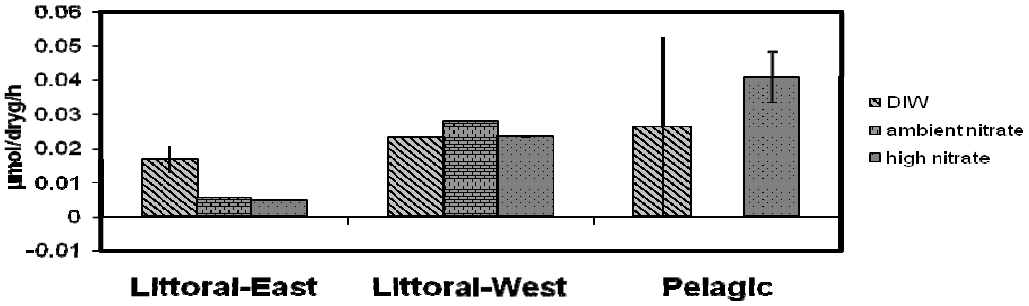

Figure 3.14. Rates of NH_4^+ production in the littoral and pelagic sediments of Onondaga Lake. Error bars represent one standard error from the mean.

The incubation results suggest that nitrate reduction in the sediments dominates over dissimilatory nitrate reduction to ammonia. In this respect, additions of nitrate would not result in substantial production of ammonia thus limiting potentially adverse effects on the lake ecosystem associated with enhanced supply of ammonia. One caution is that the procedure for the detection of NH_4^+ did not account for any NH_4^+ that might have been sorbed to sediment particles and could potentially become available. These results tentatively support the safety of maintaining 0.2 mM with respect to NO_3^- removal, NH_4^+ production (DNRA) and N_2O production.

3.5 REFERENCES FOR SECTION 3

Barkay, T., S. M. Miller, and A. O. Summers. 2003. Bacterial Mercury Resistance From Atoms to Ecosystems. FEMS Microbiology Reviews 27:355-384.

Branfireum, B. A., N. T. Routel, C. A. Kelly, and J. W. M. Rudd. 1999. In Situ Sulfate Stimulation of Mercury Production in Boreal Peatland: Toward a Link Between Acid Rain and Methylmercury Contamination in Remote Environments. Global Biogeochemical Cycles 13:743-750.

Brunet, R.C., Garcia-Gil, L.J. 1996. Sulfide-Induced Dissimilatory Nitrate Reduction to Ammonia in Anaerobic Freshwater Sediments. FEMS Microbiology Ecology. 21: 131-138.

Burgin, A. J. and S. K. Hamilton. 2007. Have We Overemphasized the Role of Denitrification in Aquatic Ecosystems? A Review of Nitrate Removal Pathways. Frontiers in Ecology and Environment 5(2):89-96.

Gilmour, C. C., Henry, E. A and R. Mitchell. 1992. Sulfate Stimulation of Mercury Methylation in Freshwater Sediments. Environmental Science and Technology 26(11): 2281-2287.

Eckley, C. and H. Hintelmann. 2006. Determination of Mercury Methylation Potential in the Water Column of Lakes Across Canada. Science of the Total Environment 368:111-125.

Mortimer, C.H. 1941. The Exchange of Dissolved Substances Between Mud and Water in Lakes. Ecology **29**: 280–329.

Sellers, P., C. A. Kelly, and J. W. M. Rudd. 2001. Fluxes of Methylmercury to the Water Column of a Drainage Lake: The Relative Importance of Internal and External Sources. Limnology and Oceanography 46:623-631.

Shippers, A. and B.B. Jorgensen. 2002. Oxidation of Pyrite and Iron Sulfide by Manganese Dioxide in Marine Sediments. Geochimica et Cosmochimica Acta 65 (6): 915-922.

Stumm, W. and J. J. Morgan. 1996. Kinetics of Redox Processes, p. 672-725. *In* W. Stumm and J. J. Morgan (eds.), Aquatic Chemistry: Chemical Equilibria and Rates in Natural Waters. John Wiley & Sons Inc., New York, NY.

Tiedje, J.M. 1988. Ecology of Denitrification and Dissimilatory Nitrate Reduction to Ammonium. *In* Zehnder, A.J.B. (ed.), Biology of Anaerobic Microorganisms, John Wiley & Sons, NY.

Ullrich, S. M., T. W. Tanton, and S. A. Abdrashitova. 2001. Mercury in the Aquatic Environments: A Review of Factors Affecting Methylation. Critical Reviews in Environmental Science and Technology 31:241-293.

U.S. Environmental Protection Agency (USEPA). Ambient Water Quality Criteria for Ammonia. Office of Water. EPA 440/5-85-001, Washington, D.C., 1985.

U.S. Environmental Protection Agency (USEPA). Methyl Mercury in Water by Distillation, Aqueous Ethylation, Purge and Trap, and CVAFC. EPA-821-R-01-020. Office of Water, Washington, D.C., 2001.

U.S. Environmental Protection Agency (USEPA). Water Quality Criterion for the Protection of Human Health: Methylmercury. USEPA-823-R-01-001. Office of Science and Technology, Office of Water. Washington, D.C. 2001.

U.S. Environmental Protection Agency (USEPA). Mercury by Oxidation, Purge and Trap, and CVAFC. EPA-821-R-02-019. Office of Water, Washington, D.C., 2002.

SECTION 4

MICROBIOLOGICAL ANALYSES OF SMU 8 SEDIMENTS

4.1 INTRODUCTION

The processes of nitrate reduction and sulfate reduction as discussed in Sections 2 and 3 are critical to the formation of methylmercury in Onondaga Lake. Both of these processes are mediated by bacteria. This study was therefore undertaken to survey the microbial populations in sediments collected in conjunction with the sediment incubations work in order to ascertain relative abundances of microbes (i.e., bacteria) involved with nitrate reduction (denitrifiers), iron reduction (iron reducers), sulfate reduction (sulfate reducers), and the final process in anaerobic carbon degradation that results in the formation of methane, methanogenesis (methanogens). The characterization of these groups of organisms covers the major groups of organisms involved in anaerobic carbon degradation and the potential mercury methylating organisms. Given the dynamic nature of these processes during the course of stratification, these microbial populations were characterized both spatially (in the vertical dimension) and temporally.

4.2 MATERIALS AND METHODS

4.2.1 Sediment Core Collection and Processing

Sediment cores were collected from South Deep on August 22 and November 17, 2008 by Syracuse University and the Upstate Freshwater Institute. Cores were sectioned into the following intervals: 0 - 0.5 cm, 0.5 - 1 cm, 1 - 1.5 cm, 1.5 - 2 cm, 2 - 4 cm, and 4 - 6 cm (note each 0.5 cm is approximately 0.2 inch). These sections were a slight modification to the work plan in that two intervals (1 - 1.5 cm and 1.5 - 2 cm) were sectioned instead of one interval between the 1 and 2 cm (0.4 to 0.8 inch) depth.

4.2.2 Identification and Enumeration of Microbial Populations

Sediment samples were analyzed by Microbial Insights Inc (www.microbe.com) using quantitative real time polymerase chain reaction (qPCR). This technique distinguishes between denitrifiers, sulfate/iron reducers, and methanogens using DNA primers specific to each microbial group. Iron and sulfate reducers cannot be distinguished from each other using this technique; however, it is anticipated that sulfate-reducers greatly outnumber iron reducers in these sediments.

qPCR was used to make multiple copies of the target genes (identified by DNA primers) for each microbial group present in each sample. The target genes were fluorescently tagged and the degree of fluorescence was measured to determine the number of copies of the target gene. The number of copies was then compared to a known standard for each microbial group and the number of cells of each microbial group in the samples was thus estimated. For denitrifiers, the method used two genes that code for enzymes involved in denitrification (nirK and nirS) and results are reported for both.

4.3 RESULTS AND DISCUSSION

To place these results in context, it is relevant to describe the chemistry of the overlying water on the two sediment sampling dates in August and November, 2008. The water quality data referenced in this section were collected as part of the baseline monitoring program for the lake and reported in the Onondaga Lake Baseline Monitoring Report for 2008 (Parsons et al. 2009). The August 22 sampling date occurred during stratification after oxygen and nitrate had become much lower relative to earlier concentrations and methylmercury appeared in the hypolimnion. The dissolved oxygen concentration at 18 m water depth on August 22 was 0.22 mg/L, while the nitrate concentration on August 18 and 25 (the closest dates to the sediment sampling date) were 0.583 and 0.721 mg/L, respectively. The methylmercury concentration at 18 meter (59 ft.) water depth on August 18 (the closest date) was 0.224 ng/L. Sulfide (the end-product of sulfate reduction) was undetected at the 18-meter water depth during August.

The November 17 sampling date occurred approximately three weeks after fall turnover when lake mixing resulted in replenishment of oxygen and nitrate to the hypolimnion and a decrease in methylmercury concentration. The dissolved oxygen, nitrate, and methylmercury concentrations at 18 m water depth on November 17 were 8.84 mg/L, 2.059 mg/L, and 0.133 ng/L, respectively. Sulfide was undetected at the 18-meter water depth during November.

4.3.1 Patterns By Microbial Groups

Figures 4.1 through 4.6 show the results for each sediment depth interval, thus allowing comparison between microbial groups and sampling dates. In August, the most abundant microbial group was nirS denitrifiers followed by nirK denitrifiers at all depths. Methanogens were slightly more abundant than iron/sulfate reducers except at 1.0 to1.5 cm (0.4 to 0.6 inch) depth where they were slightly less abundant. In November, the most abundant microbial group was methanogens at all depths, followed by the nirK and nirS denitrifiers. Iron/sulfate reducers were much more abundant at 0 to 0.5 cm depth in November than they were in August.

Interpretation of these results in terms of relative microbial activity is only approximate because population does not necessarily translate directly to activity. The patterns are, however, suggestive and also consistent with the understanding of zones of nitrate reduction and sulfate reduction described in Section 3. In August, the near surface sediment is likely a zone of active nitrate reduction because oxygen is virtually absent in overlying water while nitrate is still present and available. Therefore, the high abundance of denitrifiers is expected in near surface sediment.

Although the November sampling date was approximately three weeks after fall turnover, it is expected that the sediment takes time to recover to pre-stratification conditions because diffusion of oxygen and nitrate from the overlying water to sediment is a relatively slow process. Thus, the November microbial populations are probably reflective of conditions at fall turnover when nitrate is depleted in overlying water and the sulfate reduction zone has moved up to the sediment-water interface. The sediment in November has lower redox potential than in August and this is consistent with the greater populations of methanogens in November.

4.3.2 Patterns By Depth

Figures 4.7 through 4.10 show the results for each microbial group, thus allowing comparison between sediment depth intervals and sampling dates. Populations of nirK

denitrifiers remained approximately constant by depth for each sampling date while overall populations were slightly larger in November ($3.33x10^7$ to $6.90x10^7$) than in August ($7.66x10^6$ to $1.08x10^7$) (Figure 4.7). Populations of nirS denitrifiers remained approximately constant by depth in August ($1.87x10^9$ to $5.05x10^9$) (Figure 4.8) and were approximately 10^2 or 100 times larger than the nirK denitrifiers. Populations were generally smaller in November than in August with the lowest value ($2.89x10^6$) reported at 0 to 0.5 cm (0 to 0.2 inch) depth. The nirS denitrifier population data are consistent with the assumption that nitrate reduction in sediment was greater in August than in November, due to the availability of nitrate. The nirK denitrifier population appears to be less sensitive to changes in conditions.

Populations of iron/sulfate reducers in August were largest ($5.77x10^5$) at 1.5 – 2.0 cm depth and smallest ($1.45x10^3$) at the surface 0 to 0.5 cm depth (Figure 4.9). This pattern changed in November where the largest population ($4.36x10^6$) was observed at 0 to 0.5 cm depth and populations at the other depths ranged from $2.69x10^5$ to $1.95x10^6$. These data support the concept of the sulfate reduction zone moving up to the sediment-water interface after nitrate becomes depleted.

Methanogens were much more abundant in November than in August with populations increasing from $2x10^8$ at 0 to 0.5 cm depth to $1.81x10^9$ at 4 to 6 cm depth (Figure 4.10). In August, the population was much smaller at 0 – 0.5 cm depth ($1.95x10^3$) than at other depths, but all depths had considerably smaller populations than in November. Methanogens require low redox potential, therefore their smaller population in August (especially at 0 to 0.5 cm depth) relative to November is consistent with the shift to lower redox potential in sediment as oxygen and nitrate are consumed. There appears to be a lag time of at least several weeks before sediment re-equilibrates with oxic conditions in overlying water.

4.4 REFERENCES FOR SECTION 4

Parsons, Exponent, and Anchor QEA. 2009. Onondaga Lake Baseline Monitoring Report for 2008. Prepared for Honeywell, Inc., East Syracuse, NY.

Figure 4.1. Microbes in 0 – 0.5 cm Interval of South Deep Sediment, August 22 and November 17, 2008

Honeywell

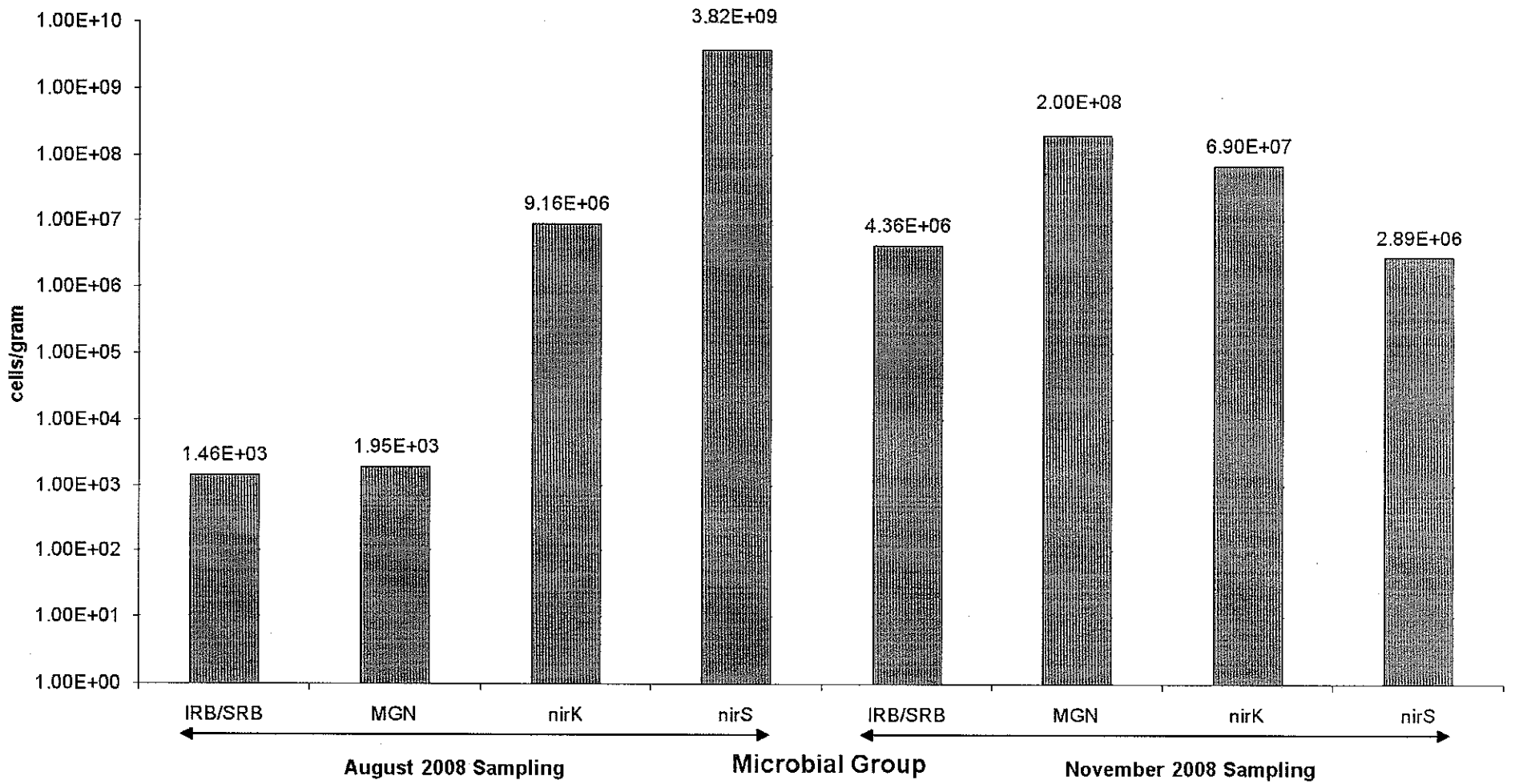

Figure 4.2. Microbes in 0.5 – 1.0 cm Interval of South Deep Sediment, August 22 and November 17, 2008

Honeywell

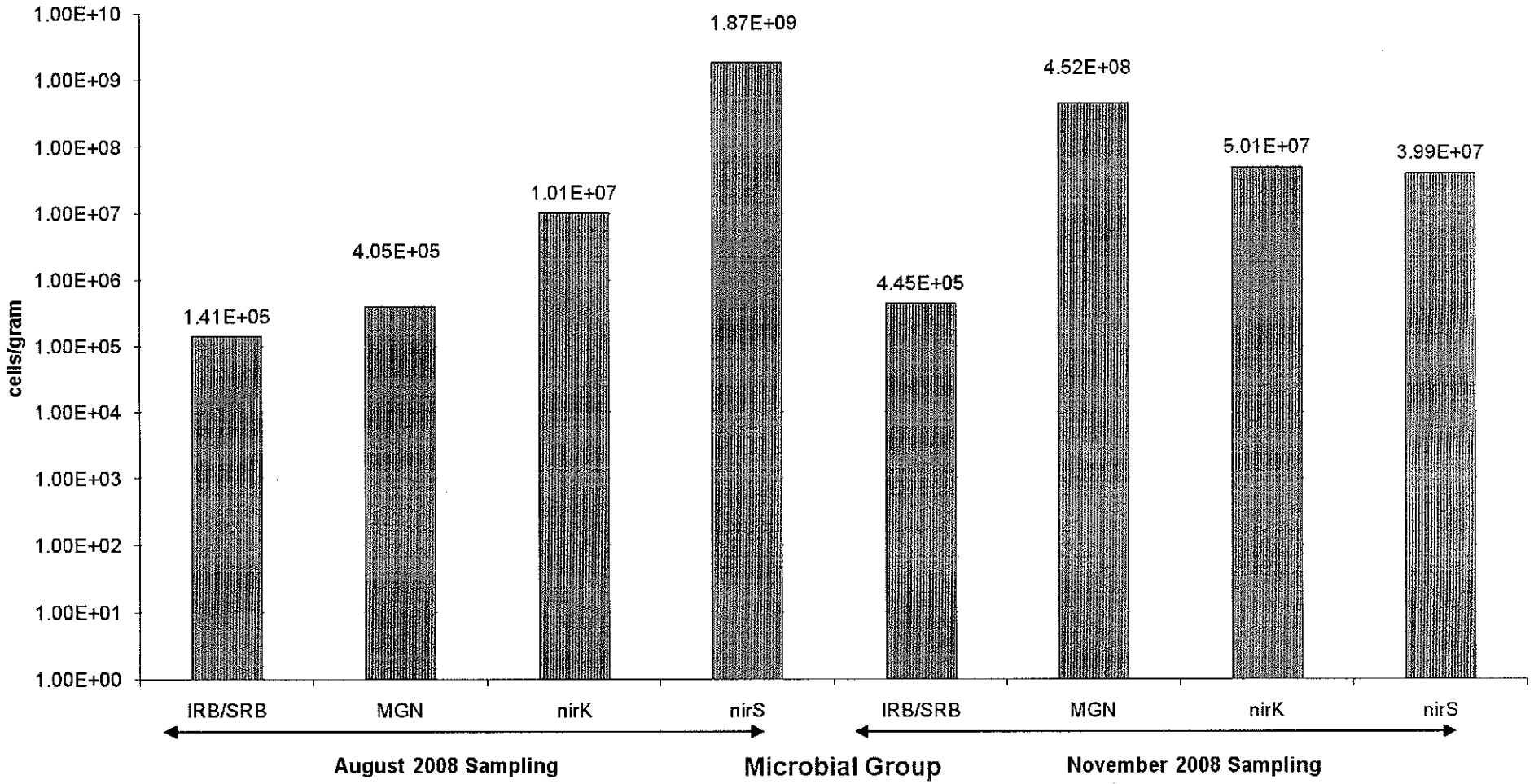

Figure 4.3. Microbes in 1.0 – 1.5 cm Interval of South Deep Sediment, August 22 and November 17, 2008

Honeywell

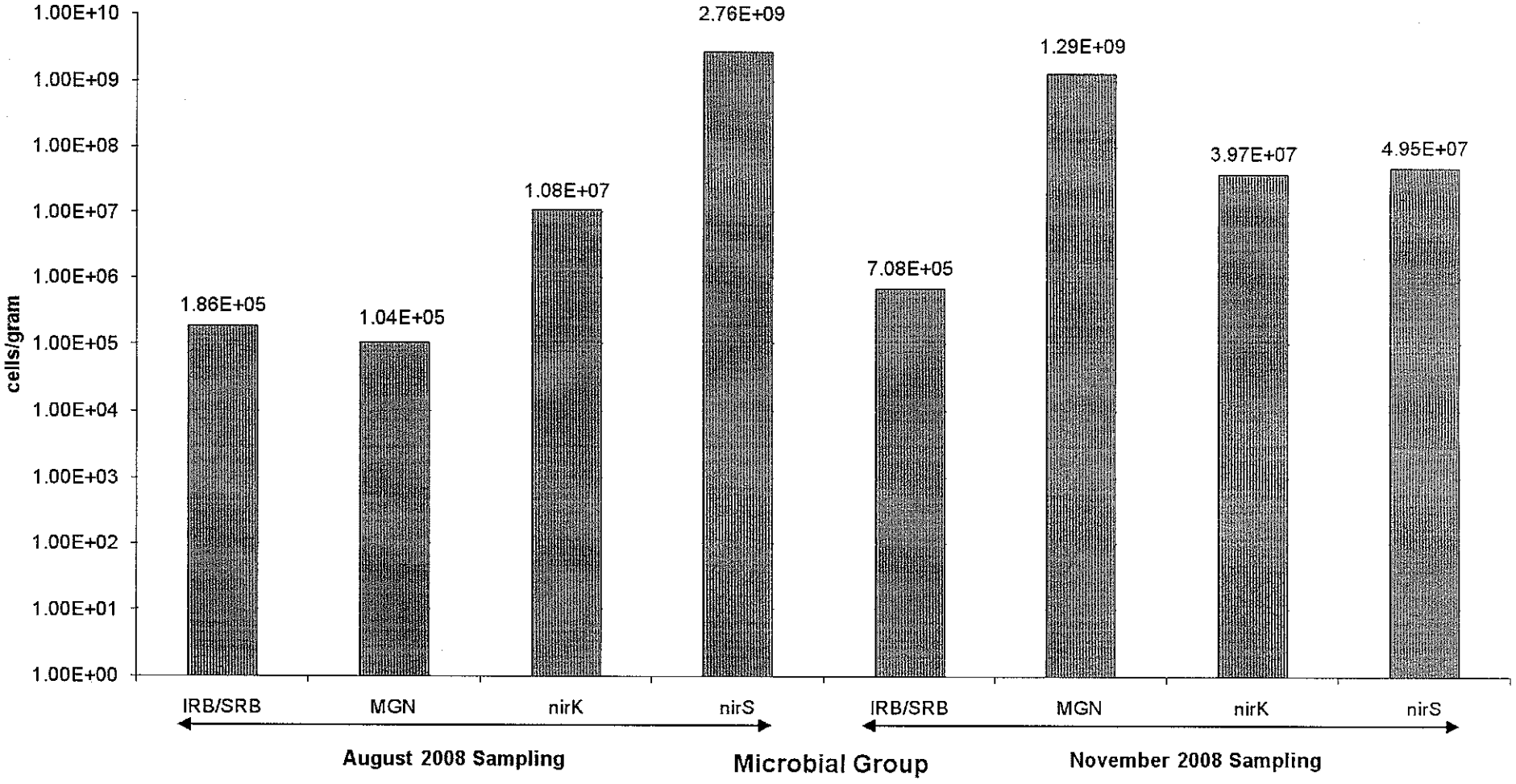

Figure 4.4. Microbes in 1.5 – 2.0 cm Interval of South Deep Sediment, August 22 and November 17, 2008

Honeywell

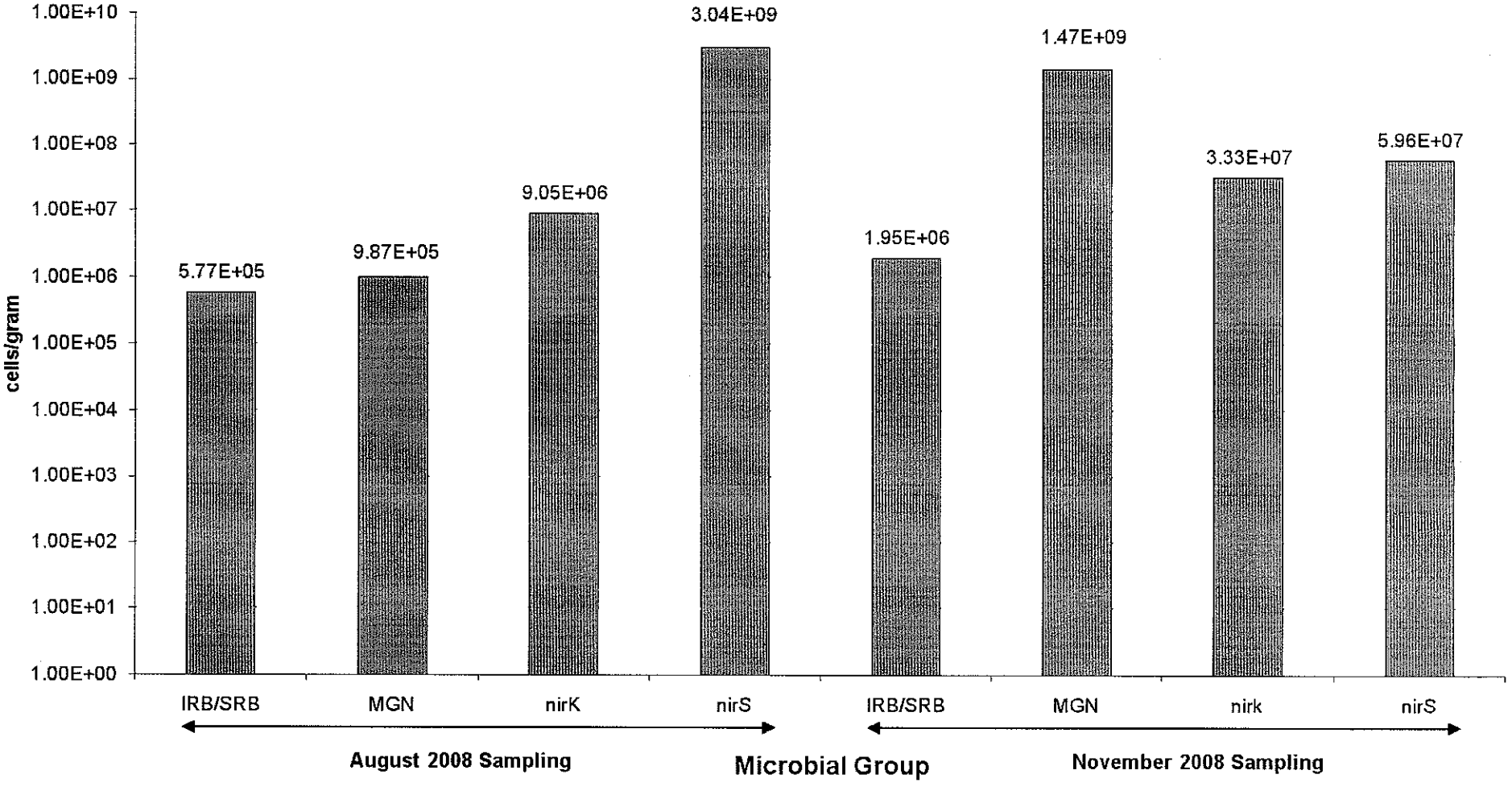

Figure 4.5. Microbes in 2.0 – 4 cm Interval of South Deep Sediment, August 22 and November 17, 2008

Honeywell

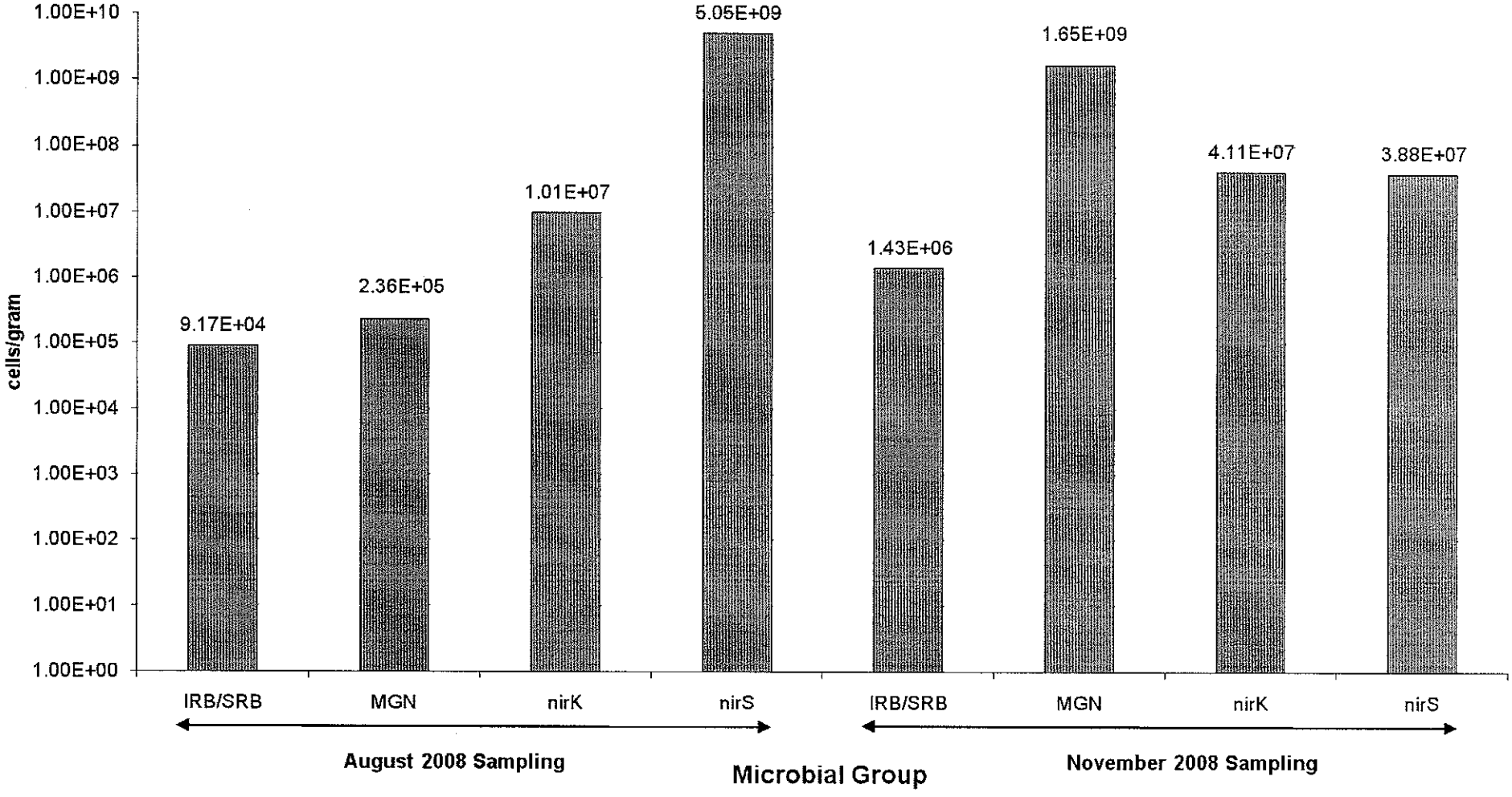

Figure 4.6. Microbes in 4 – 6 cm Interval of South Deep Sediment, August 22 and November 17, 2008

Honeywell

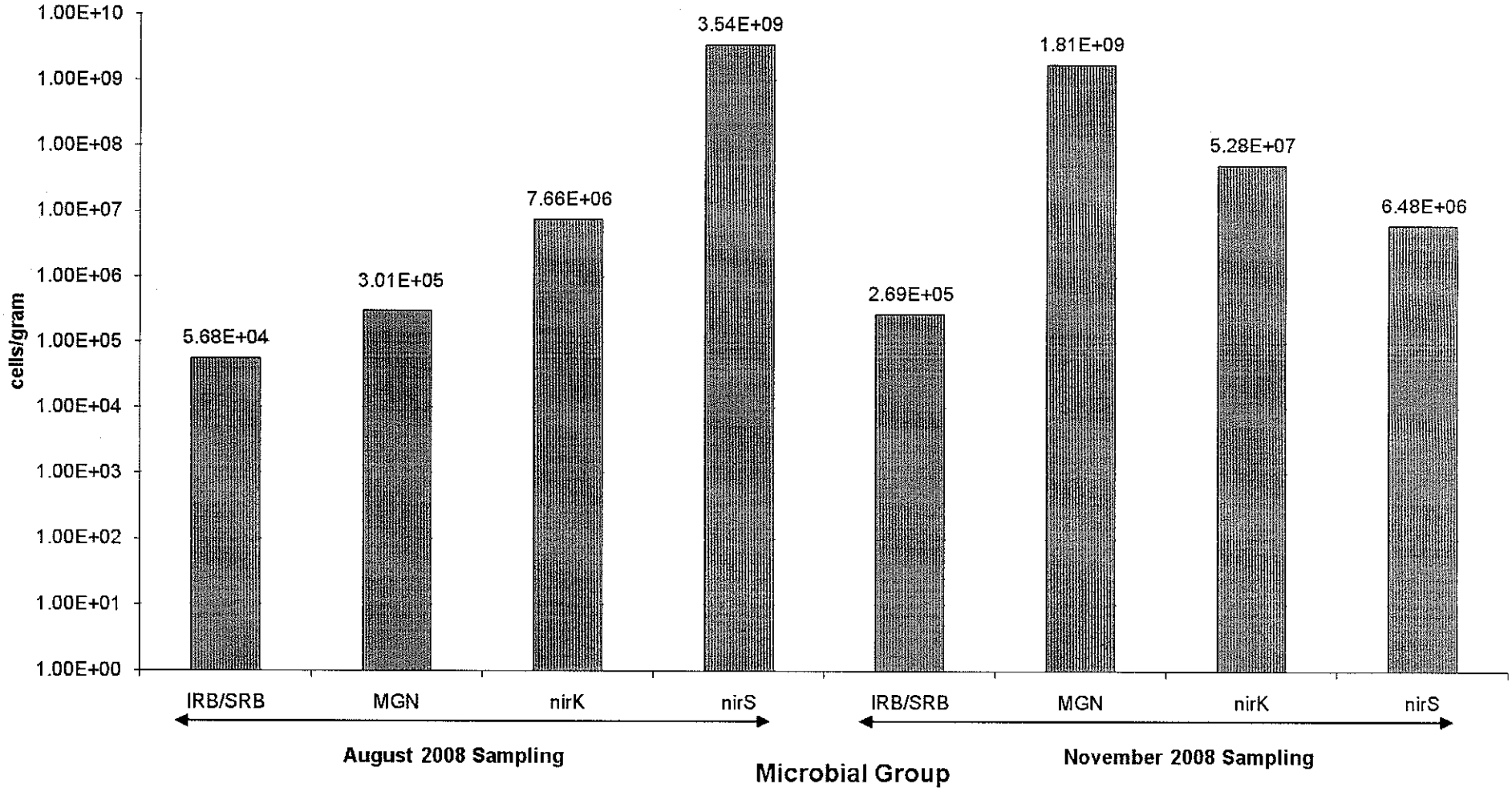

Figure 4.7. Denitrifiers (nirK) by Depth in South Deep Sediment, August 22 and November 17, 2008

Honeywell

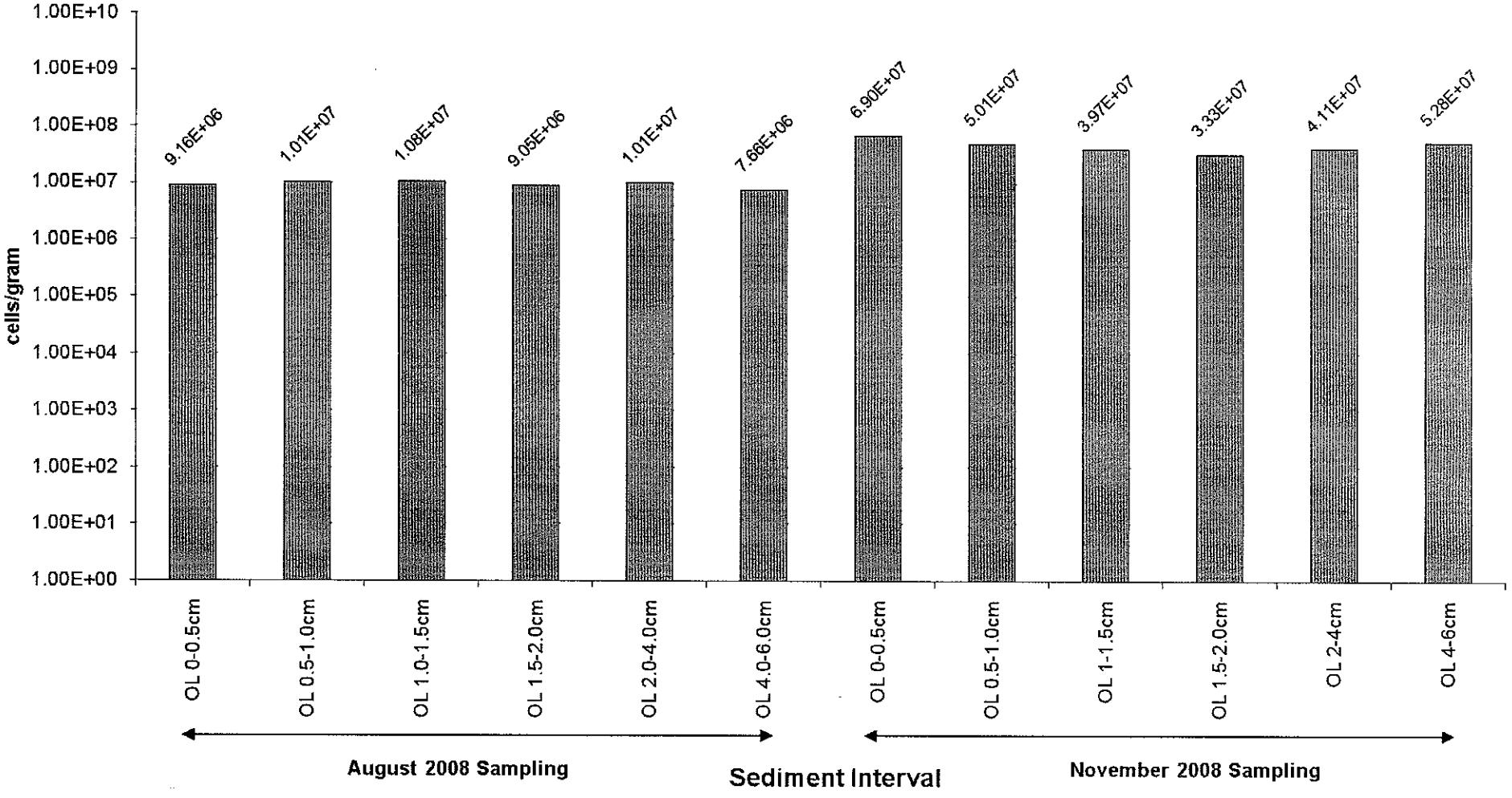

Figure 4.8. Denitrifiers (nirS) by Depth in South Deep Sediment, August 22 and November 17, 2008

Honeywell

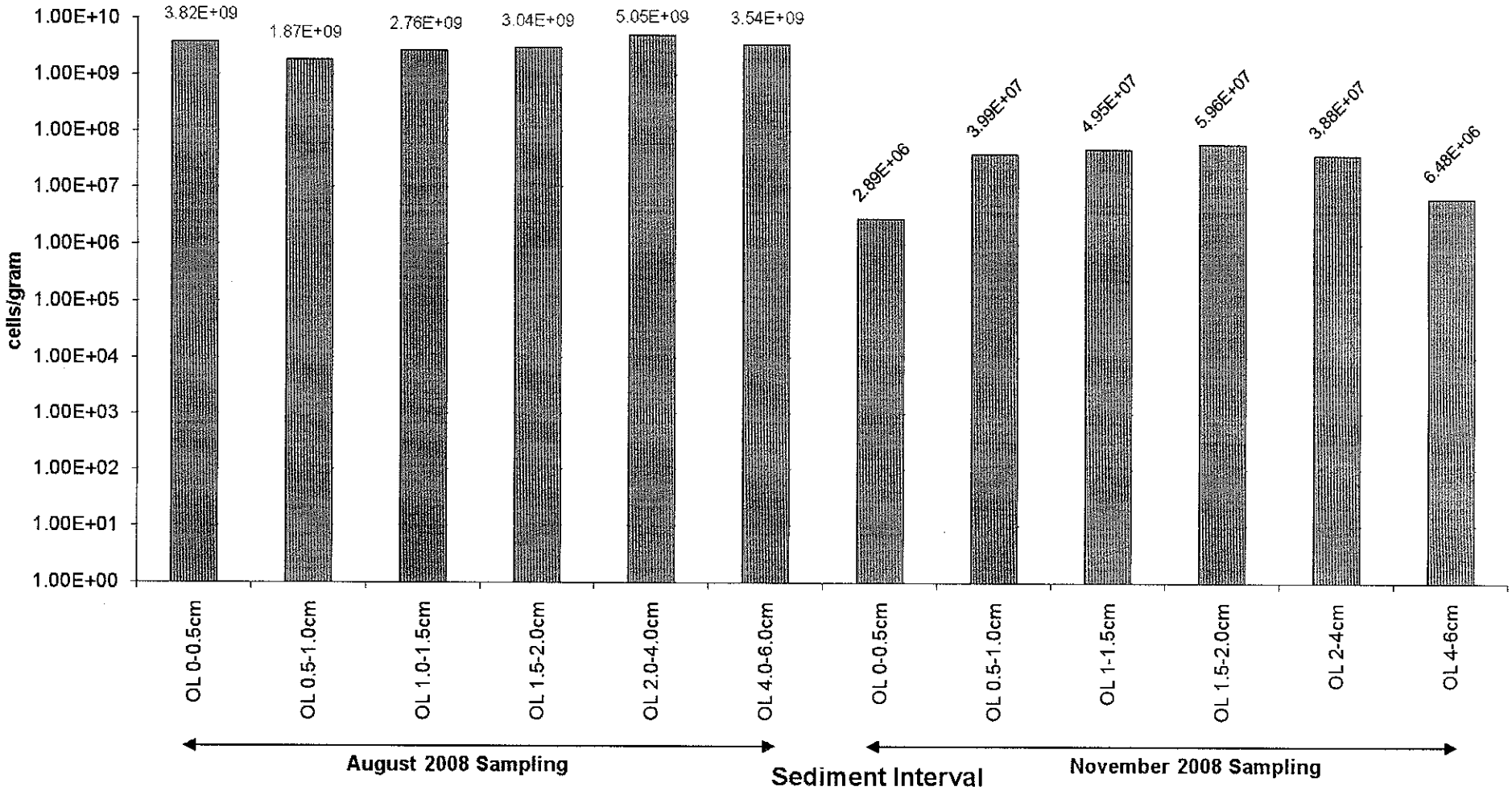

Figure 4.9.Sulfate and Iron Reducing Bacteria by Depth in South Deep Sediment, August 22 and November 17, 2008

Honeywell

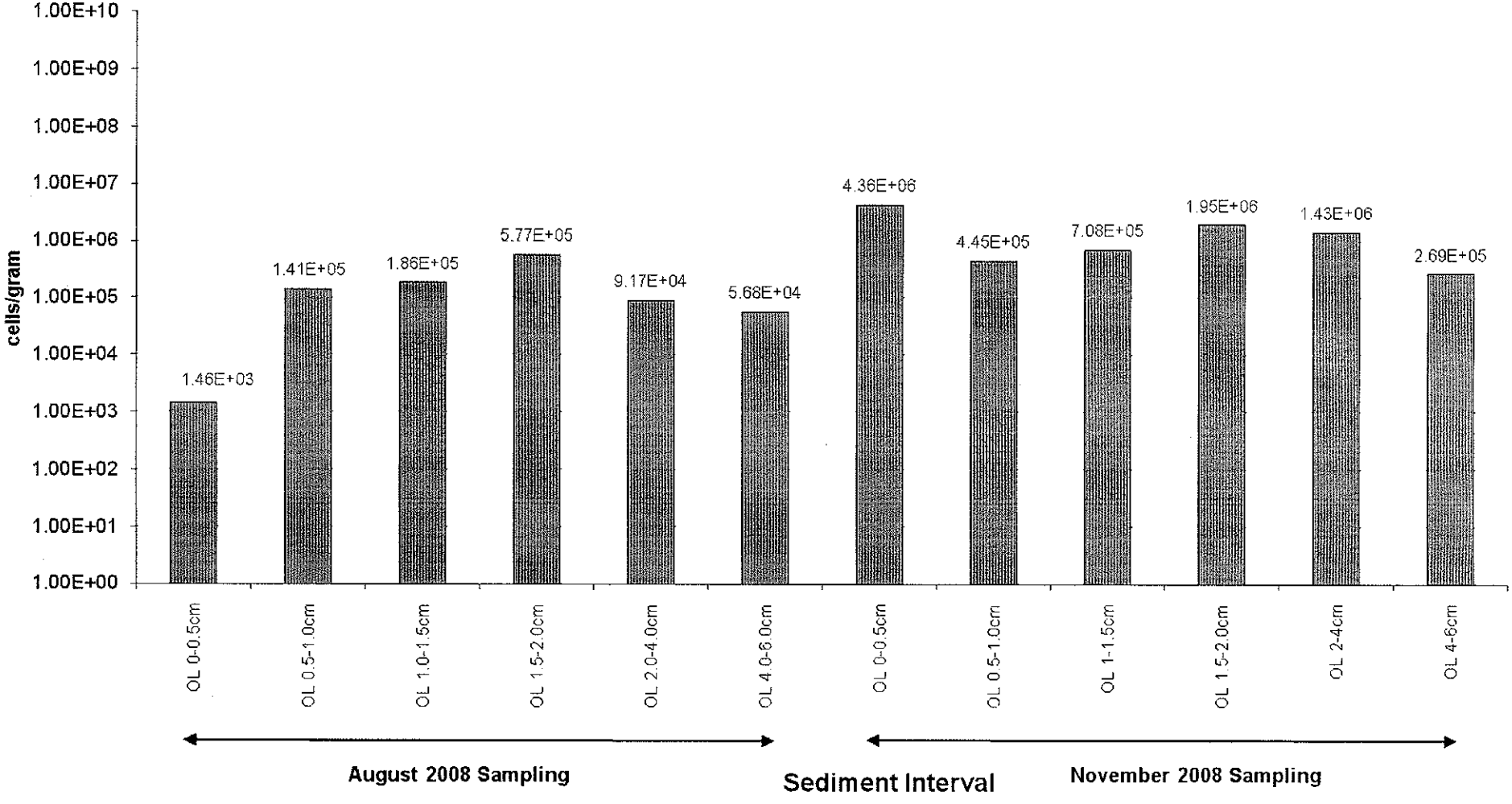

Figure 4.10. Methanogens by Depth in South Deep Sediment, August 22 and November 17, 2008

Honeywell

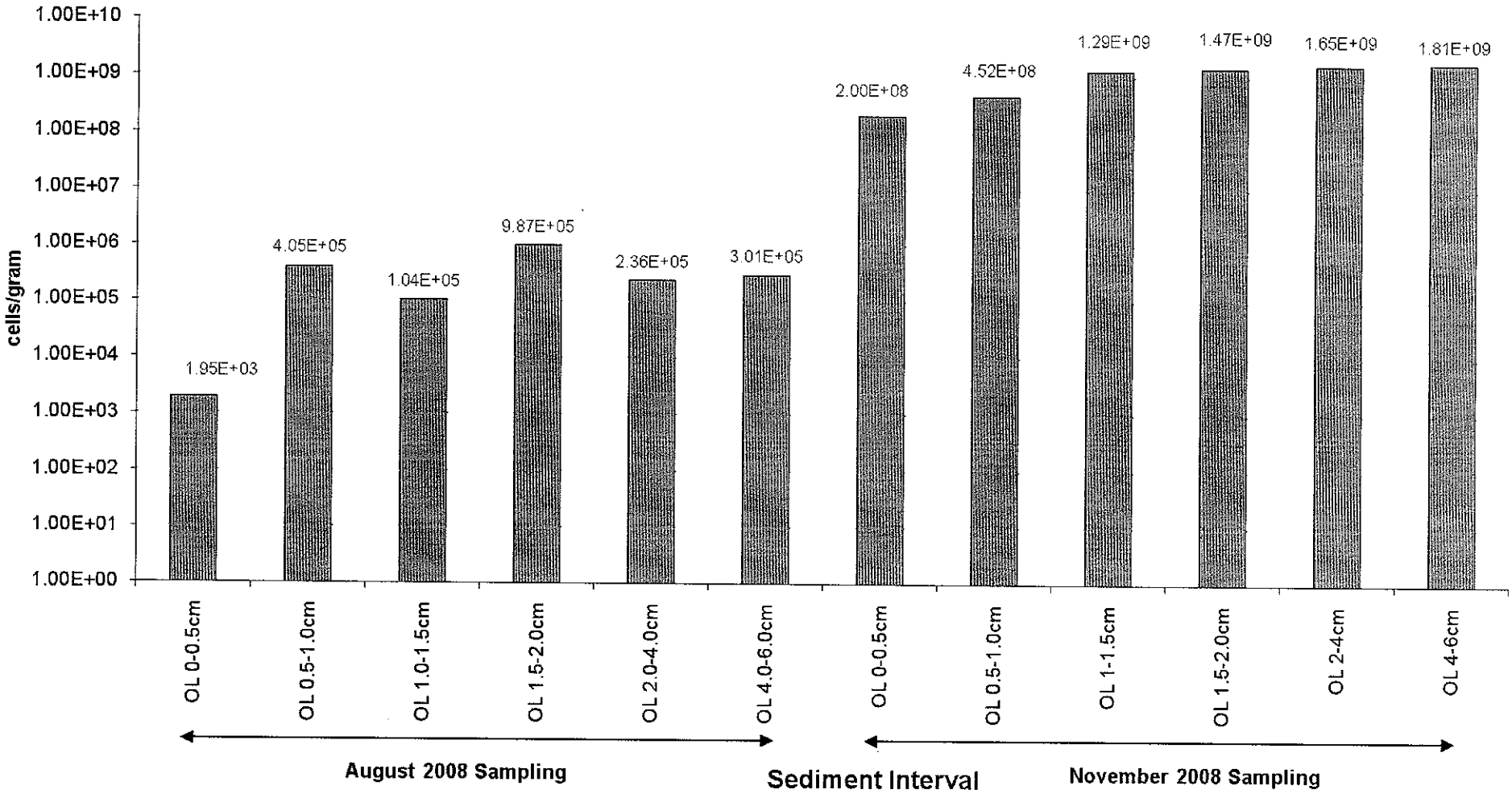

SECTION 5

CONCLUSIONS

This report documents the results of sediment incubations and other studies undertaken to assist in the evaluation of nitrate addition and oxygenation as required in the Record of Decision for the Onondaga Lake Bottom Subsite and the Statement of Work appended to the Consent Decree. The objectives of the work were to establish the efficacy of oxygen and nitrate addition in blocking methylmercury production, the quantities of nitrate and oxygen required to meet sediment demand, and the interplay between conditions in the water column and sediment dynamics.

5.1 METHYLMERCURY FLUX FROM THE SEDIMENTS OF ONONDAGA LAKE, NEW YORK AS DETERMINED USING FLOW-THROUGH SEDIMENT MICROCOSMS

Three experimental treatments, roughly corresponding to the sequential depletion of electron acceptors of Onondaga Lake, were examined: high oxygen – high nitrate, low oxygen plus nitrate and no oxygen – no nitrate. The development of porewater profiles for oxygen, nitrate, sulfide and methylmercury supported the theory of depletion of electron acceptors with depth in the sediment following the pattern oxygen → nitrate → sulfate. Below the zone of sulfate reduction, methanogenesis would be the operative process for organic carbon diagenesis.

The profiles for methylmercury and total sulfide support the hypothesis of co-occurring production within the sulfate reduction zone. The distributions of oxygen and nitrate were consistent with the operating hypothesis that methylmercury produced within the layer of sulfate reduction is sorbed or demethylated within the oxygen and nitrate bands near the sediment surface.

Baseline methylmercury flux from Onondaga Lake sediments to overlying water were estimated using three techniques: hypolimnetic accumulation, porewater gradient calculation and microcosm measurement. The results did not differ significantly from one another. Experiments conducted with zero nitrate and oxygen concentrations ranging from 0.2 – 12.2 $mgO_2 \cdot L^{-1}$ indicated a 92 percent reduction in methylmercury flux from the baseline (no oxygen – no nitrate) condition. There was no trend in flux with increasing oxygen levels, suggesting that the simple maintenance of an aerobic environment is sufficient to control methylmercury flux.

Experiments were conducted with zero oxygen and nitrate concentrations of 0.3 and 1.0 $mgN \cdot L^{-1}$ indicated a 65 percent reduction in methylmercury flux from the baseline (no oxygen – no nitrate) condition. As with the case for oxygen amendment, there was no apparent benefit from the maintenance of increasing nitrate concentrations.

The results of the sediment incubation studies support the concept of oxygen and/or nitrate addition to the hypolimnion of Onondaga Lake to control methylmercury accumulation in the hypolimnion. These results, however, will need to be interpreted in conjunction with water column observations from the ongoing baseline monitoring program as well as results from the nitrate application field trial being conducted during 2009.

5.2 THE FATE OF MERCURY AND NITROGEN IN THE WATER AND SEDIMENTS OF ONONDAGA LAKE

This study provided information on the fate of mercury and nitrogen in the surficial sediments of Onondaga Lake under three different oxidation-reduction regimes: oxic, anoxic, and anaerobic. Methylmercury was produced in the zone of sulfate reduction, as evidenced by maximum porewater methylmercury concentrations and percent mercury as methylmercury in this region. In the oxic treatment, the sulfate reduction zone was below the nitrate reduction zone which was at 0 to 2 cm (0 to 0.8 inch) sediment depth. Under anoxic conditions, when nitrate was still present in overlying water, the nitrate reduction zone occupied the 0 to 1 cm (0 to 0.4 inch) sediment depth interval while both the maximum methylmercury concentrations and the maximum percent mercury as methylmercury were observed between 1 and 2 cm depth, in the zone of sulfate reduction.

Anaerobic conditions (i.e., conditions without oxygen or nitrate) in the overlying water promoted the extension of the sulfate reduction zone to the sediment-water interface and into overlying water. Under these conditions, the average concentration of methylmercury in overlying water was approximately a factor of 10 greater than under oxic and anoxic conditions. Almost 50 percent of mercury was methylmercury in overlying water in the anaerobic treatment compared to nine and five percent, respectively, in the oxic and anoxic treatments. Unlike overlying water, the average methylmercury concentrations in porewater in the anaerobic treatments were not statistically different from the average concentrations observed in the oxic and anoxic treatments.

Regarding the fate of nitrogen in the lake, most nitrate reduction was in the form of complete denitrification to nitrogen gas, with no trend towards increased nitrous oxide or ammonium production even at ten times ambient nitrate concentrations.

5.3 MICROBIOLOGICAL ANALYSES OF SMU 8 SEDMIENT

The microbiological analyses in SMU 8 sediment support the observations made during the sediment incubations and the mercury and nitrogen fate studies. During stratification when the hypolimnion was anaerobic and nitrate was still present in water overlying the sediment, denitrifiers predominated in surface sediments indicating active nitrate reduction occurring in this zone. When nitrate was depleted, iron/sulfate reducers increased in abundance in surface sediment. Methanogens were most abundant when redox potential was low, following oxygen and nitrate depletion. There appears to be a lag time of at least several weeks before sediment re-equilibrates with oxic conditions in overlying water.

APPENDIX A

TESTING AND CALIBRATION OF TURBULENCE LEVELS WITHIN A SEDIMENT OXYGEN DEMAND CHAMBER

By

Peter J. Rusello and Edwin A. Caven
Defrees Hydraulics Laboratory
School of Civil and Environmental Engineering
Cornell University
Ithaca, NY

Testing and Calibration of Turbulence Levels within a Sediment Oxygen Demand Chamber

Peter J. Rusello and Edwin A. Cowen, DeFrees Hydraulics Laboratory
School of Civil and Environmental Engineering, Cornell University, Ithaca, NY

Cornell University
School of Civil and
Environmental Engineering

Abstract

Turbulence at the sediment-water interface can significantly alter the flux of oxygen or other scalars by sharpening gradients in the concentration boundary layer. Prior work examining sediment oxygen demand (SOD) in the hypolimnion of a reservoir in California (Beutel et al., 2007) demonstrated this effect in the laboratory but did not provide any quantitative details on the structure and intensity of the turbulence. Importantly, the applied turbulence field came from a single source, a turbulent round jet, which was not calibrated to levels typically found in the reservoir bottom boundary layer (BBL). Single jets are known to produce strong mean flows that may contribute to, or even dominate, the sediment-water interface exchange. To reproduce calibrated turbulence levels in typical laboratory SOD chambers, the randomly actuated synthetic jet array (RASJA) of Variano and Cowen (2008) was adapted to a provided SOD chamber. Turbulence is generated by randomly changing the direction of three peristaltic pumps, with the time between changes selected from a Gaussian distribution with user controllable mean and standard deviation. Particle Image Velocimetry (PIV) is used to measure the mean and turbulent velocities in the chamber and calibrate pump rotation rate to turbulence intensity. A more thorough investigation of the turbulence structure details some minor shortcomings of the smaller system, particularly at low target turbulence levels, primarily due to the limited number of degrees-of-freedom. Despite these shortcomings, the turbulence generation system is capable of producing the range of expected turbulence levels in the Onondaga Lake BBL and provides a necessary and important tool for the investigation of transport processes at the sediment-water interface.

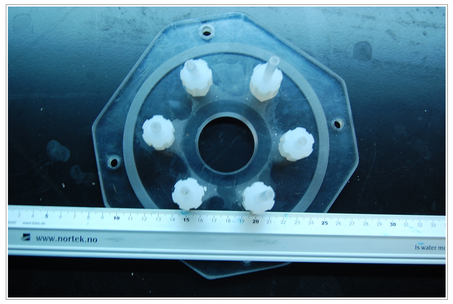

Figure 1: The top of the chamber, with six ports arrayed around the center. The scale on the ruler is in centimeters.

Chamber Design and Control

The turbulent SOD chamber tested is constructed of six inch outer diameter acrylic pipe with acrylic top and bottom plates to allow excellent optical access. An array of six ports is spaced symmetrically on the top plate around the chamber center, approximately 5 cm from the center, 5 cm from nearest neighbors, and 2.5 cm from the outer wall (Figure 1). Three peristaltic pumps (MasterFlex Model 7523-70) are plumbed to the chamber using flexible Tygon tubing, with the ends attached to opposing ports on the chamber top plate. Using the Sunbathe algorithm detailed in Variano and Cowen (2008), the pump direction is changed randomly, with the time between direction changes selected from a Gaussian distribution with user controlled mean and standard deviation. Each pump is set to the same rotation rate as a means of controlling the turbulence intensity. The pump control software permits the inclusion of a flushing cycle during which the pumps do not change direction for a specified amount of time, with the flushing cycle occurring at a user specified interval. For the present case, this was prescribed by the end-user group at Michigan Technological University for two minutes of randomization and one minute of flushing.

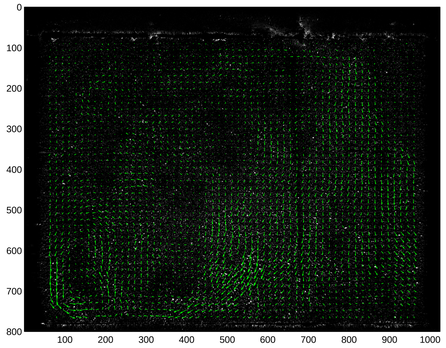

Figure 2: An example instantaneous velocity field determined by the PIV algorithm. Note the small eddies in the bottom left corner of the image.

Velocity Data Collection and Analysis

Velocity data are collected using Particle Image Velocimetry (PIV). PIV provides two velocity components, a radial and vertical velocity, on a 2-D plane located on a diameter of the chamber. Image acquisition, system timing, and pump control were all controlled via The Mathworks MATLAB's Data Acquisition Toolbox. Image pairs were processed using custom code based on cross-correlation of images (Cowen and Monismith, 1997) and including the anti-aliasing spectral continuous window technique of Liao and Cowen (2005) on a 32 x 32 pixel grid, resulting in ∼250 velocity points in the chamber for each image pair. Because of the periodic nature of the flushing and randomization cycle of the pumps, a simple phase decomposition was performed to the velocity time series, where the randomization and flushing portions were treated separately for averaging and turbulent decomposition, i.e. $u(t) = \overline{u} + u'(t)$, where $u(t)$ is the measured velocity, $\overline{u}$ is the phase dependent (random or flushing) time average mean, and $u'(t)$ represents the fluctuation from the mean. The turbulence intensities are represented as root-mean-square (RMS) values of the fluctuations and all velocities are reported in mm/s.

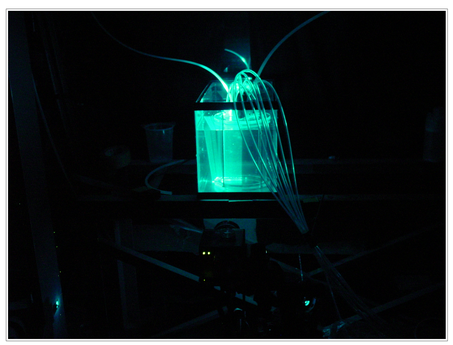

Figure 3: The chamber was placed in a small fish tank to correct distortion caused by the curved chamber walls. The light sheet is being scanned from left to right in ∼6 ms. The camera can be seen in the foreground, with the imaging plane parallel to the light sheet.

Basic Results - A Calibration Curve

After processing, vertical profiles of RMS turbulent intensities were plotted against elevation where an assumption of horizontal homogeneity was invoked and the statistics are averaged in time and space. Variano and Cowen (2008) discuss three regions in their facility, a jet merging region, a homogenous region, and a surface (wall) influenced region. There are similar regions in the SOD chamber (Figure 5) particularly at the 50 and 75 RPM pump speeds, where there is a constant turbulence intensity region lying between $z = 10 - 20mm$ and the wall influenced region occurring for $z < 10mm$. The mean value over $z = 10 - 20mm$ is used for the initial calibration presented here.

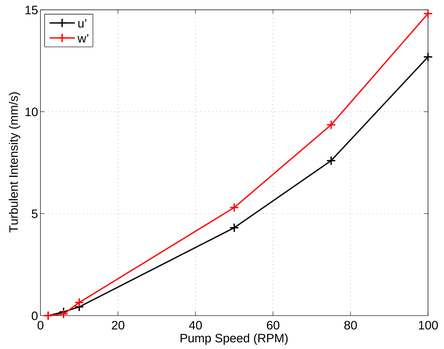

Figure 4: The basic calibration curve of RMS turbulence intensity versus pump speed in RPM.

Velocity Profiles

Assuming horizontal homogeneity, the mean (not shown) and RMS velocity fluctuations (Figure 5) are averaged at vertical levels to examine the vertical structure of the chamber. Unusual forcing is evident at lower pump speeds while the higher pump speeds produce the expected profile.

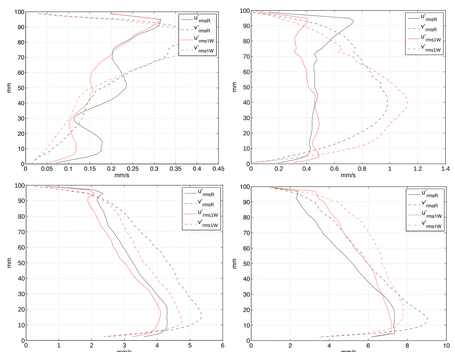

Figure 5: u'_{rms} velocity profiles averaged horizontaly in space and temporally as a function of elevation in the chamber for 6, 10, 50 and 75 RPM (top left to bottom right). Black lines are for the randomized portions of the cycle, red lines for the flushing portion of the cycle.

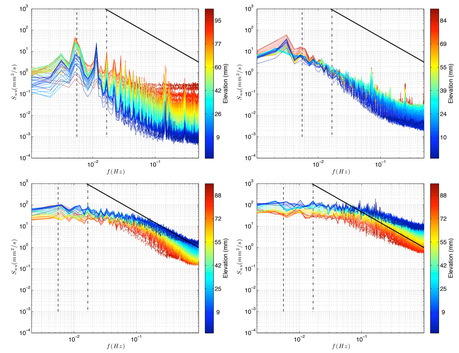

Figure 6: Temporal spectra at 6, 10, 50 and 75 RPM (top left to bottom right). The solid black line has a slope of -5/3, indicative of the inertial subrange. The dashed line (–) represents a frequency of $T = 180s$, the combined length of the random and flushing periods. The dashed-dotted line (-.) marks a frequency of $T = 60s$. Note the large number of peaks in the lower RPM cases. These indicate the randomized direction changes have not generated sufficient turbulence to stir out the individual jet-forced structure in the chamber.

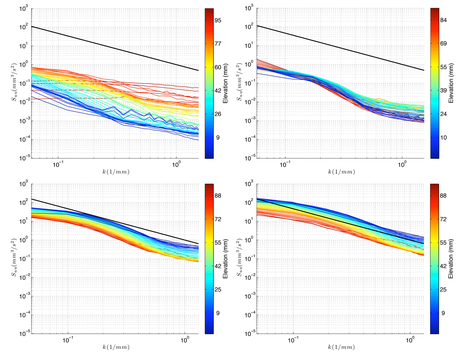

Figure 7: Spatial spectra at 6, 10, 50 and 75 RPM (top left to bottom right). The solid black line has a slope of -5/3, indicative of the inertial subrange. At higher RPM, the flow is turbulent and a roll off into the dissipative range is present.

Turbulence Verification

Temporal spectra are calculated at each interrogation point using the fluctuating velocities (n = 3 subwindows), then spatially averaged at each elevation across the tank (Figure 6). The temporal spectra provides information on the lower frequency motions in the chamber. At low RPM, there are clear peaks at $t = 180, 120,$ and $60s$ and higher frequency harmonics, which is the spectral signature of a square wave with period 3 minutes (i.e. ringing). We believe at these low flow rates the system is responding as a transition between chaotic laminar stirring states, one random and one unidirectional. Looking at the spectra the flow is not turbulent at modest to higher frequencies nor at any wavenumber (Figure 7).

Spatial spectra are calculated for each data set at vertical levels and averaged in time (Figure 7). Spatial spectra provide information on the high frequency motions in the tank. Here the spectra are much smoother due to the increased availability of temporal data for averaging. While the 6 and 10 RPM spectra appear to show some -5/3 behavior the energy level is decades lower than the 50 and 75 RPM case suggesting that this is not turbulence capable of stirring. At higher RPM a clear inertial subrange rolling off into the dissipative range is present.

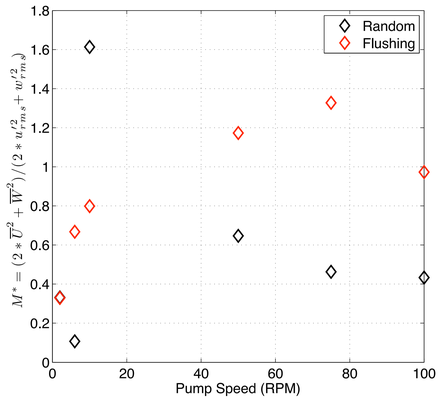

Figure 8: M^*, a ratio of the mean and turbulent energy in the tank, versus pump speed. This value is computed by averaging spatially over $z = 10 - 20mm$ and all x using temporally averaged mean flow values and the RMS fluctuations. At higher pump speeds this ratio stabilizes but is still high. The outlier for the randomized data at 10 RPM is due to the persistence of the individual jet forcing and its bias of the mean to higher values.

Chamber Performance

An important metric when examining chamber performance is the ratio of the mean velocity to the turbulent RMS velocity, a quantity termed M^* by Variano and Cowen (2008). Using the turbulent intensities from the calibration curve and the mean flow from the same region and averaged in the same manner (an RMS value averaged in vertical layers, then averaged over $z = 10 - 20mm$), M^* for both radial and vertical components is calculated (Figure 8). For comparison, Variano and Cowen (2008) report M^* in their facility < 0.1.

We attribute the high M^* values to the limited number of momentum sources and the coupled nature of those sources in setting up persistent circulation cells – leading to really only 3 degrees of freedom compared to Variano and Cowen (2008) who utilized 64 degrees of freedom. The short time between flushing cycles relative to the length of the flushing cycle also plays a part, as mean flow increases during the flushing periods. A larger number of momentum sources would permit a more dense spatial distribution leading to a wider range of energy injection length and time scales and likely reduce M^*.

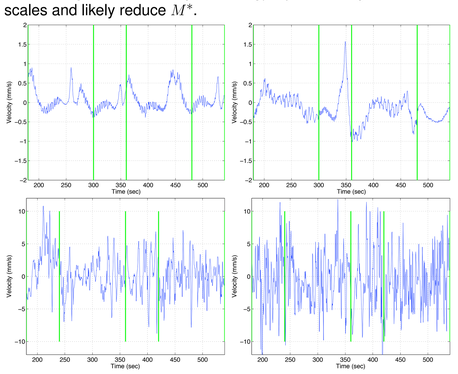

Figure 9: Example time series of radial velocities from a mid-elevation. vertical green lines denote the approximate location of cycle change from flushing to randomization. Note the unusual flow generated at lower pump settings. The higher frequency periodic components apparent in the 6 and 10 RPM cases are likely due to the direct forcing by individual changes in pump directions – the lack of turbulence allows these signatures to dominate the flow. In comparison, the 50 and 75 RPM cases reveal a typical example of a fully turbulent flow.

References

Beutel, M., I. Hannoun, J. Pasek, and K. B. Kavanagh, 2007: Evaluation of hypolimnetic oxygen demand in a large eutrophic raw water reservoir, San Vicente Reservoir, Calif. *Journal of Environmental Engineering*, **133**, 130–138.

Cowen, E. and S. Monismith, 1997: A hybrid digital particle tracking velocimetry technique. *Experiments in Fluids*.

Liao, Q. and E. Cowen, 2005: An efficient anti-aliasing spectral continuous window shifting technique for PIV. *Experiments in Fluids*.

Variano, E. and E. Cowen, 2008: A random jet stirred turbulence tank. *Journal of Fluid Mechanics*, **604**, 1–32.

APPENDIX B

ELECTRON ACCEPTOR ADDITION AND THE REGULATION OF AMMONIA AND PHOSPHORUS FLUX

APPENDIX B

ELECTION ACCEPTOR ADDITION AND THE REGULATION OF AMMONIA AND PHOSPHORUS FLUX

Prepared For:

Honeywell

Prepared By:

Michigan Technological University

and

Upstate Freshwater Institute

APRIL 2010

Electron Acceptor Addition and the Regulation of Ammonia and Phosphorus Flux From The Sediments of Onondaga Lake, New York

Addendum to Data Report: Sediment Incubations and Supporting Studies for Onondaga Lake Sediment Management Unit (SMU) 8

Martin T. Auer[1], G. Albert Galicinao[1], B.J. Ellefson[1], David A. Matthews[2] and Steven W. Effler[2]

[1] Michigan Technological University
[2] Upstate Freshwater Institute

14 April 2010

TABLE OF CONTENTS

LIST OF FIGURES

SECTION 1

SUMMARY AND CONCLUSIONS

A series of intact sediment core incubations were performed using flow-through sediment flux chambers to evaluate the efficacy of electron acceptor augmentation with oxygen and nitrate on the release of ammonia and phosphorus from Onondaga Lake sediments. Electron acceptor concentrations were maintained at the levels (2 mg nitrate-nitrogen (NO_3-N) per liter and 2 mg of oxygen (O_2) per liter) used in companion studies of methylmercury release (Exponent et al., 2009). Neither electron acceptor had a significant impact on ammonia flux, with the observed fluxes being comparable to those for unamended control incubation. Oxygen likely did not have an effect because levels were too low to support active populations of nitrifying bacteria, the primary mechanism for eliminating ammonia flux. There is no known mechanism for inhibition of ammonia flux by augmentation with nitrate. Both electron acceptors were effective in inhibiting phosphorus flux, yielding negligible rates of release. The mechanism here, in both cases, is believed to be related to mediation of redox levels and the attendant response of the ferrous-ferric iron system. Phosphorus release was initiated following cessation of electron acceptor augmentation, reaching or approaching flux levels observed in the unamended control incubation. This demonstrates that the cores in which inhibition was observed displayed the potential to yield unrestricted release of phosphorus. It is concluded that, when oxygen and nitrate levels both decline to near zero, electron acceptor amendment with either nitrate (at 2 mg NO_3-N per liter) or oxygen (at 2 mg O_2 per liter) will effectively inhibit phosphorus release. Neither amendment would be expected to impact ammonia release.

SECTION 2

ELECTRON ACCEPTOR AMENDMENT AND THE REGULATION OF CHEMICAL FLUX

The addition of electron acceptors (nitrate and/or oxygen) to the hypolimnion of lakes has been identified as a means of controlling the flux of methylmercury as needed from the sediments of mercury-contaminated Onondaga Lake. Methylmercury is produced in the sediment at locations supporting active microbial sulfate reduction. The operative principle for controlling methylmercury flux from sediment to overlying water is to maintain the presence of sediment microlayers rich in nitrate or oxygen where the biogeochemical processes (e.g. demethylation and sorption) inhibiting transport of methylmercury to the sediment-water interface are favored. Several of the biogeochemical processes associated with organic carbon diagenesis are influenced by redox conditions and it is thus reasonable to expect that fluxes other then methylmercury, e.g. ammonia and phosphorus, may be influenced by maintaining electron acceptor levels through amendment. The purpose of this report addendum is to quantify effects of electron acceptor addition on ammonia flux and phosphorus flux from the sediment when oxygen and nitrate levels in overlying hypolimnetic waters approach zero. Work reported herein is part of the sediment incubation work conducted for Honeywell by Michigan Technological University, Upstate Freshwater Institute, and Syracuse University in accordance with a work plan approved by the New York State Department of Environmental Conservation (Parsons et al., 2007) and as part of pre-design work for the Onondaga Lake Bottom remediation effort.

SECTION 3

THE BIOGEOCHEMICAL BASIS FOR REGULATION OF AMMONIA AND PHOSPHORUS FLUX

Although both ammonia and phosphorus fluxes are potentially impacted by redox conditions, the underlying biogeochemistry differs considerably for the two processes. Ammonia is introduced to the sediment pore water through the diagenesis of particulate organic nitrogen (PON) reaching the lake bottom through sedimentation. In highly productive systems such as Onondaga Lake, most of the PON deposited at the sediment-water interface is in the form of detrital algae. Concentrations of ammonia are typically higher at depth within the sediment than at the sediment-water interface where mixing with hypolimnetic waters reduces ammonia levels. The result is a concentration gradient which promotes ammonia diffusion from the sediment to the water, i.e. an ammonia flux (see Wickman, 1996). When the sediment surface microlayer contains oxygen concentrations sufficient to support nitrifying bacteria, the ammonia diffusing to the surface is converted to nitrite and then nitrate (nitrification) which may subsequently participate in reactions within the microlayer or diffuse from the sediments (Pauer and Auer 2000). In the absence of an oxic surface microlayer, nitrifying bacteria are absent and the ammonia simply diffuses across the sediment-water interface and accumulates within the hypolimnion. Ammonia in the water column is a nutrient supporting algal growth, can be toxic to aquatic life and, when oxidized, consumes oxygen. Thus management of ammonia and its release from the sediments is often an objective of water quality restoration efforts.

In contrast to the microbially-mediated case of ammonia, the flux of phosphorus across the sediment-water interface is chemically controlled through the interplay of redox conditions and iron chemistry. The mobility of phosphorus in lake sediments is governed by the presence of hydrous iron oxides possessing solid surfaces that adsorb phosphorus (Penn et al., 2000). The environmental chemistry of these oxides is such that their formation is greatly favored under oxidizing redox conditions where ferric (Fe^{3+}) iron predominates. Oxide formation is not favored under reducing conditions where ferrous (Fe^{2+}) is dominant and, as a result, soluble phosphorus accumulates in the porewater. Phosphorus and ferrous iron gradients developing in the porewater support a flux of these chemical species across the sediment-water interface (i.e., from sediment to overlying water). The redox conditions, through the ferric-ferrous iron couple, serve as a gatekeeper for phosphorus flux from the sediments. Internal loads of phosphorus, generated in this manner, have been known to retard efforts to restore lakes impacted by eutrophication.

Given the biogeochemical foundation of ammonia and phosphorus fluxes, i.e. their association with redox conditions, it is reasonable to suggest that their flux across the sediment-water interface may be amenable to control through electron acceptor augmentation.

SECTION 4

TASK SPECIFIC OBJECTIVES AND APPROACH

The objective of this work is to evaluate the utility of electron acceptor augmentation, at the levels required to achieve the desired effect on methylmercury flux, in controlling the flux of ammonia and phosphorus across the sediment-water interface. This work was accomplished using bench-scale sediment microcosms. Specifically, the objective was to:

- Quantify the flux of ammonia and phosphorus from the sediments of Onondaga Lake under conditions of electron acceptor augmentation (2 mg O_2 per liter, 2 mg NO_3-N per liter) for control of methylmercury flux and to compare those fluxes with the rates characteristic of an un-augmented environment (0 mg O_2 per liter, 0 mg NO_3-N·per liter).

This objective was accomplished through a continuous, long-term incubation simulating in-lake conditions where electron acceptors are sequentially maintained: (a) in abundance, (b) at augmentation levels and (c) in the depleted state.

SECTION 5

METHODS AND MATERIALS

Sediments were collected from the South Deep depositional basin of Onondaga Lake in May 2009 with a box corer (Model 1260, Ocean Instruments, Inc., San Diego, CA). The South Deep basin (maximum depth, 19 meters or 62 feet) is considered to be representative of conditions in the remainder of the lake's profundal zone (Effler, 1996) and was the site for collections supporting previous studies of ammonia (Wickman, 1996) and phosphorus (Auer et al., 1993; Penn et al. 2000) flux. Teflon containers (10 centimeters (4 inches) in diameter by 30 cm (12 inches) tall; Savillex Corporation) were used to subsample the box core, yielding approximately 7 centimeters (3 inches) of hypolimnetic water over 12 centimeters (5 inches) of sediment. Upon collection, sediment samples were placed in an ice chest and transported to the laboratory for storage at 4 °C until used. Particular care was taken to minimize disturbing the sediment-water interface during box coring and transportation to the laboratory.

A microcosm approach to laboratory determination of flux across the sediment-water interface using a completely-mixed flow reactor was applied here as described in Parsons et al. (2007). The sediment microcosm consisted of a cylindrical Teflon container, 10 cm (4 inches) in diameter by 30 cm (12 inches) tall, outfitted with opposing inlet-outlet ports located approximately 2 centimeters (1 inch) below the top rim (Figure B.1). The microcosm was filled with 7 centimeters (3 inches) of hypolimnetic water over 12 centimeters (5 inches) of sediment, leaving approximately 11 centimeters (4 inches) of headspace. A friction fit Teflon^{R} bottom provides a seal against leakage following sample collection. A threaded Teflon top is outfitted with six peripheral ports to provide mixing and a single, central port where gas may be introduced.

Artificial lake water (ALW), with an ionic composition similar to that of Onondaga Lake (Exponent et al., 2009), served as feed stock to the reactor with the rate of input regulated by a peristaltic pump. In its unamended state, the artificial lake water does not contain ammonia, nitrate or phosphorus, and gases are at levels dictated by the ambient environment. The impact of nitrate on chemical flux was examined by adding nitrate to the feed stock and then adjusting the feed stock flow rate until the desired nitrate concentration was achieved. Gas was bubbled into the microcosm as a means of regulating redox conditions. Air (for oxygen saturation), a mixed gas (nitrogen gas with 5 percent hydrogen and 1,600 parts per million (ppm) carbon dioxide; for anoxic conditions) or an air-mixed gas combination (to establish 2 mg O_2 per liter; digital gas mixer Mix 1000 model, Applied Analytics, Inc.) were utilized depending on the desired condition. Mixing in the microcosm was provided by three re-circulating channels (Teflon tubes; six ports) attached to a computer-controlled peristaltic pump. The pump was set at a re-circulating rate that provided random mixing at a turbulence level comparable to that observed at the sediment-water interface of Onondaga Lake (Exponent et al., 2009, Appendix A). All experiments were conducted in a temperature-controlled room or incubator maintained at 8°C, a representative hypolimnetic temperature for Onondaga Lake. Ammonia and phosphorus flux

were determined in three single incubations: (a) in the absence of nitrate and oxygen, (b) with nitrate only added and (c) with oxygen only added. Where experimental conditions required the absence of oxygen, experiments were conducted in an anaerobic chamber (mixed gas; Coy Laboratory Products). The maintenance of anoxic conditions within the chamber was confirmed through daily monitoring.

The theory of microcosm operation establishes that chemical flux may be calculated once the system has reached steady state, i.e. chemical conditions in the effluent stream are unchanged with respect to time. The achievement of steady-state conditions was established by monitoring of nitrate (Thermo Fisher Scientific Inc., Model 9707BNWP Ionplus® Nitrate Combination Electrode) and oxygen (Hach Model LBOD 10101 luminescent dissolved oxygen probe) in the chamber effluent. Once effluent conditions indicated steady state condition, effluent samples were collected daily for five days and composited. Subsamples were collected and filtered (0.45 micron disc filter, Vipor Inc.) daily, placed in glass (phosphorus) or plastic (ammonia) vials and stored temporarily at 4ºC. Daily subsamples collected over a 5-day interval were composited to yield a weekly sample and frozen prior to shipment to Upstate Freshwater Institute for analysis (ammonia by U.S. EPA, Method 350.1 Rev. 2.0, O'Dell 1993 and phosphorus by Standard Methods, 20th Edition, Method 4500-PE, APHA 1998).

Chemical fluxes are calculated by assuming that the sediment microcosm is a completely-mixed flow reactor. The mass balance on that reactor may be given as,

$$V \cdot \frac{dC}{dt} = Q \cdot C_{in} - Q \cdot C + J \cdot A \qquad (1)$$

where:

V = microcosm volume, m^3

Q = feed stock flow rate, $m^3 \cdot d^{-1}$

C = microcosm ammonia-nitrogen (NH_3-N) or phosphorus (P) concentration, mg per cubic meter

C_{in} = influent NH_3-N or P concentration, mg·per cubic meter

J = NH_3-N or P flux, mg·per square meter per day

A = area of the sediment surface, square meters

Given that the ammonia and phosphorus concentrations in the influent (i.e., the artificial lake water) are zero and that, at steady-state, dC/dt = 0, Equation 1 becomes,

$$J = QC_{ss} / A \qquad (2)$$

Thus, at steady state, the ammonia or phosphorus flux may be calculated as a function of the flow, the steady state effluent ammonia or phosphorus concentration (C_{ss}) and the sediment surface area of the reactor.

SECTION 6

RESULTS AND DISCUSSION

6.1 BASELINE CONDITIONS – NO NITRATE OR OXYGEN ADDED

The reactor not receiving electron acceptor augmentation, colloquially termed the 'nono' condition provides a baseline with which to compare the efficacy of nitrate and oxygen addition in reducing ammonia and phosphorus flux. The baseline condition simulates the interval of anaerobic conditions in the hypolimnion anoxia of the lake, i.e. where both oxygen and nitrate have been depleted and ammonia and phosphorus diffuse readily from the sediment. The sediment flux chamber used for the baseline condition was incubated in the anaerobic chamber and fed with artificial lake water containing neither nitrate nor oxygen. Concentrations of nitrate and oxygen in this chamber dropped rapidly over a 30-day equilibration period approaching the limit of detection well before flux sampling commenced. Once strongly reducing conditions were established, interferences prevented additional nitrate monitoring. However, given knowledge that nitrate had been depleted from this reactor and that no nitrate was added over the course of the experiment, it is reasonable to conclude that the system remained nitrate-free. Oxygen concentrations remained at zero mg O_2 per liter over the course of the incubation (Figure B.2a). Flows were reasonably constant (0.4 to 0.5 liter per day) over the course of the incubation (Figure B.2a).

The baseline ammonia and phosphorus fluxes, averaged over the 7 weeks of incubation (Figures B.2b and B.2c), were 18.0±3.0 mg NH_3-N per square meter per day and 5.2±1.6 mg P per square meter per day, respectively. As points of reference, these fluxes are significantly less than those measured for Onondaga Lake sediments by Wickman (1996; 78.0 mg NH_3-N per square meter per day in 1995), Auer et al. (1993; 13.3 mg P per square meter per day in 1987) and Penn et al. (2000; 10.0 mg P per square meter per day in 1992). These reduced fluxes are consistent with the projected response of the system to reduced phosphorus loadings and attendant rates of primary production and organic matter deposition.

6.2 ELECTRON ACCEPTOR AUGMENTATION – NITRATE ADDITION

The reactor simulating electron acceptor augmentation with nitrate was operated at a steady state nitrate concentration of 2.0±0.2 mg NO_3-N per liter (Figure B.3a). This level is comparable to that present in the hypolimnion of Onondaga Lake at the onset of thermal stratification and was one of the nitrate levels tested in examining the impact of electron acceptor augmentation on methylmercury flux (Exponent et al. 2009). Following 4 weeks of incubation, nitrate addition was discontinued and the system allowed to assume a steady state equivalent to that of the no nitrate – no oxygen baseline reactor. Oxygen was absent from the reactor (Figure B.3a) and flows remained relatively constant, ranging from 0.5 to 0.6 liter per day, over the course of the incubation (Figure B.3a).

The ammonia flux in the nitrate-added reactor (Figure B.3b) averaged 25.8±2.5 mg NH3-N·per square meter per day for the 4 weeks during which nitrate was added and 24.2±7.4 mg NH3-N per square meter per day during the 3 weeks simulating no nitrate – no oxygen conditions . The ammonia flux in the nitrate added reactor (Figure B.3b) was significantly ($p<0.001$) higher than that observed in the no nitrate-no oxygen reactor (Figure B.2b). It is concluded from this that electron acceptor augmentation with nitrate, at a nominal concentration of 2 mg N per liter has no inhibitory effect on ammonia flux from Onondaga Lake sediments (as expected because there is no candidate biogeochemical sink for achieving such an effect). The fact that nitrate addition (Figure B.3b) yielded fluxes higher than the no nitrate-no oxygen control (Figure B.2b) suggests an additional source of ammonia such as dissimilatory nitrate reduction (DNRA, NO3 → NH3). The fact that the ammonia flux in the nitrate-added reactor fell, when nitrate addition was discontinued, to levels comparable to those observed for the no-nitrate – no oxygen reactor, suggests the DNRA ammonia source was lost after this step (Figure B.3b). The lag in the DNRA response (weeks 5 and 6 in Figure 3b) is similar to that noted in other sediment microcosm incubations.

The average phosphorus flux in the nitrate-added reactor for the 4-week period of electron acceptor augmentation was 0.2±0.1 mg P per square meter per day (Figure B.3c), significantly ($p<0.001$) lower than the no nitrate – no oxygen flux. This flux is considered negligible and reflects essentially complete inhibition of phosphorus flux. Over the 3 weeks following cessation of nitrate addition, the phosphorus flux increased from 0.1 to 1.9 mg P per square meter per day. It is anticipated that the phosphorus flux would have continued to increase had the incubation period been extended, approaching the flux attained in the no nitrate-no oxygen reactor. It is concluded from these results that electron acceptor augmentation with nitrate, at a nominal concentration of 2 mg N per liter, is effective in inhibiting phosphorus flux from the sediments of Onondaga Lake.

6.3 ELECTRON ACCEPTOR AUGMENTATION – OXYGEN ADDITION

The reactor simulating electron acceptor augmentation with oxygen was operated at saturation for the first week, spent a week in transition and stabilized at a steady state oxygen concentration of 2.0 mg O_2 per liter, remaining there for two weeks (Figure B.4a). Saturation concentrations are comparable to levels present in the hypolimnion of Onondaga Lake at the onset of thermal stratification, while the steady state concentration corresponds to one of the oxygen levels tested in examining the impact of electron acceptor augmentation on methylmercury flux (Exponent et al. 2009). Following four weeks of incubation, oxygen addition was discontinued and the system allowed to assume a steady state equivalent to that of the no nitrate – no oxygen baseline reactor. Flows remained relatively constant, ranging from 0.3 to 0.4 liter per day, over the course of the incubation (Figure B.4a).

The ammonia flux in the oxygen-added reactor averaged 9.4±4.4 mg NH_3-N per square meter per day for the four weeks of oxygen augmentation and 20.9±3.1 mg NH_3-N per square meter per day for the three weeks simulating no nitrate – no oxygen conditions (Figure B.4b). The ammonia flux was low initially, but climbed steadily over the course of the incubation, reaching a plateau with a rate in the last two weeks (Figure B.4b) comparable to that achieved in

the no nitrate-no oxygen reactor. It is inferred from this response that nitrifying bacteria were initially present (flux less than 5 mg NH_3-N· per square meter per day), but were not sustained at the level of oxygen augmentation used here. Beutel (2006) observed that oxygenation at concentrations of 7 to 8 mg O_2 per liter (M. Beutel, personal communication) successfully inhibited ammonia release. The conclusion here, however, is that electron acceptor augmentation with oxygen, at a nominal concentration of 2 mg O_2·per liter, is not capable of sustaining the microbial populations required to reduce ammonia flux from Onondaga Lake sediments.

The average phosphorus flux in the oxygen-added reactor for the 4-week period of oxygen augmentation was 0.1±0.05 mg P per square meter per day (Figure B.4c), significantly (p less than 0.001) lower than the no nitrate – no oxygen flux. This flux is considered negligible and reflects essentially complete inhibition of phosphorus flux. Over the three weeks following cessation of oxygen addition the phosphorus flux increased from 0.3 to 5.7 mg P per square meter per day (Figure B.4c), a rate little different from the average for the no nitrate-no oxygen reactor (5.2 mg P per square meter per day). It is concluded from these results that electron acceptor augmentation with oxygen, at a nominal concentration of 2 mg O_2 per liter, is effective in inhibiting phosphorus flux from the sediments of Onondaga Lake.

SECTION 7

LITERATURE CITED

American Public Health Association (APHA). 1998. *Standard Methods for the Examination of Water and Wastewater*, 20th edition. American Public Health Association, Washington, DC.

Auer, M.T., Johnson, N.A., Penn, M.R., and Effler, S.W. 1993. Measurement and verification of sediment phosphorus release rates for a hypereutrophic urban lake. *Hydrobiologia*, 253: 301-309.

Beutel, M.W. 2006. Inhibition of ammonia release from anoxic profundal sediments in lakes using hypolimnetic oxygenation. *Ecological Engineering*, 28:271-279.

Effler, S.W. (ed.) 1996. *Limnological and Engineering Analysis of a Polluted Urban Lake: Prelude to the Management of Onondaga Lake, New York*. Springer-Verlag Publishers, New York, NY, 831 pp.

Exponent, Michigan Technological University, Upstate Freshwater Institute, and Syracuse University. 2009. Data Report: Sediment Incubations and Supporting Studies for Onondaga Lake Sediment Management Unit (SMU) 8. Prepared for Honeywell. June 2009. Draft.

O'Dell, J.W. (ed.) 1993. Method 350.1. Determination of ammonia nitrogen by semi-automated colorimetry. Revision 2. U.S. Environmental Protection Agency, Cincinnati, OH.

Parsons, Exponent, Syracuse University, and Upstate Freshwater Institute. 2007. Work Plan for Onondaga Lake SMU 8 Sediment Incubations and Supporting Studies. Prepared for Honeywell. Revised December 2007.

Pauer, J.J. and M.T. Auer. 2000. Nitrification in the water column and sediment of a hypereutrophic lake and adjoining river system. *Water Research*, 34(4): 1247-1254.

Penn, M.R., Auer, M.T., Doerr, S.M., Driscoll, C.T., Brooks, C.M. and Effler, S.W. 2000. Seasonality in the rate of phosphorus release from the sediments of a hypereutrophic lake under a matrix of pH and redox conditions. *Canadian Journal of Fisheries and Aquatic Sciences*, 57(5): 1033-1041.

Wickman, T.R. 1996. Nitrogen diagenesis and the flux of ammonia from lake sediments. M.S. Thesis, Department of Civil and Environmental Engineering, Michigan Technological University, Houghton, MI.

Figure B.1. Schematic drawing (left) of the sediment microcosm used to measure methylmercury flux under controlled conditions of mixing and electron acceptor concentration and photograph (right) of the anaerobic chamber used for incubation. Only two of six mixing jets are included in the schematic drawing.

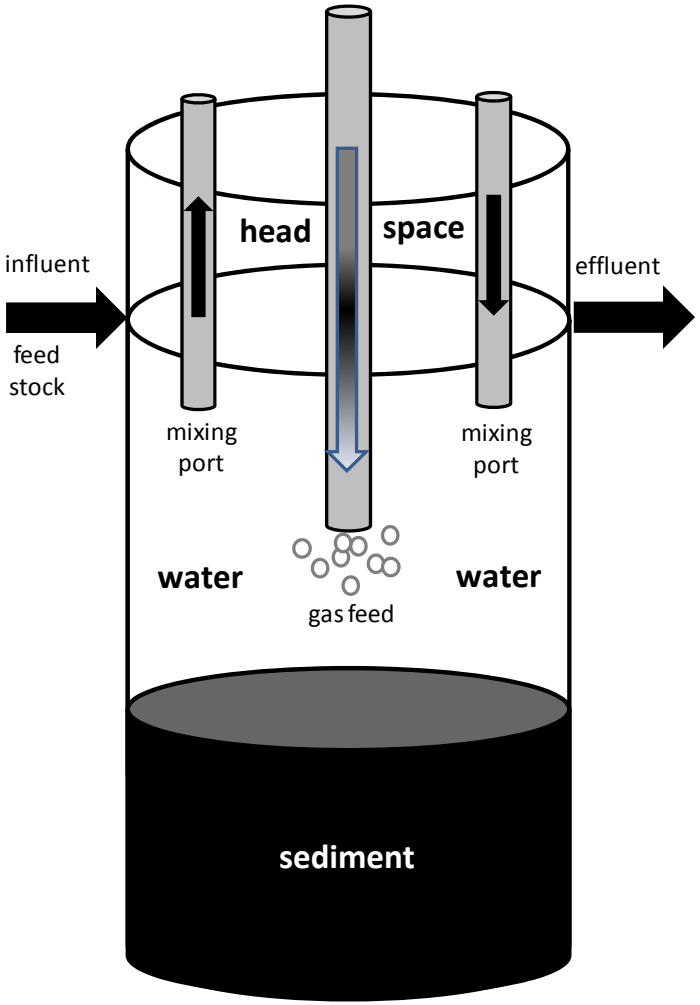

Figure B.2a. Incubation conditions, 2b. NH_3 flux and 2c. Soluble reactive phosphorus (SRP) flux in a reactor receiving no electron acceptor augmentation.

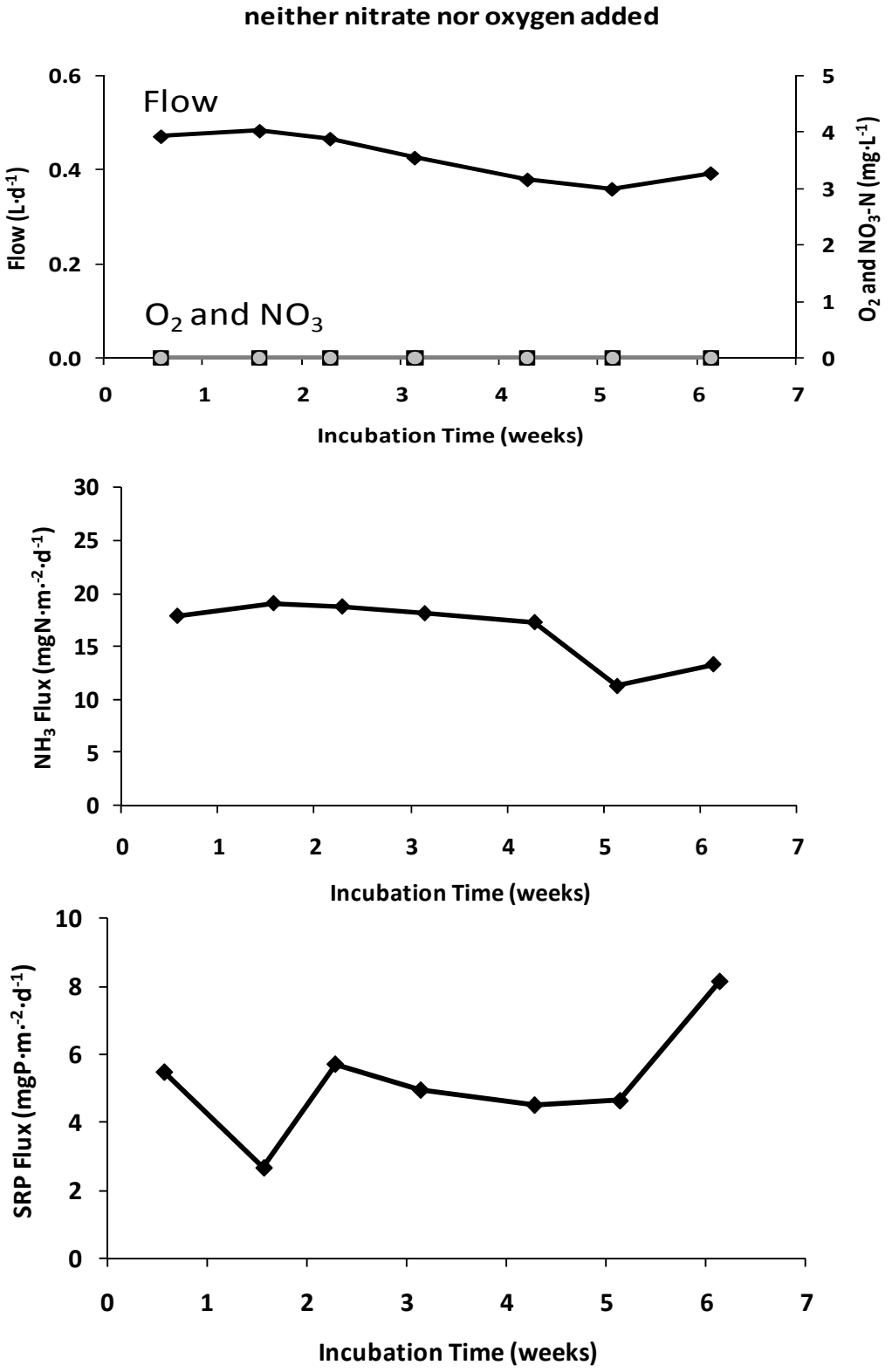

Figure B.3a. Incubation conditions, 3b. NH_3 flux and 3c. SRP flux in a reactor receiving electron acceptor augmentation with nitrate.

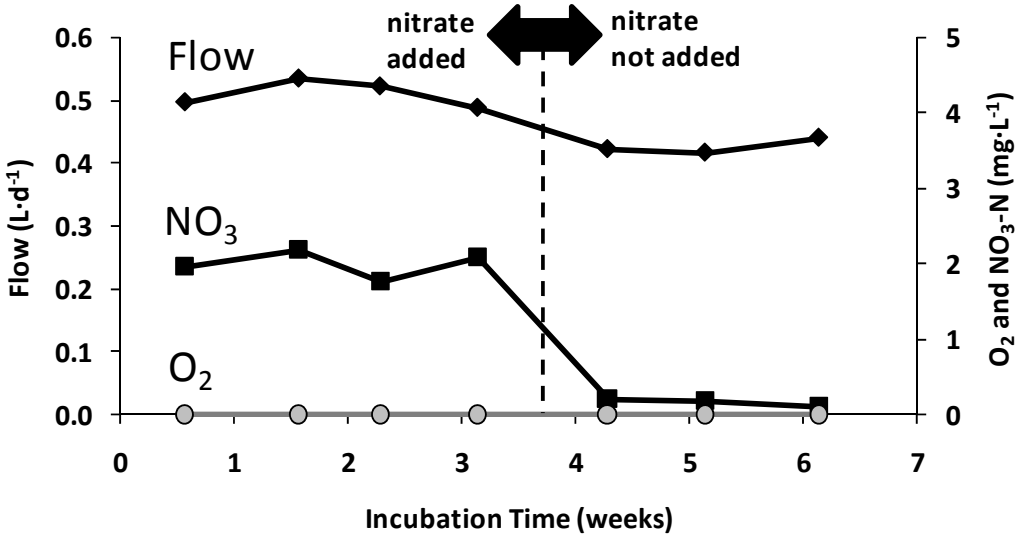

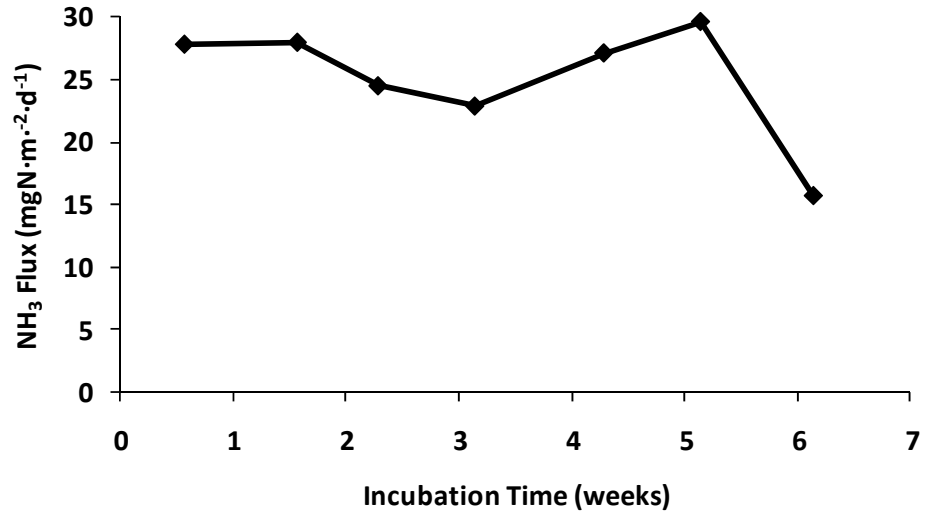

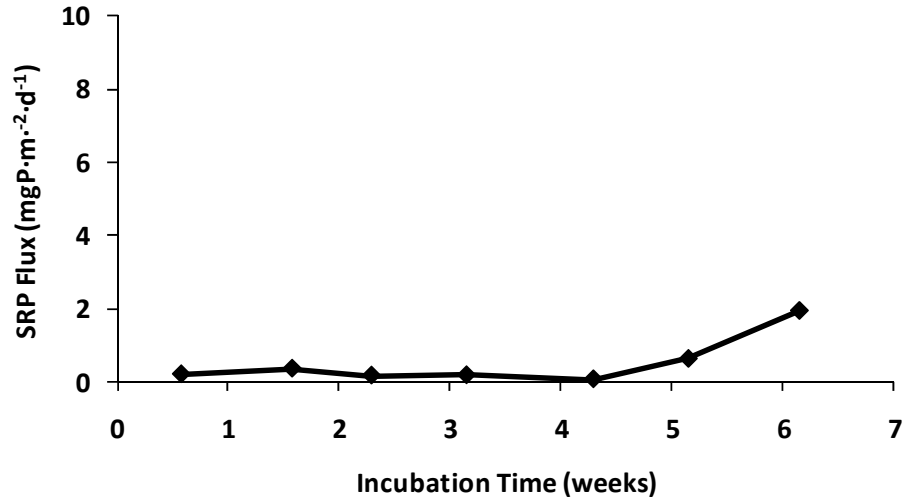

\

Figure B.4a. Incubation conditions, 4b. NH_3 flux and 4c. SRP flux in a reactor receiving electron acceptor augmentation with oxygen.

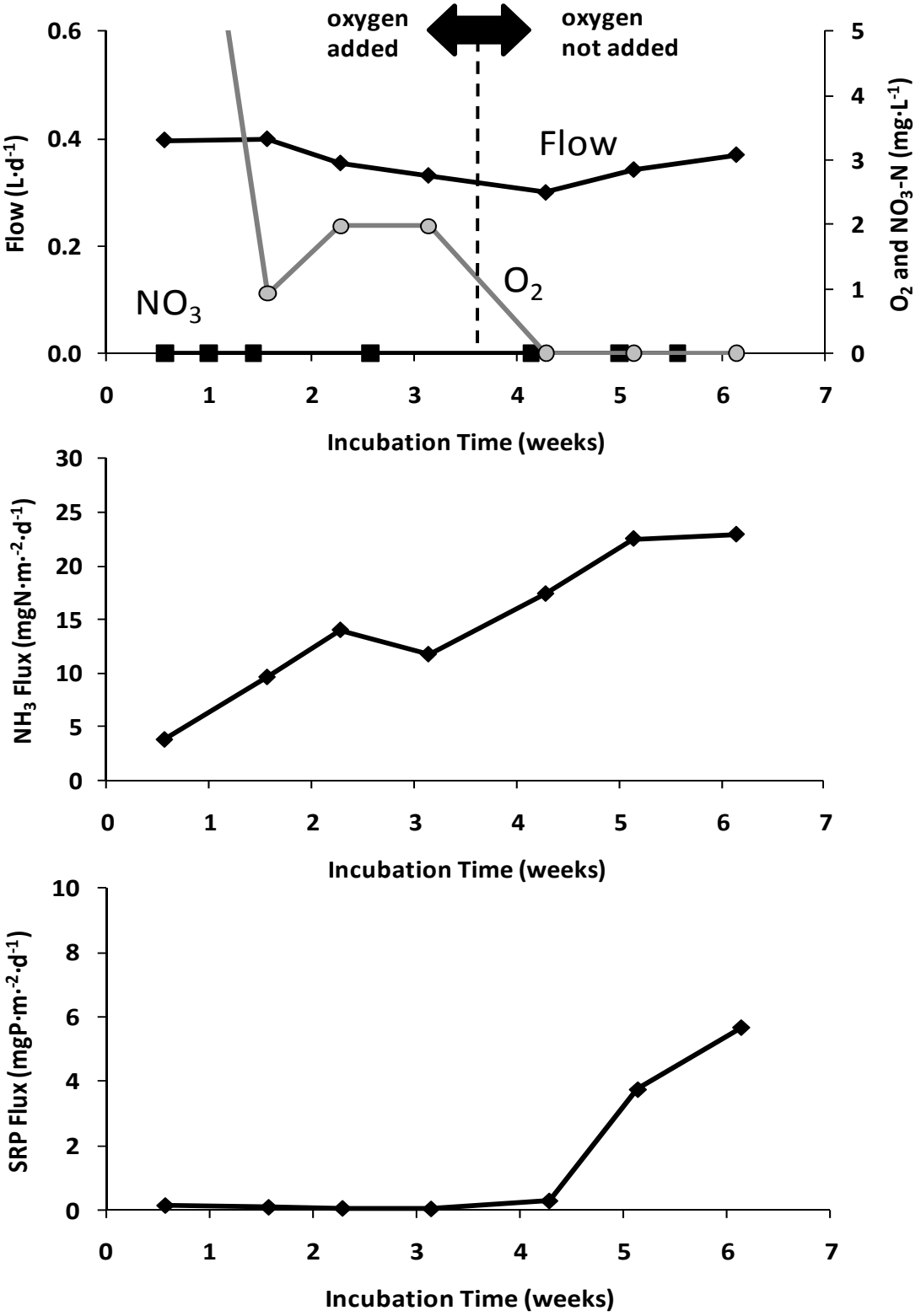

APPENDIX C

INDUCED OXYGEN DEMAND AND ELECTRON ACCEPTOR AMENDMENT IN ONONDAGA LAKE, NEW YORK

APPENDIX C

INDUCED OXYGEN DEMAND AND ELECTRON ACCEPTOR AMENDMENT IN ONONDAGA LAKE, NEW YORK

Prepared For:

Honeywell

301 Plainfield Road
Suite 330
Syracuse, New York 13212

Prepared By:

Martin T. Auer[1], Brandon J. Ellefson[1], P.J. Rusello[2], Edwin A. Cowen[2], Steven C. Chapra[3], David A. Matthews[4] and Steven W. Effler[4]

[1] Michigan Technological University

[2] Cornell University

[3] Tufts University

[4] Upstate Freshwater Institute

JULY 2011

TABLE OF CONTENTS

LIST OF TABLES

TABLE OF CONTENTS (CONT.)

LIST OF FIGURES

INDUCED OXYGEN DEMAND AND ELECTRON ACCEPTOR AMENDMENT IN ONONDAGA LAKE

EXECUTIVE SUMMARY

Onondaga Lake has been identified as a candidate for electron acceptor amendment (with nitrate or oxygen) as a means of reducing the flux of methylmercury from its sediments. Past experience at other sites indicates that such amendments may influence electron acceptor demand by altering the turbulence regime of the hypolimnion and by increasing concentration gradients at the sediment-water interface. Where the induction effect is significant, augmentation systems may be under-designed, with engineering and economic consequences. This research presents the results of experiments characterizing the relationship between hypolimnetic turbulence and electron acceptor (nitrate and oxygen) demand. Measurements of ambient turbulence in the lake's hypolimnion are applied in assessing the vulnerability of the system to induced demand. It is concluded that the anticipated induced demand effect would be modest for Onondaga Lake, ranging from 1-4% for sediment oxygen demand and 5-10% for sediment nitrate demand (*SND*). It is believed that the projected lack of sensitivity to induced demand evolves from the lake's orientation with respect to prevailing winds and attendant seiche activity; i.e. ambient hypolimnetic turbulence naturally places the system near the upper turbulent intensity threshold for the induction phenomenon. A second component of induced demand would arise if the augmentation system increased the average bulk water concentrations above that used for quantifying baseline demand. Experiments, where higher SND was observed, involved nitrate concentrations approximately double those of average concentrations during the historical depletion periods and double the proposed target nitrate concentration for the pilot test (1 mgN/L at 18m). Such conditions are highly unlikely in the field and, therefore, it is not anticipated that induced demand generated by concentration increases would be significant. It is recommended that projections of a modest induced electron acceptor demand effect be accommodated in the design of a pilot system.

Acronyms Used In This Report

AHOD	Areal hypolimnetic oxygen deficit
MT	Metric ton
DBL	Diffusive boundary layer
SND	Sediment nitrate demand
SOD	Sediment oxygen demand
VOD	Volumetric oxygen demand

1.0 HYPOLIMNETIC AERATION/OXYGENATION AND INDUCED OXYGEN DEMAND

Hypolimnetic oxygen depletion is one manifestation of the eutrophication of lakes. Where nutrient enrichment yields rates of organic matter delivery to the sediment in excess of the system's capacity to mineralize those materials, legacy deposits accumulate. Decomposition of contemporary and legacy deposits of organic matter leads to oxygen depletion with attendant

extirpation of the benthic invertebrate and fish communities and the release of a variety of chemical species from the sediments (ammonia, iron and manganese, methane, mercury, phosphorus and sulfide; Penn et al. 2000; Beutel 2006; Beutel et al. 2008b; Matthews et al. 2008). The long-term solution to this problem is to reduce phytoplankton growth and attendant organic matter deposition by managing nutrient inputs. The result is that legacy deposits of labile organic matter undergo diagenesis over time, the system comes into equilibrium with contemporary rates of organic matter deposition and the demand on hypolimnetic oxygen resources is reduced to levels where depletion does not lead to water quality problems. As a short-term solution, or where the requisite level of load management is infeasible, hypolimnetic aeration (introduction of air) or oxygenation (introduction of pure oxygen) may be employed to maintain oxygen resources (McQueen and Lean 1986; Beutel and Horne 1999) and limit the flux of chemical species from the sediment (Gemza 1997; Beutel 2006; Beutel et al. 2008b).

Hypolimnetic aeration/oxygenation systems are designed based on a knowledge of the sediment oxygen demand (*SOD*, $gO_2 \cdot m^{-2} \cdot d^{-1}$), i.e. the flux of oxygen from the hypolimnion into the sediment. Estimates of *SOD* may be derived in several ways, e.g. through a flux-gradient approach using sediment porewater oxygen microprofiles (Sweerts et al. 1989), through laboratory incubations using intact sediment cores (Gelda et al. 1995) and by calculation of the areal hypolimnetic oxygen deficit (*AHOD*, $gO_2 \cdot m^{-2} \cdot d^{-1}$; Matthews and Effler 2006). In this last case, a volume-weighted hypolimnetic oxygen concentration is determined at intervals over the stratified period and the *AHOD* is calculated based on sediment surface area and hypolimnetic volume, corrected for inputs from vertical mass transport. Of these three methods, *AHOD* is the approach most commonly applied in design of aeration/oxygenation systems (Ashley 1985; Moore et al. 1996; Beutel 2003; Beutel et al. 2007).

It has been noted in practice, however, that pre-implementation determinations of oxygen demand may underestimate the oxygen supply later required to maintain target concentrations in the hypolimnion, a phenomenon termed induced oxygen demand (Smith et al. 1975; Taggart and McQueen (1982); Ashley 1983; McQueen et al. 1984; Ashley et al. 1987; Soltero et al. 1994; Moore et al. 1996; Beutel 2003; Beutel et al. 2007; Gantzer et al. 2009). The degree of underestimation can be significant, with post-implementation *SOD* values increasing by 57% (Moore et al. 1996) and factors of 2 (Soltero et al. 1994), 2-3 (Smith et al. 1975), 2-4 (Beutel 2003; Beutel et al. 2007) and 2-6 (depending on aeration rate, Gantzer 2009), and leading to design failures with both engineering and economic implications. Induced oxygen demand effects have led designers to include a safety factor in the sizing of hypolimnetic aeration systems (Cooke et al. 2005). The induced oxygen effect is thought to result from an increase in mixing within the hypolimnion (post-implementation turbulence effect; Moore et al. 1996; Gantzer et al. 2009) and from an increase in the bulk liquid oxygen concentration, i.e. the driving force for diffusion at the sediment-water interface (Jørgensen and Revsbech, 1985; Cai and Sayles 1996; Moore et al. 1996; Beutel 2003; Beutel et al. 2007; but see also Gantzer et al. 2009; the review by Hall et al. 1989 and the theoretical development presented in the following section).

2.0 THE MECHANISTIC BASIS FOR INDUCED OXYGEN DEMAND

The phenomenon termed induced demand is a manifestation of changes in mass transport and thus has application to any chemical species exchanged at the sediment-water interface. The

mechanistic basis for the phenomenon is developed here using oxygen as an example. Sediment oxygen demand refers to the process through which oxygen is consumed in the conversion of ammonia to nitrate, dissolved organic carbon to carbon dioxide and selected reduced species end products of organic carbon diagenesis (Mn^{2+}, Fe^{2+}, S^{2-} and CH_4) to their oxidized counterparts.

2.1 Fate, Transport and the Physical Environment

The physical environment hosting and interacting with this phenomenon includes the bulk liquid, the diffusive boundary layer and the sediment (Figure C.1a). Assuming that turbulent diffusion dominates, i.e. advection and horizontal gradients are negligible in this system, a steady-state, one-dimensional mass balance for oxygen can be written as,

$$0 = D \cdot \frac{d^2C}{dz^2} - k \cdot C \qquad [1]$$

where: C is concentration, $g \cdot m^{-3}$

t = time, d

D is the diffusion coefficient (layer-specific), $m^2 \cdot d^{-1}$

z is depth measured downward, m

k is a first order decay coefficient, d^{-1}

The first term to the right of the equal sign describes diffusive mass transport and the second represents consumption of oxygen resulting from the diagenesis of organic matter. In the absence of oxygen consumption, the oxygen profile ($C = f(z)$) will be linear and vertical through all three layers, with oxygen extending indefinitely into the sediment (Figure C.1b). Profiles in the presence of sediment oxygen consumption vary among the three layers.

Mass transport in the bulk liquid is dominated by turbulent diffusion. Oxygen consumption within the bulk liquid is assumed to be negligible and Equation 1 reduces to,

$$0 = D \cdot \frac{d^2C}{dz^2} \qquad [2]$$

This equation states that the profile within the bulk liquid will be linear (i.e., the second derivative of a straight line is zero). In addition to being linear, the profile in the bulk liquid will be vertical (Figure C.1c) because intense turbulent mixing tends to eliminate vertical concentration gradients.

The bulk liquid and sediment are separated by the diffusive boundary layer (*DBL*). In this region the internal friction (viscosity) of the water creates a laminar film that does not participate in the general circulation of the bulk liquid (Vogel 1981) and mass transport is by molecular diffusion (Santschi et al. 1983). It is assumed that no oxygen consumption occurs within the film. Adopting as a top boundary condition the bulk liquid oxygen concentration and as a bottom boundary condition the concentration at the sediment-water interface, the oxygen profile for the

DBL (Figure C.1c) will again be linear as described by Equation 2. However, for the case where sediment oxygen demand causes the sediment porewater concentration to be lower than the bulk concentration, the resulting profile will be non-vertical (as required by the boundary conditions).

In the sediment, mass transport is by molecular diffusion (as modified by porosity and tortuosity effects); here the reaction term is significant and Equation 1 applies. As a consequence, the resulting oxygen profile (Figure C.1c) is non-linear (as in Equation 1, the second-derivative is non-zero) and non-vertical (as required by the lower boundary condition; that is, that oxygen eventually goes to zero with depth).

The *DBL*, existing as a thin (~1 mm or less in thickness; Santschi et al. 1983; Jørgenson and Revsbech 1985; Gunderson and Jørgenson 1990) layer above the sediment, constitutes a significant barrier to the exchange of chemical species into (oxygen, nitrate) and out of (nutrients, metals, reduced species end products) the sediment (see Gunderson and Jørgenson 1990). The conceptual treatment of fate and transport within the bulk liquid – *DBL* – sediment environment provided here offers a basis for quantifying *SOD* and its relationship to the rate of organic matter diagenesis, the thickness of the *DBL* and the bulk liquid oxygen concentration.

2.2 Factors Mediating Sediment Oxygen Demand

Sediment oxygen demand is appropriately quantified as a flux across the sediment-water interface, equal to the product of the diffusion coefficient and the concentration gradient between the sediment and the overlying water well described by Fick's 1st Law,

$$J_{O_2} = -D \cdot \frac{dC}{dz} \qquad [3]$$

where: J, a generic representation of *SOD*, is the diffusive flux, $g \cdot m^{-2} \cdot d^{-1}$

At steady state, the flux of oxygen at the sediment-water interface and the flux across the *DBL* are equal. As described above, because of the absence of significant oxygen depleting reactions, the oxygen profile within the *DBL* is well described by a linear representation which links the dependence of flux (*SOD*) to the bulk liquid oxygen concentration and the thickness of the *DBL*,

$$\frac{dC}{dz} = \frac{C_{bulk} - C_{swi}}{z_{DBL}} \qquad [4]$$

where: C_{bulk} is the bulk liquid oxygen concentration, $gO_2 \cdot m^{-3}$

C_{swi} is the oxygen concentration at the sediment-water interface, $gO_2 \cdot m^{-3}$

z_{DBL} is the thickness of the diffusive boundary layer, m

Models developed by Bouldin (1968) and Hall et al. (1989) provide a means of quantifying these relationships. Bouldin (1968) introduced the concept of volumetric oxygen demand (*VOD*),

an intrinsic property representing the carbon undergoing diagenesis with oxygen as the electron acceptor. *VOD* may be estimated from measurements of three parameters typically included in sediment studies: *SOD*, *D* and C_{bulk},

$$VOD = \frac{SOD^2}{2 \cdot D \cdot C_{bulk}} \quad [5]$$

where: *VOD* is the volumetric oxygen demand, $gO_2 \cdot m^3 \cdot d^1$

As an intrinsic property, *VOD* does not exhibit short term changes in response to environmental conditions and thus proves useful in calculating other features of sediment oxygen dynamics. Hall et al. (1989) extended Bouldin's (1968) development, accommodating the presence of a diffusive boundary layer and permitting calculation (for specified values of *D* and *VOD*) of sediment oxygen demand,

$$SOD = VOD \cdot \left[\sqrt{\frac{2D_{sed} \cdot C_{bulk}}{VOD} + \left(\frac{D_{sed}}{D_{DBL}} \cdot z_{DBL} \right)^2} - \frac{D_{sed}}{D_{DBL}} \cdot z_{DBL} \right] \quad [6]$$

the maximum depth of oxygen penetration (z_{ox}),

$$z_{ox} = \sqrt{\frac{2D_{sed} \cdot C_{bulk}}{VOD} + \left(\frac{D_{sed}}{D_{DBL}} \cdot z_{DBL} \right)^2} - \frac{D_{sed}}{D_{DBL}} \cdot z_{DBL} \quad [7]$$

and the attendant oxygen profile ($C(z)$),

$$C(z) = \frac{VOD}{2 \cdot D_{sed}} \left[\sqrt{\frac{2 \cdot D \cdot C_{bulk}}{VOD} + \left(\frac{D_{sed}}{D_{DBL}} \cdot z_{DBL} \right)^2} - \frac{D_{sed}}{D_{DBL}} \cdot z_{DBL} \right]^2 - \frac{VOD}{D_{sed}} \left[\sqrt{\frac{2 \cdot D \cdot C_{bulk}}{VOD} + \left(\frac{D_{sed}}{D_{DBL}} \cdot z_{DBL} \right)^2} - \frac{D_{sed}}{D_{DBL}} \cdot z_{DBL} \right] \cdot z + \frac{VOD}{2 \cdot D} z^2 \quad [8]$$

as functions of C_{bulk} and z_{DBL}.

Illustrative applications of Equations 6-8 are presented here with values of *VOD* (2900 $gO_2 \cdot m^{-3} \cdot d^{-1}$) and *D* ($8.64 \times 10^{-5}$ $m^2 \cdot d^{-1}$) representative of Onondaga Lake sediments. The response of the oxygen profile to changes in C_{bulk} in the absence of a *DBL* ($z_{DBL} = 0$) is presented in Figure C.2a. Note that as C_{bulk} increases, the depth of oxygen penetration and the slope of the

profile (~*SOD*) both increase. The role of the *DBL* in mediating *SOD* is considered for two cases (z_{DBL} =1.0 mm and 0.1 mm) in Figure C.2b. Here, the driving force for *SOD* is not C_{bulk}, but rather C_{swi} (the oxygen concentration at the base of the *DBL*). Reducing the *DBL* thickness leads to a higher value of C_{swi}, an increased depth of oxygen penetration and a greater slope (~*SOD*). This effect is illustrated in model-predicted oxygen profiles for a range of sediment-water interface oxygen concentrations in Figures 3a (without a *DBL*) and 3b (with a *DBL*). It can be seen here that increasing C_{swi} increases both the depth of oxygen penetration and the slope of the profile (~*SOD*).

Thus model-predicted *SOD* is seen to be a function of an intrinsic *VOD*, the oxygen concentration in the bulk liquid (and thus at the sediment-water interface, Figure C.4a) and the thickness of the diffusive boundary layer (Figure C.4b). The combined effect of the two factors is illustrated in Figure C.4c. These relationships are consistent with the observations of Moore et al. (1996), Beutel (2003), Beutel et al. (2007) and Beutel et al. (2008a) that induced oxygen demand is mediated by both C_{bulk} and mixing conditions, but stands in contrast to the conclusion of Gantzer et al. (2009) and several studies summarized by Hall et al. (1989) that hypolimnetic oxygen consumption is independent of C_{bulk}.

It is clear that, for given values of *VOD* and C_{bulk}, *SOD* decreases with increasing boundary layer thickness. Thus it may be appropriate to consider *SOD* for a minimum z_{DBL} (unburdened by mass transport limitations) as a maximum value and *SOD* as z_{DBL} increases to be apparent or realized values.

3.0 MOTIVATION, OBJECTIVES, AND APPROACH

Sediments at the study site, Onondaga Lake, are contaminated with mercury as a result of industrial discharges, leading to production of methylmercury and attendant ecosystem impacts. Remediation at upland and nearshore in-lake locations is expected to significantly reduce mercury inputs to the lake's depositional basins with attenuation of methylmercury formation as legacy deposits become buried and overlain by uncontaminated sediment. It has been observed here that methylmercury flux from the sediments is initiated once oxygen and nitrate have been depleted from the hypolimnion (Todorova et al. 2009). Electron acceptor augmentation with nitrate or oxygen is thus being considered as a means of controlling methylmercury flux as the sediments approach equilibrium with contemporary conditions of deposition (United States District Court 2007).

An examination of the potential response of chemical flux at the sediment-water interface of Onondaga Lake to changes in turbulence levels, i.e. induced demand, is an appropriate pre-condition to field-scale testing of the electron acceptor augmentation technology. The objectives of this study are to:

(a) quantify the relationship between *SND*/*SOD* and turbulence for Onondaga Lake sediments;

(b) place that relationship within the context of the bottom boundary layer turbulence measured for Onondaga Lake; and

(c) apply those results in assessing the sensitivity of the system to the induced demand following implementation of electron acceptor augmentation.

Sediment nitrate and oxygen demand were measured using sediment flux chambers designed to provide varying levels of isotropic turbulence at the sediment-water interface. Rates of *SND* and *SOD* were measured over a range of turbulences and plotted to provide the desired relationship. A quantitative characterization of the bottom boundary layer turbulence for Onondaga Lake (Rusello and Cowen 2010) is used to place ambient conditions within the context of the turbulence – *SND*/*SOD* relationship. Evaluation of that result permits estimation of the degree to which induced electron acceptor demand will be manifested following implementation of electron acceptor augmentation.

4.0 METHODS

4.1 Sediment Core Collection and Handling

Sediments were collected from the South Deep station in the south depositional basin of Onondaga Lake on 4 dates between 12 June 2008 and 26 April 2009, supporting 12 measurements of sediment nitrate demand and 13 measurements of sediment oxygen demand. The South Deep station (maximum depth, 19m) is considered representative of sediment conditions in the depositional basins of Onondaga Lake (Effler 1996). Sediment was collected using a stainless steel box corer (Model 1260, Ocean Instruments, Inc., San Diego, CA). The box core was sub-sampled using 15 cm (6-inch) diameter polycarbonate reactor housings and capped with friction-fit tops and bottoms. The sealed cores were placed on ice and transported to the laboratory where they were stored at 4 °C. Particular care was taken to minimize disturbance of the sediment-water interface during box coring and transportation to the laboratory.

The organic matter content of sediments in nature decreases over time with exposure to electron acceptors (see Gantzer et al. 2009). This is also the case with the organic matter in sediment cores when stored or utilized in sediment flux chambers (incubations; see Sundby 1986), altering the associated *SND*/*SOD*. We observed that our cores had a 'shelf life' of about 3 months, i.e. values of *SND*/*SOD* began to decline after this period. Where measured values of SND_{max}/SOD_{max} declined significantly (due to length or storage or utilization in measurements) the core was discarded and a fresh core utilized.

4.2 Sediment Flux Chamber Design

A sediment flux chamber (i.e. completely-mixed flow reactor) has identifiable sources and sinks of chemical mass and, when operating at steady state, supports determination of an unknown source/sink when the other source/sink terms and physical conditions (area, volume and flow) are known. The application of this approach and detailed calculations are provided in Section 4.5 below.

The chambers were specifically designed to support quantification of chemical flux at the sediment-water interface by:

- Housing an intact sediment core
- Providing an inlet for addition of feed stock
- Permitting establishment of specified turbulence levels
- Maintaining isotropic mixing conditions
- Providing an outlet for sample collection.

Chambers consisted of a cylindrical Plexiglas container, 15 cm diameter by 25.4 cm tall, outfitted with opposing inlet-outlet ports located approximately 1.3 cm below the top rim. When filled, chambers contained ~13 cm of sediment and ~12 cm of overlying water. Plexiglas top and bottom pieces, inlayed with flexible gaskets and placed within clamping devices sealed the system against gas penetration and leakage of liquid. The chamber top had six peripheral jet ports where the liquid content of the chamber water was circulated via peristaltic pumps to provide mixing and control turbulence. The system was operated with zero head space.

4.3 Regulation of Turbulence

The objective of this work, quantification of the effect of turbulence on the thickness of the diffusive boundary layer and thus chemical flux, demands particular attention to characterization and regulation of that turbulence. Direct field measurement of these effects is challenging due to the small length scales associated with boundary layers. Sediment flux chambers provide an alternative approach, but yield estimates representative of the ambient environment only when natural boundary conditions are reproduced (Boynton et al. 1981; Hall et al. 1989). It is necessary to overcome several challenges in order to meet this criterion.

The first challenge is to insure that turbulent flux dominates within the chamber (i.e. mean advective flux is eliminated). Mass transport in the hypolimnion of lakes and attendant chemical renewal at the sediment-water interface occurs primarily through vertical turbulent mixing. Horizontal advective flux in the hypolimnion (spatial scale of 100s of meters) does not serve to renew conditions at the interface, but rather moves water of a relatively constant chemical composition over the bed. In chambers (spatial scale of centimeters), however, horizontal advective transport quickly moves water to the boundary (chamber wall), setting up a circulation pattern that provides chemical renewal at the sediment-water interface. Thus it is the goal of chamber design to establish isotropic conditions, i.e. no net flow. To meet this challenge, a novel chamber was developed based on proven isotropic turbulence generation techniques (Rusello and Cowen 2010). The chamber design minimizes advective horizontal transport by utilizing an array of jets arranged symmetrically on the chamber top and oriented with the jet axes perpendicular to the sediment bed. The jets are driven by peristaltic pumps which randomly change direction, generating nearly isotropic turbulence that is horizontally homogenous with very low mean flows.

The second challenge is to quantitatively characterize turbulence within the chamber. Particle image velocimetry (PIV) was used for this purpose, characterizing chamber turbulence under various forcing conditions (pump speeds; Figure C.5). Vertical turbulent intensity, calculated as the root mean square difference between the instantaneous and mean velocities, was selected as the metric representing turbulence in the chamber. The turbulent intensity is a common turbulence statistic and provides a measure of the strength of the turbulence readily comparable to field measurements. With appropriate assumptions it can also be used for comparison to other systems where turbulence statistics are not reported. The third challenge is to scale chamber turbulence to that of the ambient environment. Vertical turbulent intensity, the metric adopted for laboratory chambers, is readily measured in the field and its use in characterizing turbulence in the ambient environment facilitates direct comparison of conditions. Measurements in the bottom boundary layer of Onondaga Lake (Rusello and Cowen 2010) showed classic turbulent boundary layer conditions, although with weaker mean flows than

expected. Because of the slow mean flows, measurement noise dominates the horizontal turbulence statistics, leaving the vertical turbulence measurements (which have significantly lower measurement noise) as the most reliable estimates of *in-situ* turbulence conditions. Turbulent intensities and turbulent dissipation rates in the chamber were compared to estimates from the field measurements with good agreement at a representative turbulent intensity of 1-2 mm/s. Chamber turbulence conditions were calibrated to the pump speed in RPM, yielding a vertical turbulent intensity appropriate for modeling scalar flux at both current *in-situ* conditions and with enhanced turbulence as may be imparted through electron acceptor augmentation. Vertical turbulent intensity can also be scaled to yield the friction velocity (u*, a common boundary layer parameter) to facilitate comparison of our findings with those from other systems where direct turbulence measurements have not been performed.

In this application, the top of the chamber was outfitted with six jets that were flush with the reactor/water interface. Tygon tubes were run from these jets through 3 peristaltic pumps (Masterflex L/S Computerized Drive; Masterflex Easy Load II Model #77202-50). The pumps were programmed (MATLAB) to randomly reverse the recirculation direction to achieve isotropic conditions. The degree of turbulence was varied by adjusting the pump speed (Figure C.5). At intervals of 60 minutes, the pumps operated in a single direction for several minutes to flush the tubing system. Velocities employed here (~0-4.5 mm/s, pump speeds of 0-50 RPM) reflect the range of ambient fluid velocities observed near the sediment-water interface of Onondaga Lake. Higher velocities (25 and 50 RPM) represent a minimum *DBL* thickness and thus an appropriate condition for determination of SOD_{max}/SND_{max}. Above 50 RPM, sediment resuspension occurred. Given that implementation of electron acceptor amendment would be designed to prevent sediment resuspension, this range of velocities also represents expected conditions should the technology be utilized.

4.4 Chamber Operation and Monitoring

The continuous-flow sediment flux chamber and supporting system components are described schematically in Figure C.6. Incubations were performed in a constant temperature room (8°C; mimicking ambient hypolimnetic conditions) with two reactors (one *SND* and one *SOD*) operated simultaneously at turbulent intensities of 0.07 – 4.57 $mm \cdot s^{-1}$. Artificial lake water (Table C.1), with an ionic composition similar to that of the lake, served as feed stock to the reactor with the rate of input regulated by metered gravity flow or a peristaltic pump. Feed stock for the oxygen reactor (measurement of *SOD*) was continuously bubbled with an air-nitrogen mixture (Mix-1000 Digital Gas Mixer/Blender) to achieve the desired oxygen concentration. Feed stock for the nitrate reactor (measurement of *SND*) was augmented with potassium nitrate (~4-6 $mgNO_3\text{-}N \cdot L^{-1}$) and continuously bubbled with nitrogen gas to purge oxygen from the system.

It is necessary that the bulk liquid nitrate/oxygen concentration be controlled, as this represents a driving force for diffusion (Jørgensen and Revsbech 1985; Moore et al. 1996). Further, by controlling the bulk liquid electron acceptor concentration, turbulence (*DBL* thickness) is isolated as the sole factor mediating realized *SND*/*SOD*. Target bulk liquid concentrations (nominally, 2-4 $mgNO_3\text{-}N \cdot L^{-1}$ and 2-4 $mgO_2 \cdot L^{-1}$) were those proposed for control of MeHg flux through electron acceptor amendment (Auer et al. 2009). Target concentrations were maintained at steady-state levels of 2.2±0.8 $mgNO_3\text{-}N \cdot L^{-1}$ (n = 12) and 3.0±1.9 $mgO_2 \cdot L^{-1}$

(n = 13) through regulation of feed stock inflow (rotameters and gravity feed, initially, and peristaltic pumps, later). Feed stock nitrate (Orion Thermo Scientific Nitrate Sensor 9700B NWP) and oxygen (HACH HQ 40d LDO probe) concentrations were monitored daily. Effluent nitrate concentrations were monitored four times daily using the ion-specific electrode. Effluent oxygen levels were monitored continuously using a Unisense in-line oxygen microprobe (50 and 100 μm tip diameter). The LDO and nitrate probes were calibrated daily, while the in-line oxygen microprobe was calibrated only at the beginning and end of the incubation to avoid disturbing the system. Effluent concentrations were monitored for several days after placing the core at 8°C and flux measurements initiated once the system stabilized, i.e. achieved steady state (Figure C.7). The stabilized sediment flux chambers were then monitored for 2-4 days and the average concentration applied in calculating *SND* and *SOD* as described below.

4.5 Flux Calculation

The sediment reactors were run to steady state and the effluent concentration noted. The flux (J = *SND*, *SOD*) was then calculated by conducting a mass balance on the electron acceptor concentration (C) in the reactor,

$$V \cdot \frac{dC}{dt} = Q \cdot C_{in} - Q \cdot C - J \cdot A \qquad [9]$$

where: V is the liquid volume in the sediment flux chamber, m^3

Q is the reactor flow rate, $m^3 \cdot d^{-1}$

C_{in} is the influent electron acceptor concentration, $g \cdot m^{-3}$

A is the reactor surface area, m^2

At steady state, the change in concentration (dC/dt) is zero, and Equation 9 becomes,

$$0 = Q \cdot C_{in} - Q \cdot C - J \cdot A \qquad [10]$$

The flux may be solved for by rearranging Equation 10,

$$J = \frac{Q \cdot (C_{in} - C)}{A} \qquad [11]$$

The values for Q, C_{in}, C, and A are all known or measured during the conduct of the experiment.

The fluxes generated by this calculation were obtained using sediment cores collected at various times of the year and thus reflecting a range of sedimentation fluxes (Soltero 1994) and carbon content and lability. These differences manifest themselves in variation in the maximum value of J, i.e. that associated with a minimal *DBL* thickness. Thus, fluxes determined for a

particular core were normalized to their respective maxima (SND_{max} and SOD_{max}) value before being placed within the pool of data used to define the demand/turbulence relationship.

5.0 RESULTS AND DISCUSSION

Sediment flux chambers containing Onondaga Lake sediment were exposed to controlled environments characterized by turbulent intensities ranging from 0.07 – 4.57 $mm \cdot s^{-1}$. Chambers were operated and monitored for several days until the effluent electron acceptor concentration reached a steady state condition (Figure C.7). Effluent oxygen and nitrate concentrations were then monitored for 2-4 days and the average concentration applied in calculating *SND* and *SOD* according to Equation 11.

5.1 Maximum Rates of Sediment Nitrate and Oxygen Demand

A total of 12 incubations were conducted with nitrate as the electron acceptor, yielding SND_{max} values ranging from 0.079 - 0.258 $gN \cdot m^{2} \cdot day^{-1}$ with an average of 0.17±.07 $gN \cdot m^{-2} \cdot day^{-1}$ (Table C.2). These values are roughly double those of contemporary rates of hypolimnetic nitrate depletion observed for Onondaga Lake (0.07 and 0.09 $gN \cdot m^{-2} \cdot day^{-1}$ for 2008 and 2009, respectively; Upstate Freshwater Institute unpublished). In-lake nitrate depletion rates are expected to be less than those observed in flux chambers due to differences in bulk liquid nitrate concentrations, i.e., in-lake levels are depleted over the stratified interval and thus are, on average, less than those utilized in experiments where concentrations are held constant. (It should also be noted that the target concentration to be maintained during the pilot test at 18m is 1 mgN/l, approximately half the value used in the experiments.) SND_{max} values observed here compared favorably with those determined for sediment from Lake Perris, California (0.04-0.17 $gN \cdot m^{-2} \cdot day^{-1}$; Beutel et al. 2008a) for similar bulk liquid nitrate concentrations (1-5 $mgN \cdot L^{-1}$).

A total of 13 incubations were performed with oxygen as the electron acceptor, yielding values of SOD_{max} ranging from 1.01 to 1.25 $gO_2 \cdot m^{-2} \cdot day^{-1}$ and averaging 1.09 ±0.11. $gO_2 \cdot m^{-2} \cdot day^{-1}$ (Table C.3). The average value for SOD_{max} compares favorably with that determined for Onondaga Lake as *AHOD* (1.02 $gO_2 \cdot m^{-2} \cdot day^{-1}$ for both 2008 and 2009; Upstate Freshwater Institute, unpublished); exact correspondance is not expected due to differences in C_{bulk}. An increase in SOD corresponding to maintenance of oxygen levels was not observed, perhaps because the average condition in the lake reasonably approximated that used in the measurements. The range observed for SOD_{max} in Onondaga Lake falls between that reported in chamber studies by Beutel (2003) for nine California reservoirs (0.1–0.8 $gO_2 \cdot m^{-2} \cdot day^{-1}$) and by Arega and Lee (2005) in primarily semi-artificial cores (2-6 $gO_2 \cdot m^{-2} \cdot day^{-1}$).

5.2 Turbulence and Induced Electron Acceptor Demand

Determinations of SND_{max} and SOD_{max} were made at mixing pump speeds of 25 and 50 rpm, yielding turbulent intensities associated with a minimum *DBL* thickness. Additional measurements were made at lesser turbulent intensities (pump speeds of 2, 6, 10 and 17.5 rpm) to explore the induced demand effect. Here, *SND* and *SOD* values for each turbulent intensity were normalized to the SND_{max} or SOD_{max} value for their particular collection and plotted as a function of turbulent intensity (Figure C.8). In each case, the relationship between turbulent intensity ($mm \cdot s^{-1}$) and electron acceptor demand ($gO_2 \cdot m^{-2} \cdot day^{-1}$) was well described by a rectangular hyperbola,

$$J_i = \alpha \cdot J_{max} \cdot \frac{i}{\beta + i} \quad [12]$$

where: J_i is the normalized flux, i.e. at turbulent intensity i,

$J_{i,max}$ is the maximum flux, 1.0 for the normalized case,

α, β are dimensionless fitting parameters

The model represented in Equation 12 was fit to the normalized *SND* and *SOD* data (Figures 8a and b) using Microsoft Excel Solver yielding values of the fitting parameters α and β were 1.05 $gNO_3\text{-}N \cdot m^{-2} \cdot d^{-1}$and 0.15 $mm \cdot s^{-1}$ for *SND* and 1.05 $gO_2 \cdot m^{-2} \cdot d^{-1}$and 0.09 $mm \cdot s^{-1}$ for *SOD*. The root mean square errors for fits to the *SND* and *SOD* results were 0.07 $gNO_3\text{-}N \cdot m^{-2} \cdot d^{-1}$ and 0.27 $gO_2 \cdot m^{-2} \cdot d^{-1}$. The relationship embodied in Equation 12 may then be applied for measured ambient and projected future (post amendment) turbulent intensities to quantify the system's sensitivity to the induced demand effect.

5.3 Management Application: Induced Electron Acceptor Demand in Onondaga Lake

The motivation for this research was to enhance the reliability of an electron acceptor augmentation design for Onondaga Lake by quantifying the sensitivity of the system to the induced demand effect. The theoretical and experimental development presented above demonstrates that induced demand occurs in response to increased turbulence (decreased boundary layer thickness) and increased bulk liquid electron acceptor levels.

The turbulent intensity-electron acceptor demand relationship presented as Figure C.8 provides a means of assessing the sensitivity of a system to the phenomenon. Ambient turbulent intensities for Onondaga Lake measured in late September and October of 2007 ranged from 1.0 – 1.5 $mm \cdot s^{-1}$ (Rusello and Cowen 2010). Application of Equation 12 for this range of ambient velocities using the electron acceptor-specific coefficients α and β (as illustrated in Figure C.9) indicates that an increase in turbulent intensity at the sediment water interface yielding J_{max} values would increase *SND* by 5-9% and *SOD* by 1-4%. Assuming a sediment surface area of 6.75 km^2 for the Onondaga Lake profundal, this would correspond to an additional requirement of 5-10 MT-NO_3-N and 7-27 MT-O_2 over a stratified interval of 100 days.

These projected induced demand effects are modest in comparison to those reported for other systems (e.g., increases by a factor of 2-4; see Section 1.0). It is surmised that this lack of projected sensitivity involves both of the factors believed to mediate the induced demand effect. First, the major axis of Onondaga Lake is oriented in the direction of prevailing westerly and northwesterly winds. Exposure to this energy source promotes seiche activity in the lake (Effler 2004), the primary driving force for turbulence in the hypolimnion. Elevated turbulent intensities would reduce the *DBL* thickness, enhancing diffusive mass transport and increasing ambient J_{max}. Thus Onondaga Lake would potentially lie further to the right (i.e. $SOD \rightarrow SOD_{max}$) along the velocity-demand continuum presented as Figure C.9 than would some other systems and would be less sensitive to further increases in turbulence imparted by electron acceptor addition.

However, differences inthe bulk liquid concentration play a role as well. Flux chamber measurements conducted here for Onondaga Lake sediments utilized C_{bulk} levels averaging 2.2 $mgNO_3\text{-}N\cdot L^{-1}$ and 3.0 $mgO_2\cdot L^{-1}$. The theoretical development summarized in Figure C.4a and the findings of Moore et al. (1996) suggest that *SOD* may increase by a factor of 2-3 for an increase in the bulk concentration from 2 to 6 or 8 $mgO_2\cdot L^{-1}$. The maintenance of electron acceptor levels through chemical conditioning may thus be expected to induce demand compared with contemporary in-lake rates where bulk concentrations fall over the stratified period due to microbial consumption. A prediction of induced demand due to concentration effects under an augmentation regime requires a comparison of average bulk water concentrations over the historical nitrate depletion periods (starts at 2.0 mgN/l, ends at 0 mgN/l, averaged approximately 1 mgN/l) to concentrations maintained during the experiments (2.2 mgN/l), to proposed concentrations during the pilot test (1 mgN/l). Thus for the ambient mixing conditions determined for Onondaga Lake by Rusello and Cowen (2010) and the bulk concentrations proposed for augmentation, the prospect of a modest induced electron acceptor demand effect seems reasonable. It is recommended that projections of an induced electron acceptor demand effect be accommodated in the design of a pilot system.

6.0 REFERENCES

Arega, F. and J.H.W. Lee. 2005. Diffusional mass transfer at sediment–water interface of cylindrical sediment oxygen demand chamber. Journal of *Environmental Engineering*, 131:755-766.

Ashley, K.I. 1983. Hypolimnetic aeration of a naturally eutrophic lake: Physical and chemical effects. *Canadian Journal of Fisheries and Aquatic Sciences*, 40: 1343-1359.

Ashley, K.I., S. Hay and G.H. Scholten. 1987. Hypolimnetic aeration: A field test of the empirical sizing method. *Water Resources*, 21(2): 223-227.

Auer, M.T., Matthews, S.A., Driscoll, C.T., Effler, S.W., Galicinao, G.A., Elefson, B.J. and Todorova, S. 2009. Methylmercury Flux From The Sediments of Onondaga Lake, New York as Determined Using Flow-Through Sediment Microcosms. Draft Project Report submitted to Honeywell Corporation by Michigan Technological University, Houghton, Michigan. 46 pp.

Beutel, M. W., 2003. Hypolimnetic anoxia and sediment oxygen demand in California drinking water reservoirs. *Lake and Reservoir Management*, 19: 208–221.

Beutel, M. W., 2006. Inhibition of ammonia release from anoxic profundal sediments in lakes using hypolimnetic oxygenation. *Ecological Engineering*, 28(3): 271-279.

Beutel, M.W. and A.J. Horne. 1999. A review of the effects of hypolimnetic oxygenation on lake and reservoir water quality. *Lake and Reservoir Management*, 15(4): 285-297.

Beutel, M.W., I. Hannoun, J. Pasek and K. Bowman Kavanagh. 2007. Hypolimnetic oxygenation pre-design study for a large eutrophic raw water reservoir, San Vicente Reservoir, CA. *ASCE Journal of Environmental Engineering*, 133(2): 130-138.

Beutel, M.W., N.R. Burley and S.R. Dent. 2008a. Nitrate uptake rate in anoxic profundal sediments from a eutrophic reservoir. *Hydrobiologia*, 610: 297-306.

Beutel, M.W., T.M. Leonard, S.R. Dent and B.C. Moore. 2008b. Effects of aerobic and anaerobic conditions on P, N, Fe, Mn and Hg accumulation in waters overlaying profundal sediments of an oligo-mesotrophic lake. *Water Research*, 42: 1953-1962.

Bouldin, D.R. 1968. Models for describing the diffusion of oxygen and other mobile constituents across the mud-water interface. *Journal of Ecology*, 56: 77-87.

Boynton, W. R., Kemp, W. M., Osborne, C. G., Kaymeyer K. R., Jenkins, M. C., 1981. Influence of water circulation rate on in situ measurements of benthic community respiration. *Marine Biology* 65 (2): 185-190.

Cai, W. J. and F. Sayles. 1996. Oxygen penetration depths and fluxes in marine sediments. *Marine Chemistry*, 52(2): 123-131.

Cooke, G.D., E.B. Welch, S.A. Peterson and S.A. Nichols. 2005. *Restoration and Management of Lakes and Reservoirs*, 3rd Edition. CRC Press, Boca Raton, Florida, 591 pp.

Effler, S.W. (ed.), 1996. *Limnological and Engineering Analysis of a Polluted Urban Lake: Prelude to the Management of Onondaga Lake, New York*. Springer-Verlag Publishers, New York, New York, 831 pp.

Effler, S. W., Wagner, B. A., O'Donnell, D. M., O'Donnell, S. M., Matthews, D. A., Gelda, R. K., Matthews, C. M. and Cowen, E.A. 2004. An upwelling event at Onondaga Lake, NY: Characterization, impact and recurrence. *Hydrobiologia*, 511: 185-199.

Gantzer, P.A., L.D. Bryant and J.C. Little. 2009. Effect of hypolimnetic oxygenation on oxygen depletion in two water-supply reservoirs. *Water Research*, 43: 1700-1710.

Gelda, R.K., Auer, M.T., and S.W. Effler. 1995. Determination of sediment oxygen demand by direct measurement and by inference from reduced species accumulation. *Marine and Freshwater Research*, 46: 81-88.

Gemza, A. F., 1997. Water quality improvements during hypolimnetic oxygenation in two Ontario lakes. *Water Quality Research Journal of Canada*, 32(2): 365-390.

Gundersen, J. K. and B.B. Jorgensen. 1990. Microstructure of diffusive boundary layers and the oxygen uptake of the sea floor. *Nature*, 345: 604-607.

Hall, P. O. J., L.G. Anderson, M.M. Rutgers van der Loeff, B. Sundby and S.F.G. Westerlund. 1989. Oxygen uptake kinetics in the benthic boundary layer. *Limnology and Oceanography*, 34(4): 734-746.

Jørgensen, B. B., Revsbech, N. P., 1985. Diffusive boundary layers and the oxygen uptake of sediments and detritus. *Limnology and Oceanography*, 30(1): 111-122.

Matthews, D. A. and S.W. Effler. 2006. Long-term changes in the areal hypolimnetic oxygen deficit (*AHOD*) of Onondaga Lake: Evidence of sediment feedback. *Limnology and Oceanography*, 51(1): 702-714.

Matthews, D. A., S. W. Effler, S. M. O'Donnell, C. T. Driscoll and C. M. Matthews. 2008. Electron budgets for the hypolimnion of a recovering urban lake, 1989-2004: Response to changes in organic carbon deposition and availability of electron acceptors. *Limnology and Oceanography,* 53(2): 743-759.

McQueen, D. J. and D.R.S. Lean. 1986. Hypolimnetic aeration: An overview. *Water Quality Research Journal of Canada*, 21(2): 205-217.

McQueen, D.J., S.S. Rao and D.R.S. Lean. 1984. Hypolimnetic aeration: changes in bacterial populations and oxygen demand. *Archiv für Hydrobiologie*, 99: 498-514.

Moore, B. C. 1996. A model for predicting lake sediment oxygen demand following hypolimnetic aeration. *Journal of the American Water Resources Association*, 32(4): 723-731.

Penn, M.R., Auer, M.T., Doerr, S.M., Driscoll, C.T., Brooks, C.M. and S.W. Effler. 2000. Seasonality in the rate of phosphorus release from the sediments of a hypereutrophic lake under a matrix of pH and redox conditions. *Canadian Journal of Fisheries and Aquatic Sciences*, 57(5): 1033-1041.

Rusello, P.J. and Cowen, E.A. 2010. A turbulent microcosm chamber for laboratory scalar flux estimates. In preparation for *Water Resources Research*.

Soltero, R. A., L.M. Sexton, K.I. Ashley and K.O. McKee. 1994. Partial and full lift hypolimnetic aeration of Medical Lake, WA to improve water quality. *Water Research*, 28: 2297–2308.

Smith, S. A., D. R. Knauer, and T. L. Wirth. 1975. *Aeration as a lake management technique.* Technical Bulletin No. 87, Wisconsin Department of Natural Resources, Madison, Wisconsin, 40 pp.

Sundby, B. 1986. The effect of oxygen on release and uptake of cobalt, manganese, iron and phosphate at the sediment-water interface. *Geochimica et cosmochimica acta*, 50: 1281-1288.

Sweerts, J,-P. R. A., V. St. Louis, and T. E. Cappenberg. 1989. Oxygen concentration profiles and exchange in sediment cores with circulated overlying water. *Freshwater Biology*. 21: 401-409.

Taggart, C. T. and D.J. McQueen. 1982. A model for the design of hypolimnetic aerators. *Water Research*, 16(6): 949-956.

Todorova, S.G., C.T. Driscoll, Jr., D.A. Matthews, S.W. Effler, M.E. Hines and E.A. Henry. 2009. Evidence for regulation of monomethyl mercury by nitrate in a seasonally stratified, eutrophic lake. *Environmental Science and Technology*, 43: 6572-6578.

United States District Court. 2007. *Consent Decree Onondaga Lake Bottom Subsite of the Onondaga Lake Superfund Site, Syracuse, NY*. Northern District of New York.

Table C.1. Composition of artificial lake water (ALW), mimicking the ionic composition of Onondaga Lake water.

a. Components as salts.

Salt	Concentration (mM)	Concentration ($mg \cdot L^{-1}$)
$CaCl_2.2H_2O$	5.84	858.83
$NaHCO_3$	4.24	356.20
$(Na)_2SO_4$	1.67	237.21
NaCl	3.21	187.45
$MgCl_2.6H_2O$	0.99	200.87
KCl	0.44	32.43
NaF	0.02	1.01

b. Components as ions and ion balance.

Cations	($meq \cdot L^{-1}$)	(mM)	($mg \cdot L^{-1}$)
Ca^{2+}	11.68	5.84	234.14
K^+	0.44	0.44	17.01
Mg^{2+}	1.98	0.99	24.03
Na^+	10.81	10.81	248.57
Total	**24.908**		
Anions	($meq \cdot L^{-1}$)	(mM)	($mg \cdot L^{-1}$)
Cl^-	17.303	17.303	611.54
HCO_3^-	4.241	4.241	258.64
SO_4^{2-}	3.340	1.670	160.42
F^-	0.024	0.024	0.46
Total	**24.908**		

Table C.2. Summary of results from measurements of nitrate and oxygen demand as a function of turbulence for Onondaga Lake sediments.

a. Sediment nitrate demand, non-normalized values (SND_{max} in **bold**)

Date	Pump Speed (rpm)	Turbulent Intensity ($mm \cdot s^{-1}$)	*SND*, mean $gN \cdot m^{-2} \cdot d^{-1}$	*SND*, s.d. $gN \cdot m^{-2} \cdot d^{-1}$
6-12-2008	2.0	0.07	0.023	0.008
	6.0	0.24	0.052	0.004
	10.0	0.44	0.063	0.006
	50.0	4.57	**0.079**	0.006
10-16-2008	25.0	1.55	**0.176**	0.003
4-28-2009	2.0	0.07	0.096	0.022
	25.0	1.55	0.252	0.028
	25.0	1.55	0.254	0.030
	50.0	4.57	**0.258**	0.036
7-29-09	10.0	0.44	0.123	0.004
	17.5	0.93	*0.181*	0.010
	50.0	4.57	**0.158**	0.006
Grand Mean, SND_{max}			**0.168**	0.073

b. Sediment nitrate demand, average normalized values (data source for Figure C.8a)

Pump Speed (rpm)	Turbulent Intensity ($mm \cdot s^{-1}$)	n	*SND*, mean $gN \cdot m^{-2} \cdot d^{-1}$	*SND*, s.d. $gN \cdot m^{-2} \cdot d^{-1}$
2.0	0.07		0.33	0.06
6.0	0.24		0.66	
10.0	0.44		0.79	0.01
25.0	1.55		0.98	0.00
50.0	4.57		1.00	0.00

Table C.3. Summary of results from measurements of oxygen demand as a function of turbulence for Onondaga Lake sediments.

a. Sediment oxygen demand, non-normalized values (SOD_{max} in **bold**)

Date	Pump Speed (rpm)	Turbulent Intensity ($mm \cdot s^{-1}$)	*SOD*, mean $gO_2 \cdot m^{-2} \cdot d^{-1}$	*SOD*, s.d. $gO_2 \cdot m^{-2} \cdot d^{-1}$
8-8-2008	2.0	0.07	0.50	0.02
	6.0	0.24	0.79	0.01
	6.0	0.24	0.84	0.02
	25.0	1.55	1.01	0.02
	25.0	1.55	**1.07**	0.01
10-7-2008	10.0	0.44	0.80	0.01
	25.0	1.55	**1.25**	0.01
4-14-2009	10.0	0.44	0.73	0.00
	25.0	1.55	*1.37*	0.03
	50.0	4.57	1.01	0.02
	50.0	4.57	**1.01**	0.01
7-28-2009	10.0	0.44	0.63	0.01
	17.5	0.93	0.97	0.02
	50.0	4.57	**1.03**	0.00
Grand Mean, SOD_{max}			**1.09**	0.11

b. Sediment oxygen demand, average normalized values (data source for Figure C.8b)

Pump Speed (rpm)	Velocity ($mm \cdot s^{-1}$)	n	*SOD*, mean $gO_2 \cdot m^{-2} \cdot d^{-1}$	*SOD*, s.d. $gO_2 \cdot m^{-2} \cdot d^{-1}$
2.0	0.07	1	0.47	
6.0	0.24	2	0.76	0.03
10.0	0.44	3	0.66	0.06
17.5	0.93	1	0.94	
25.0	1.55	3	0.98	0.03
50.0	4.57	3	1.00	0.00

Figure C.1. Sediment oxygen demand and the diffusive boundary layer: (a) the physical environment; (b) oxygen profile with no consumption in the sediment; (c) oxygen profile with consumption in the sediment.

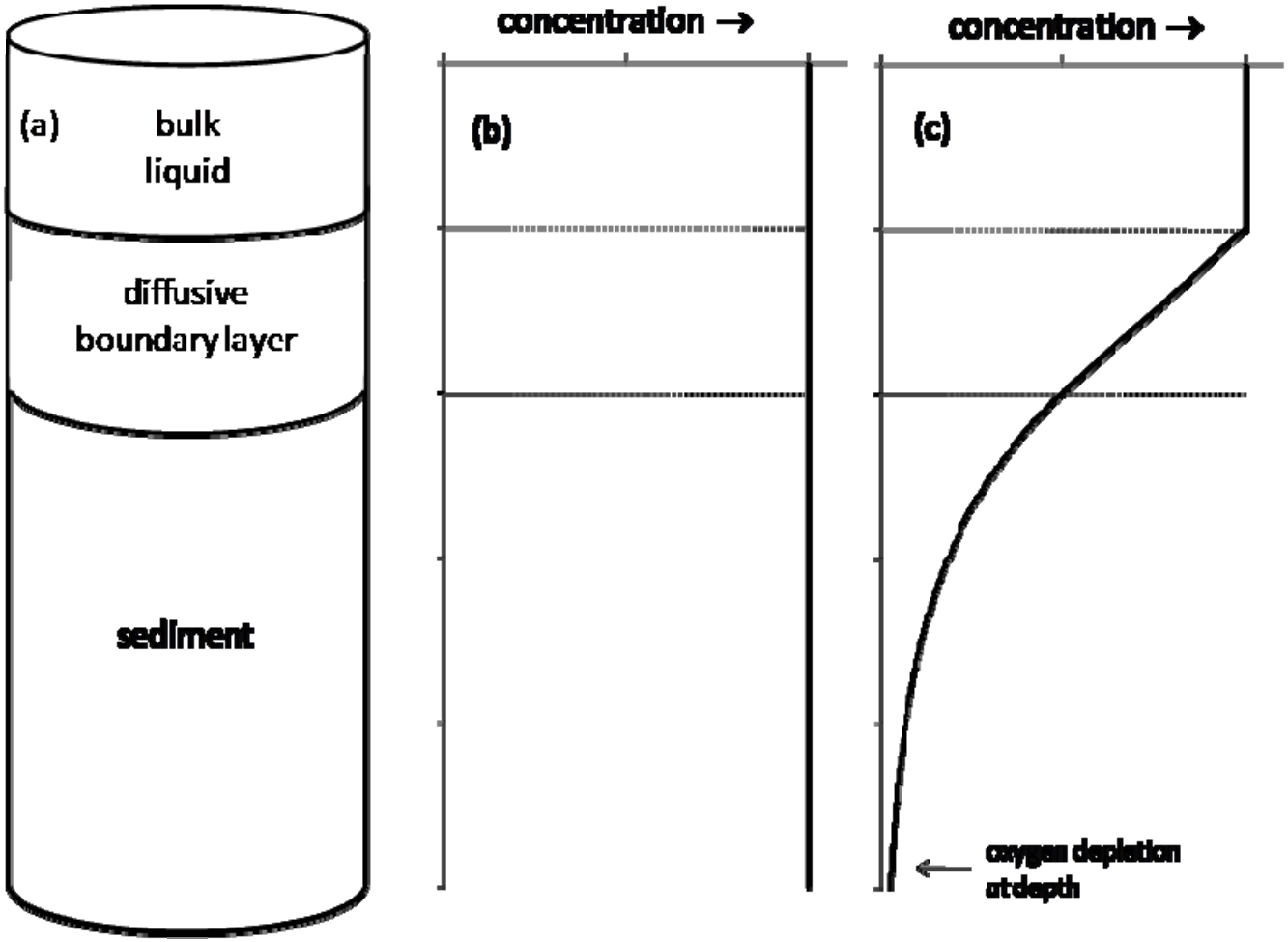

Figure C.2. The effect of changes in (a) the bulk liquid concentration and (b) the diffusive boundary layer thickness on sediment oxygen demand. In Panel A, a doubling of the bulk liquid oxygen concentration increases the profile slope (and thus the *SOD*) by a factor of 1.4. In Panel B, a 10-fold reduction in the thickness of the *DBL* increases the profile slope (and thus the *SOD*) by a factor of 2.4.

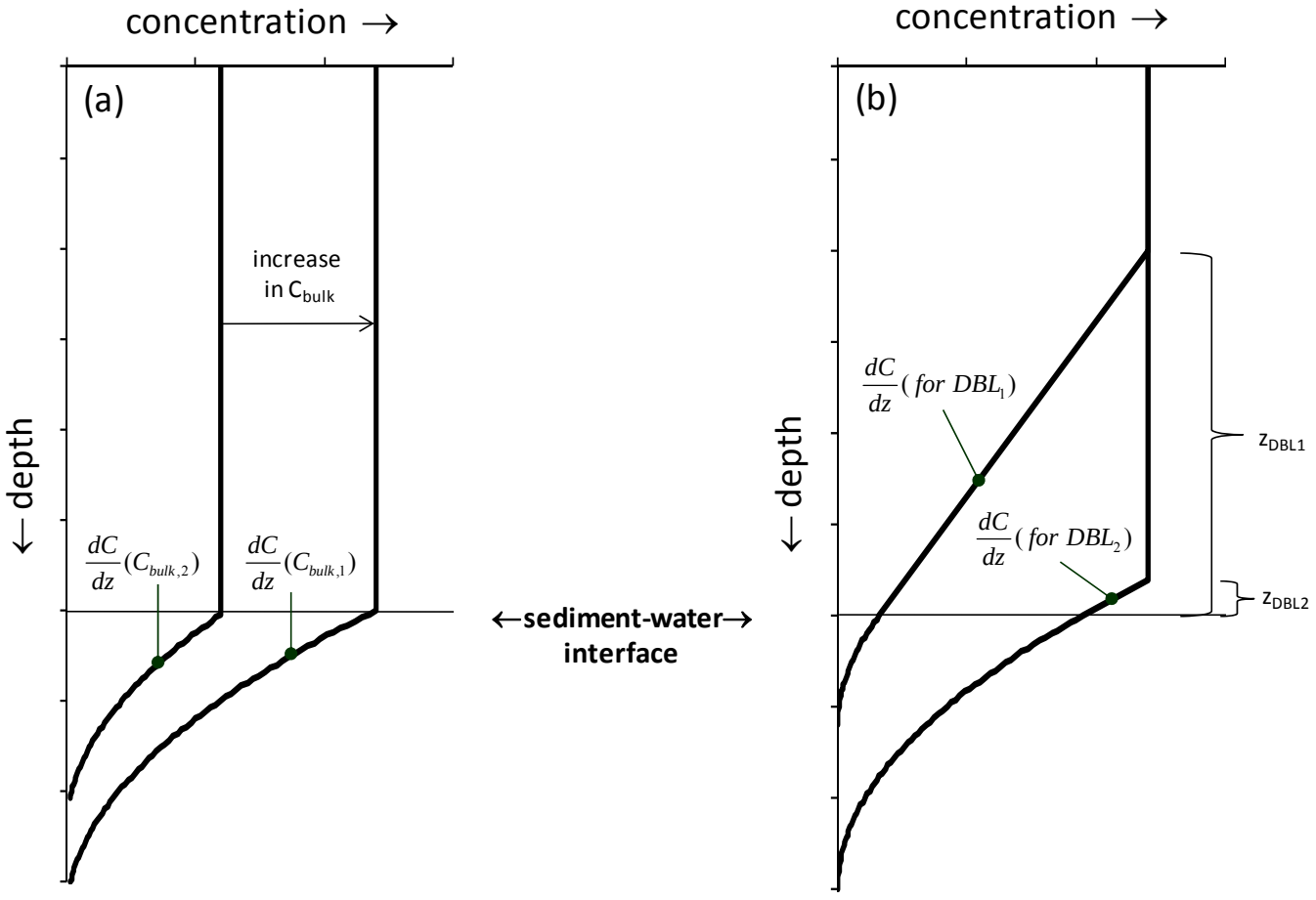

Figure C.3. Model-predicted oxygen profiles (a) without and (b) with a diffusive boundary layer. The bulk liquid oxygen concentration (C_{bulk} = 2→10 $gO_2 \cdot m^{-3}$) is the same in both cases. In the absence of a *DBL*, the oxygen concentration at the sediment-water interface (C_{swi}) equals that of the bulk liquid (C_{bulk}). In the presence of a *DBL* (see Figure C.2b), C_{swi} is less than C_{bulk}, reducing the concentration gradient and thus the *SOD*.

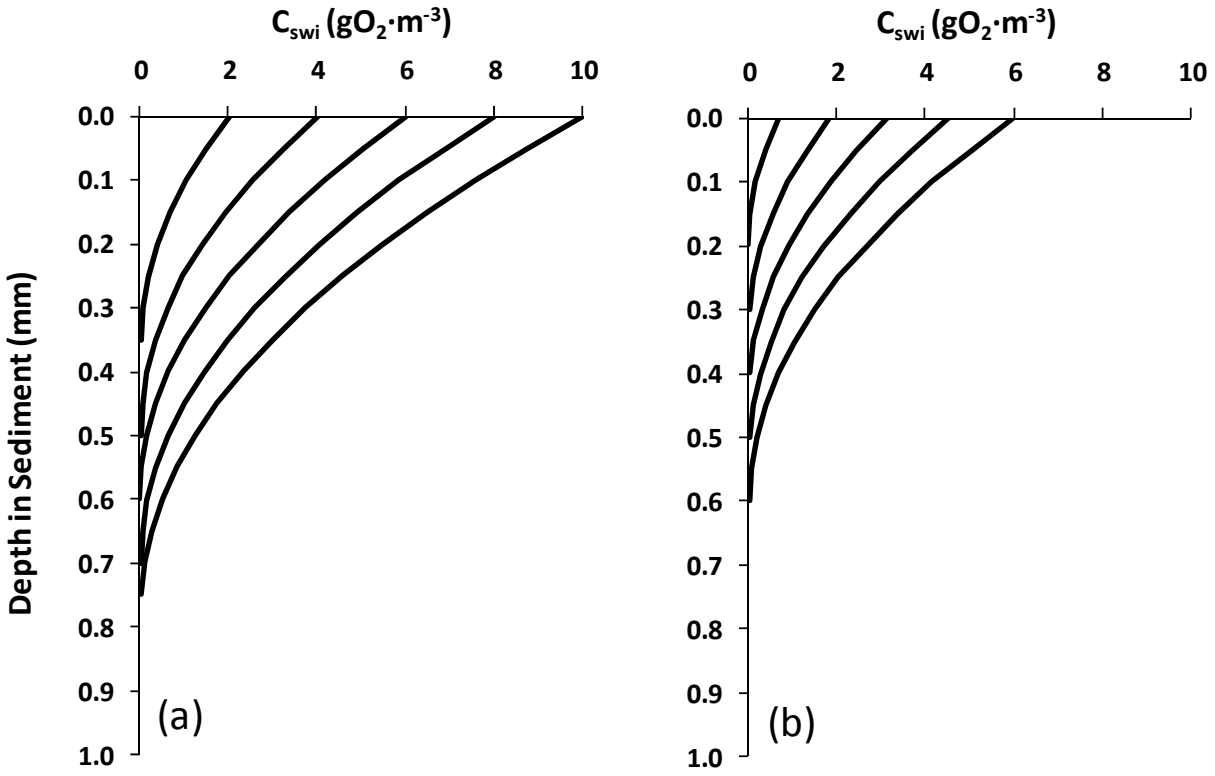

Figure C.4. Illustrating the role of (a) the bulk liquid concentration and (b) the diffusive boundary layer thickness in mediating model-predicted *SOD* separately and (c) together.

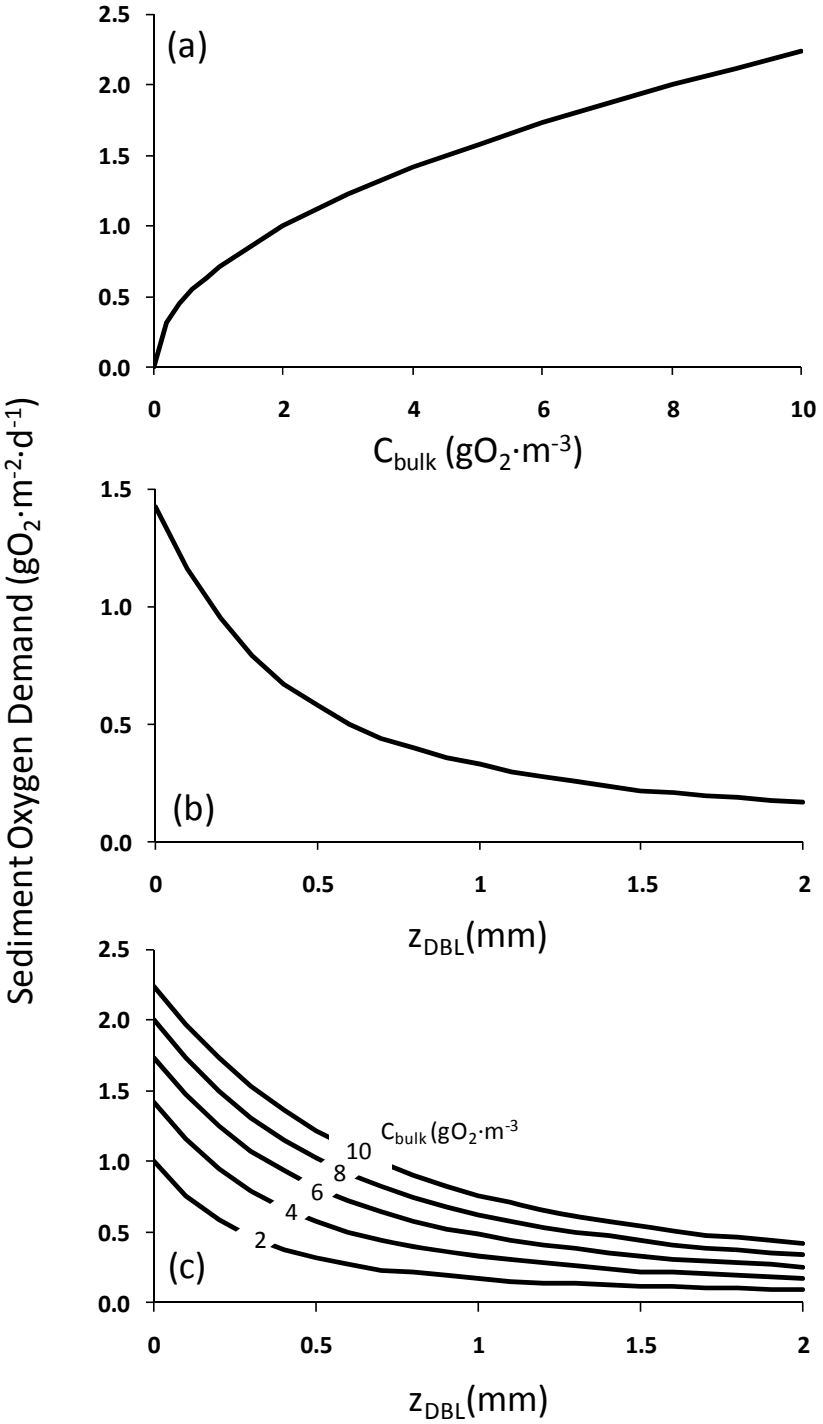

Figure C.5. Sediment flux reactor turbulence calibration.

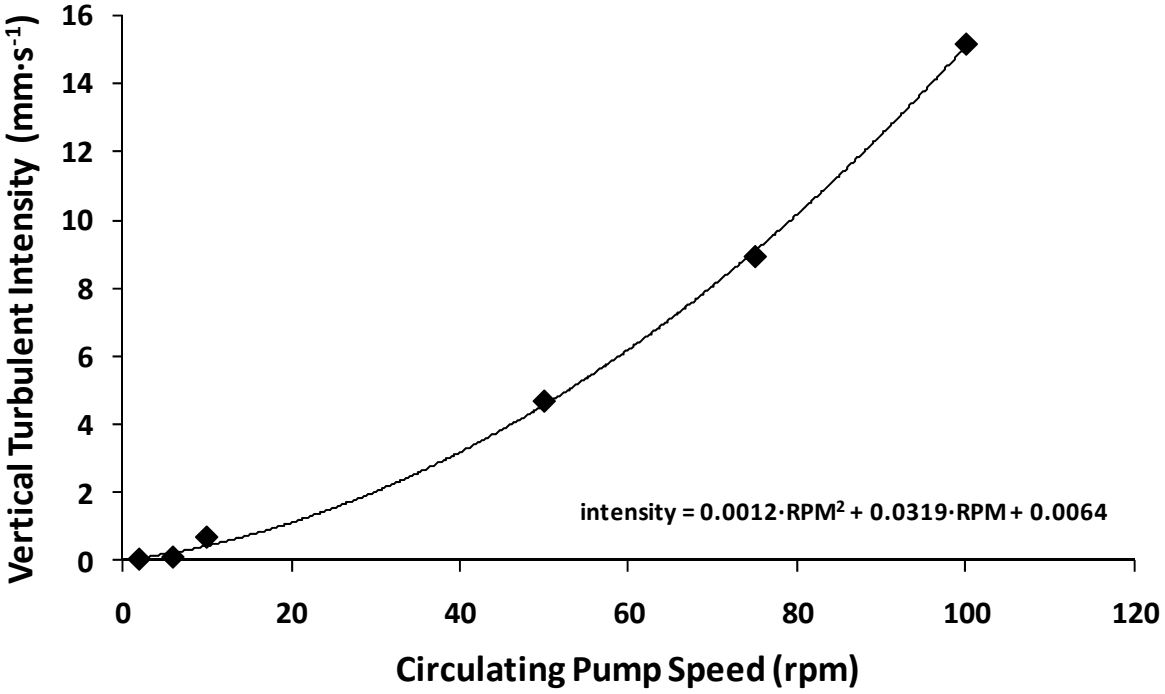

Figure C.6. Schematic drawing of the sediment flux chamber and supporting apparatus.

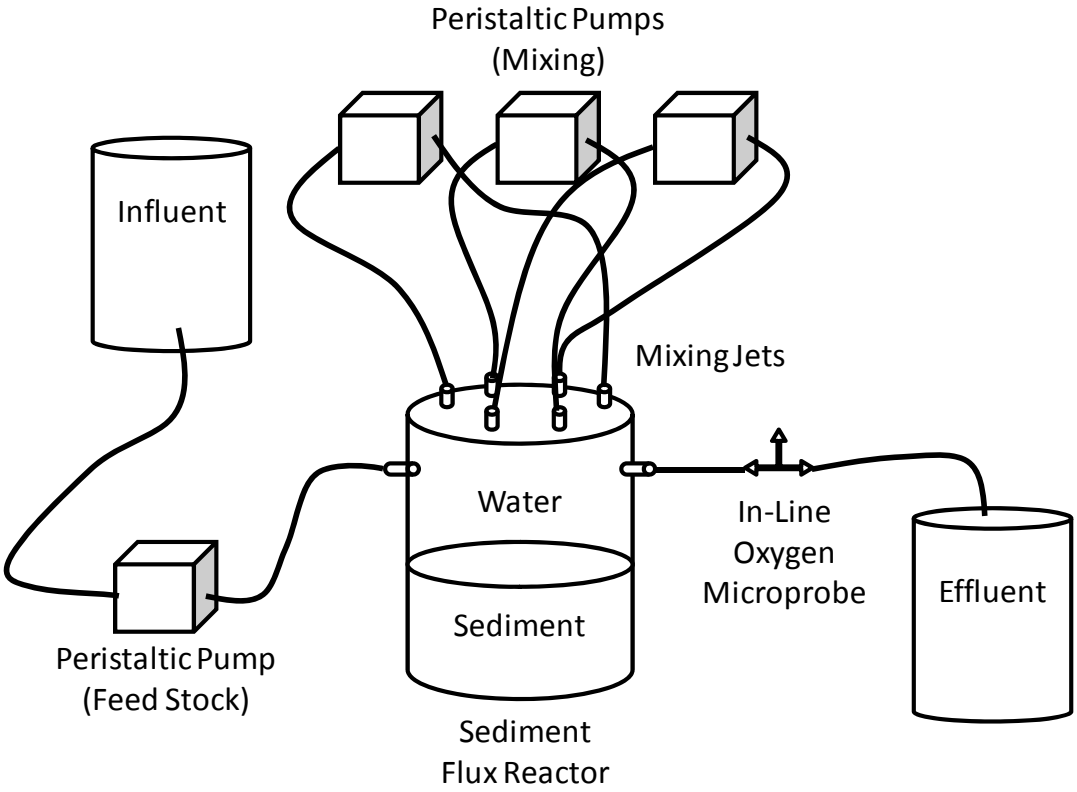

Figure C.7. Approach to steady state in the sediment flux chamber for (a) *SOD* and (b) *SND*.

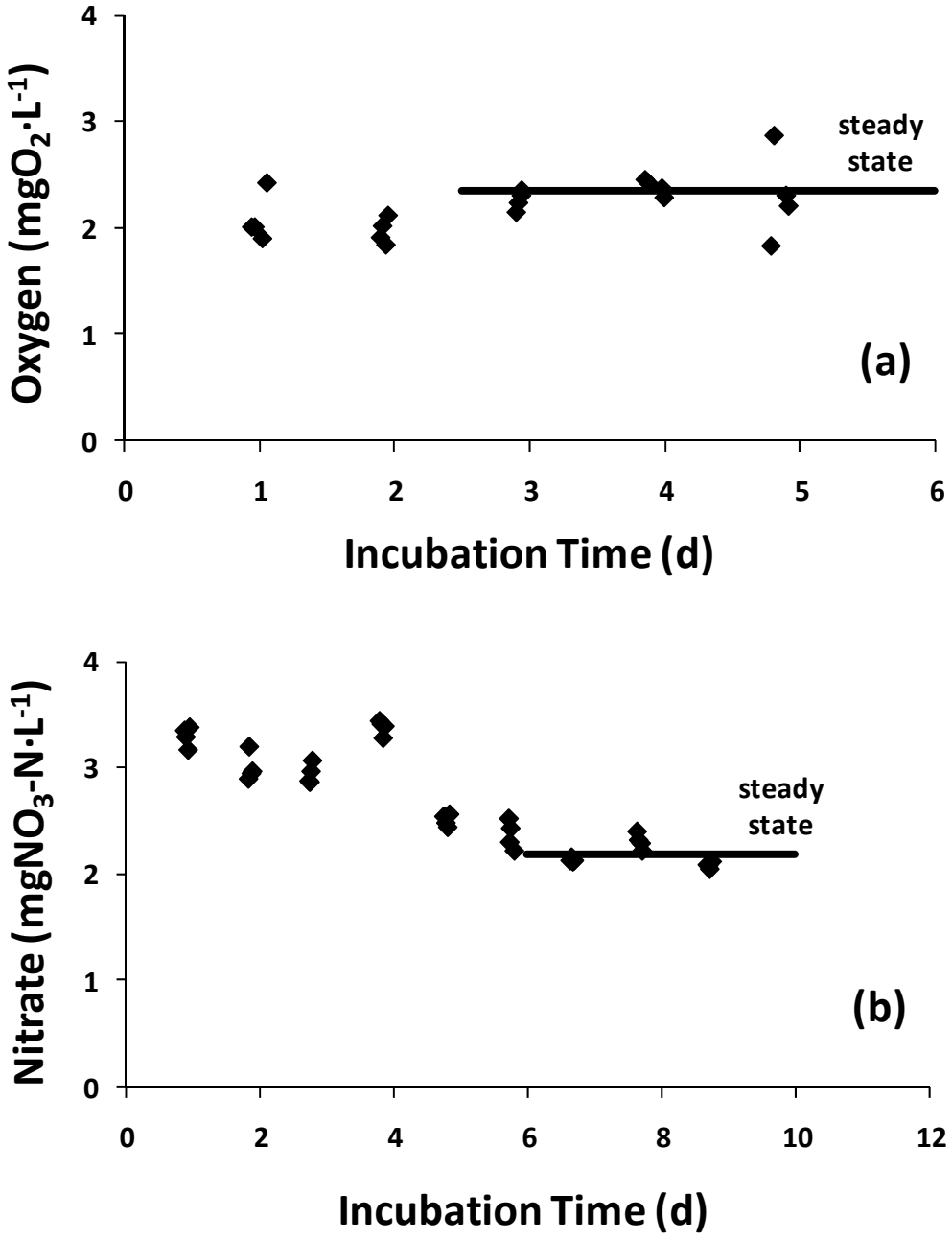

Figure C.8. Relationship between normalized electron acceptor flux and turbulent intensity for (a) *SND* and (b) *SOD*.

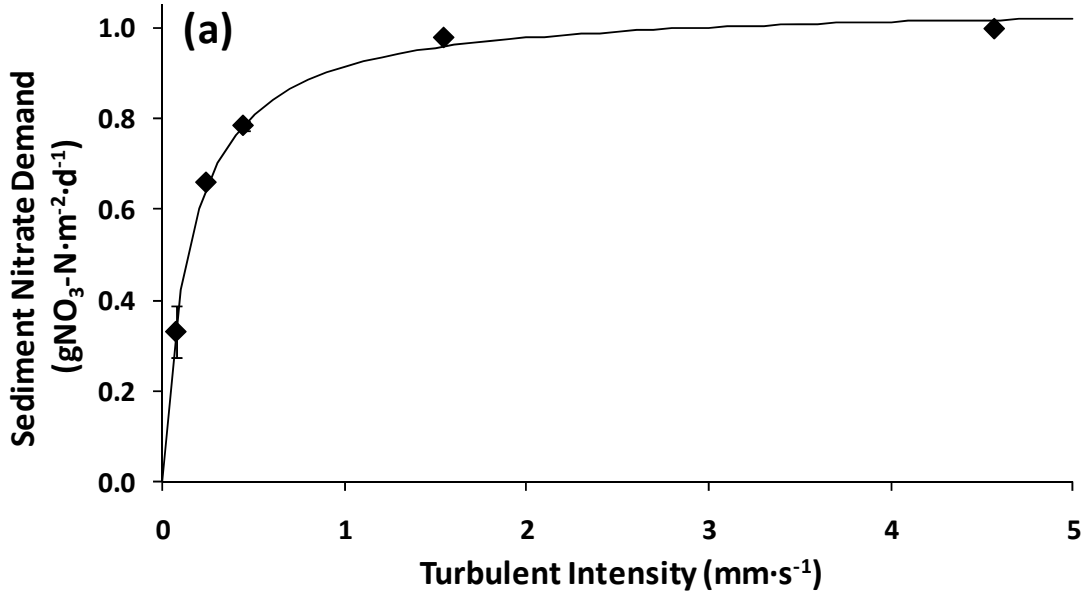

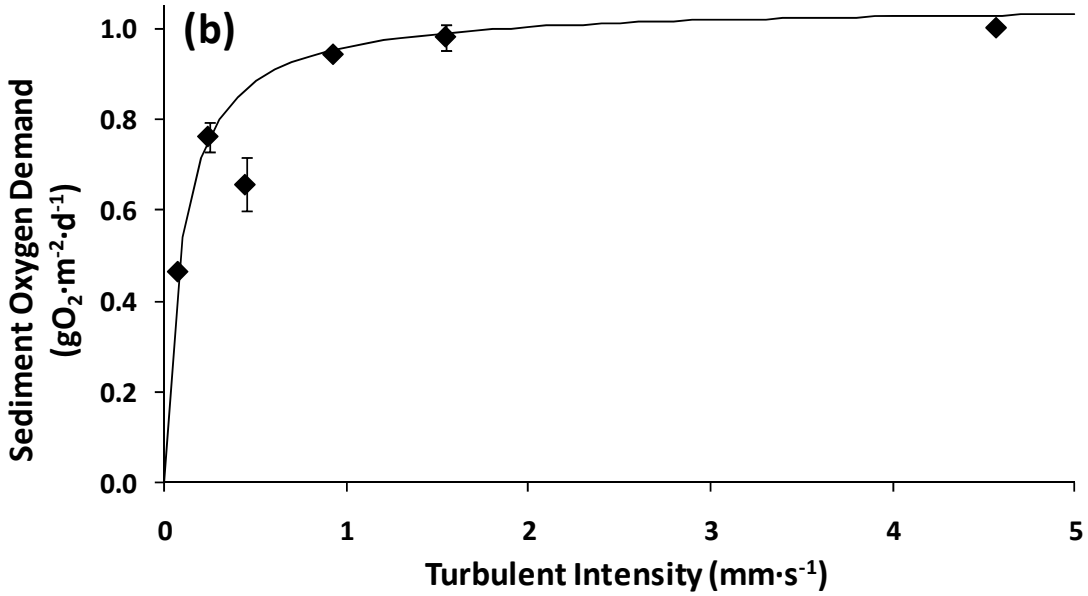

Figure C.9. Management application of the turbulent intensity – electron acceptor flux relationship.